XAFS
(X-ray Absorption Fine Structure)

The k-edge absorption in isolated atoms and in a solid

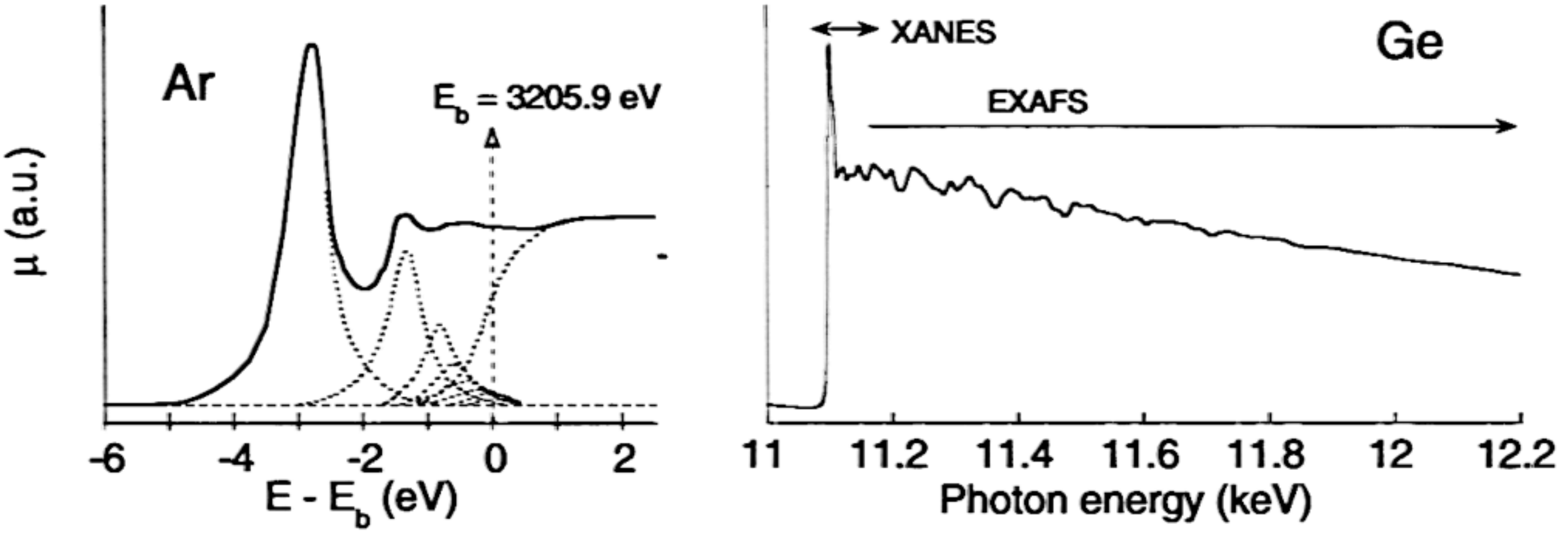

The atomic absorption cross section

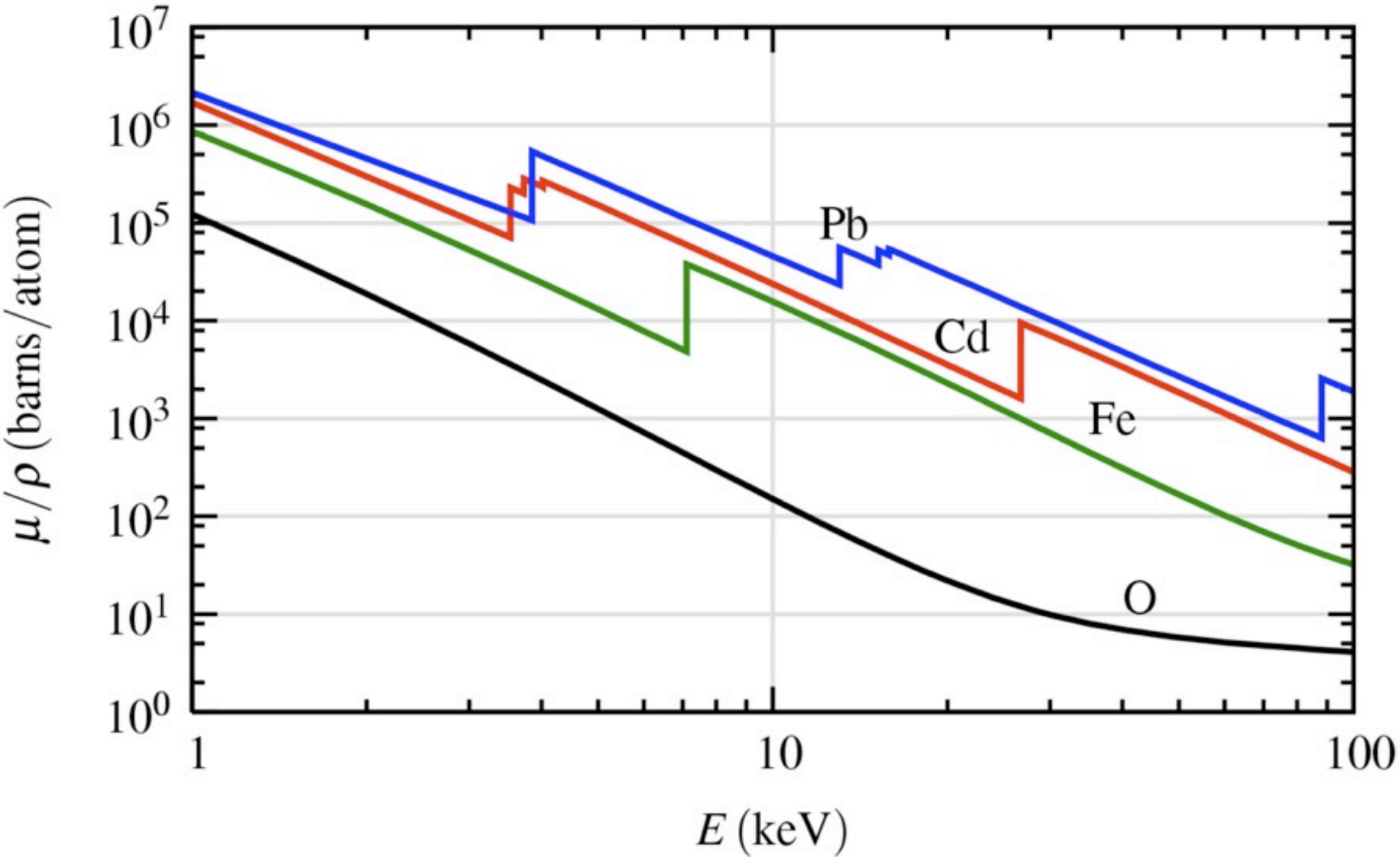

The photoabsorption energy

The photoabsorption energy

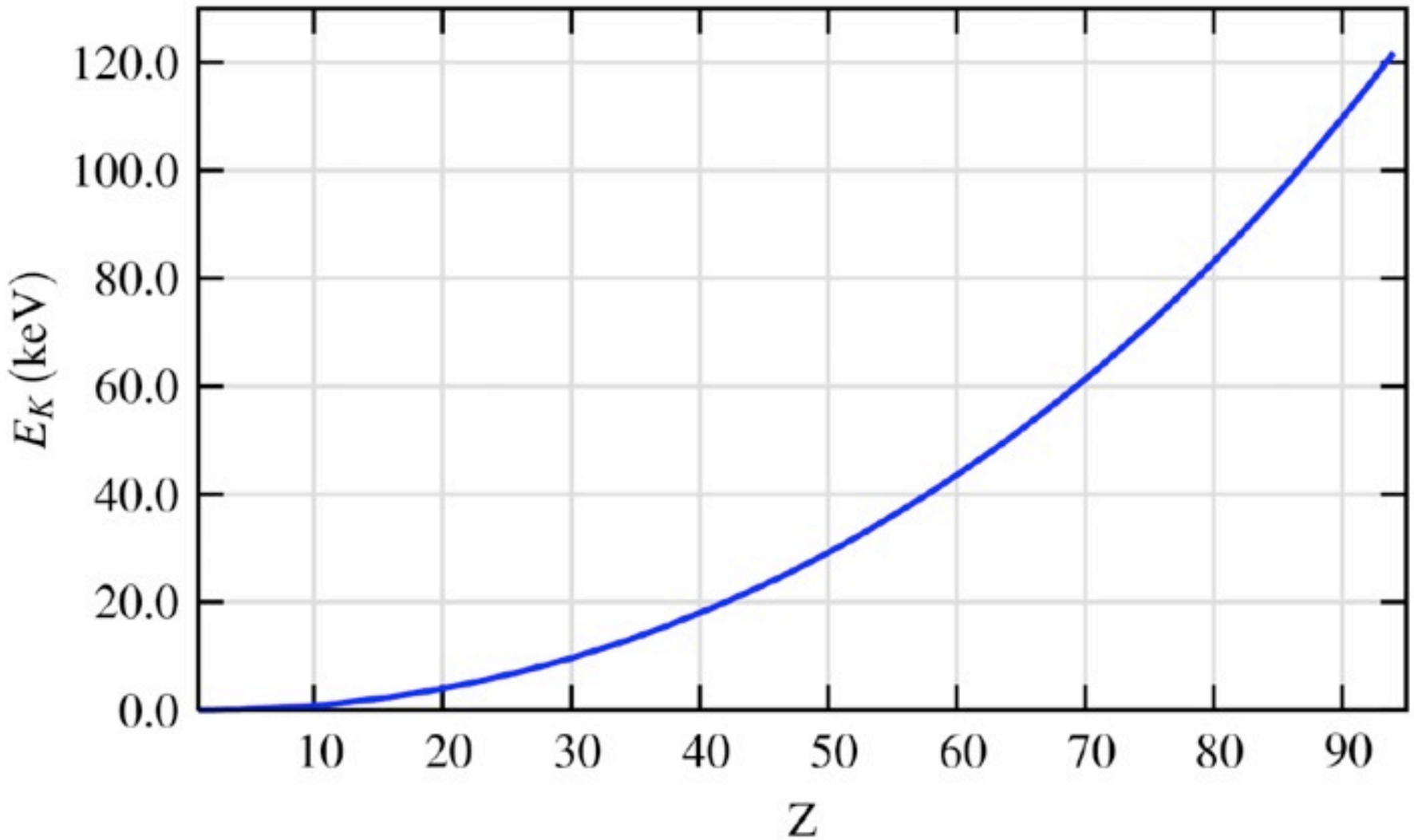

The photoabsorption energy

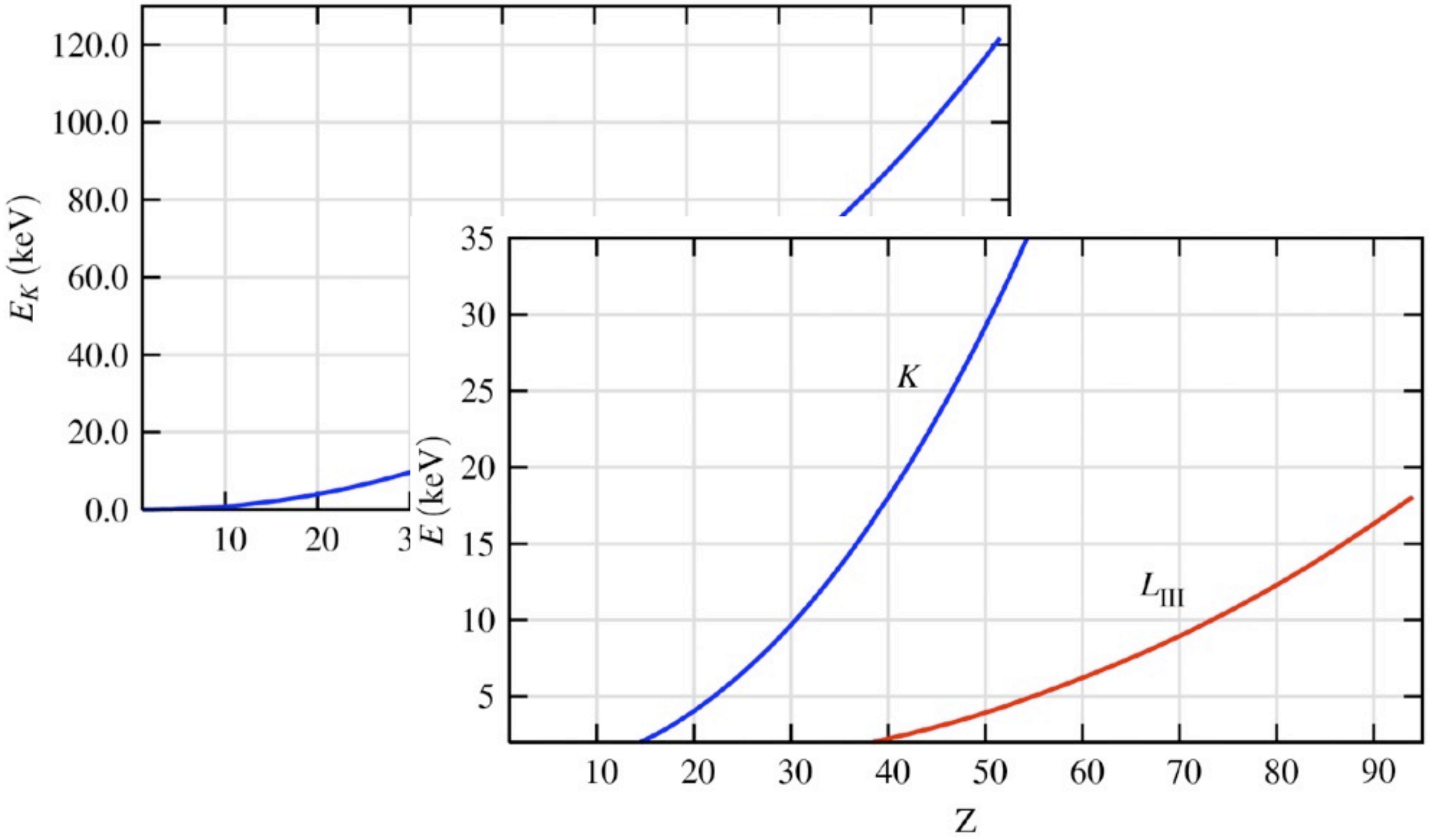

A typical (FeO) solid state k-edge spectrum.

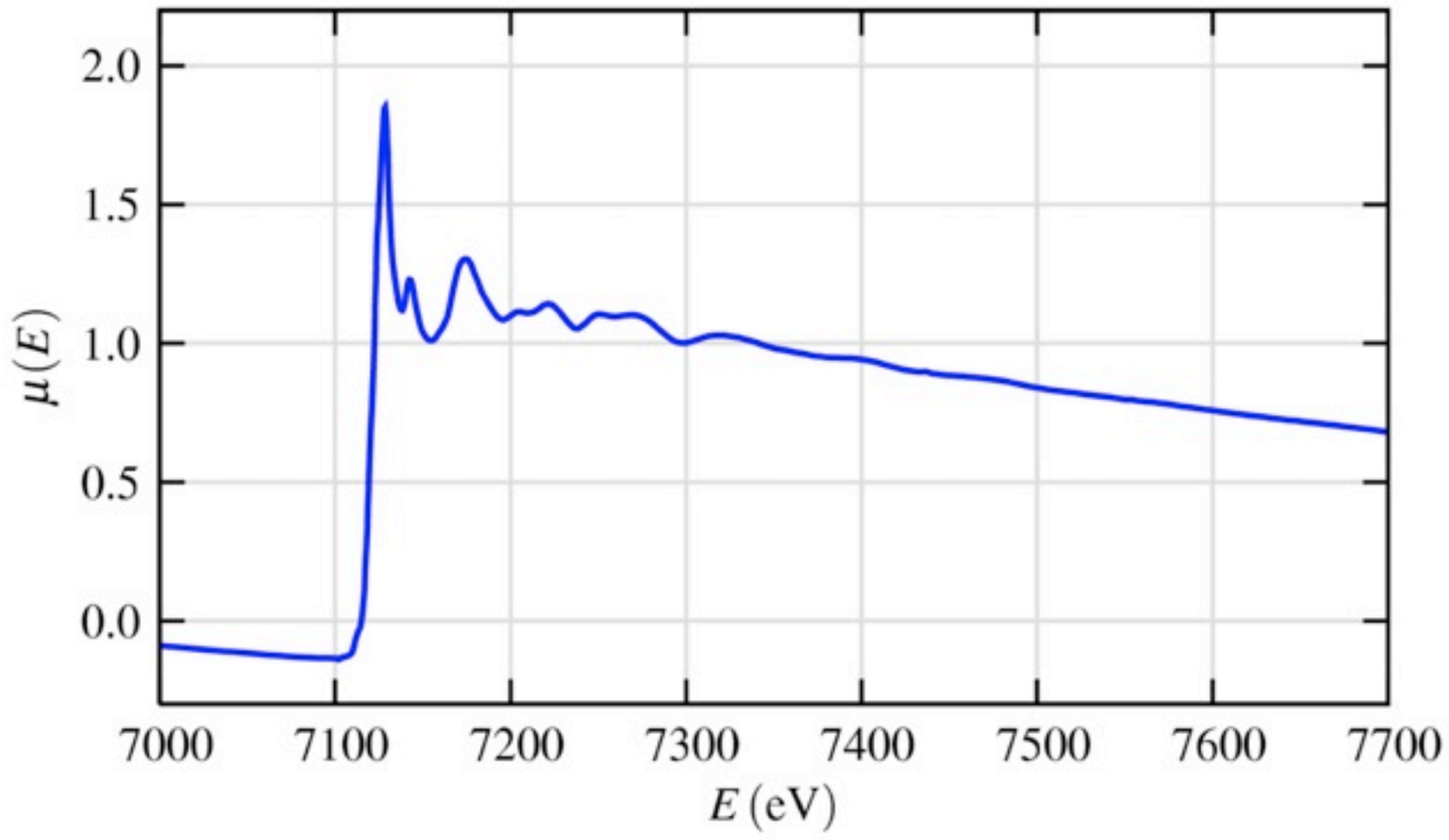

A typical (FeO) solid state k-edge spectrum.

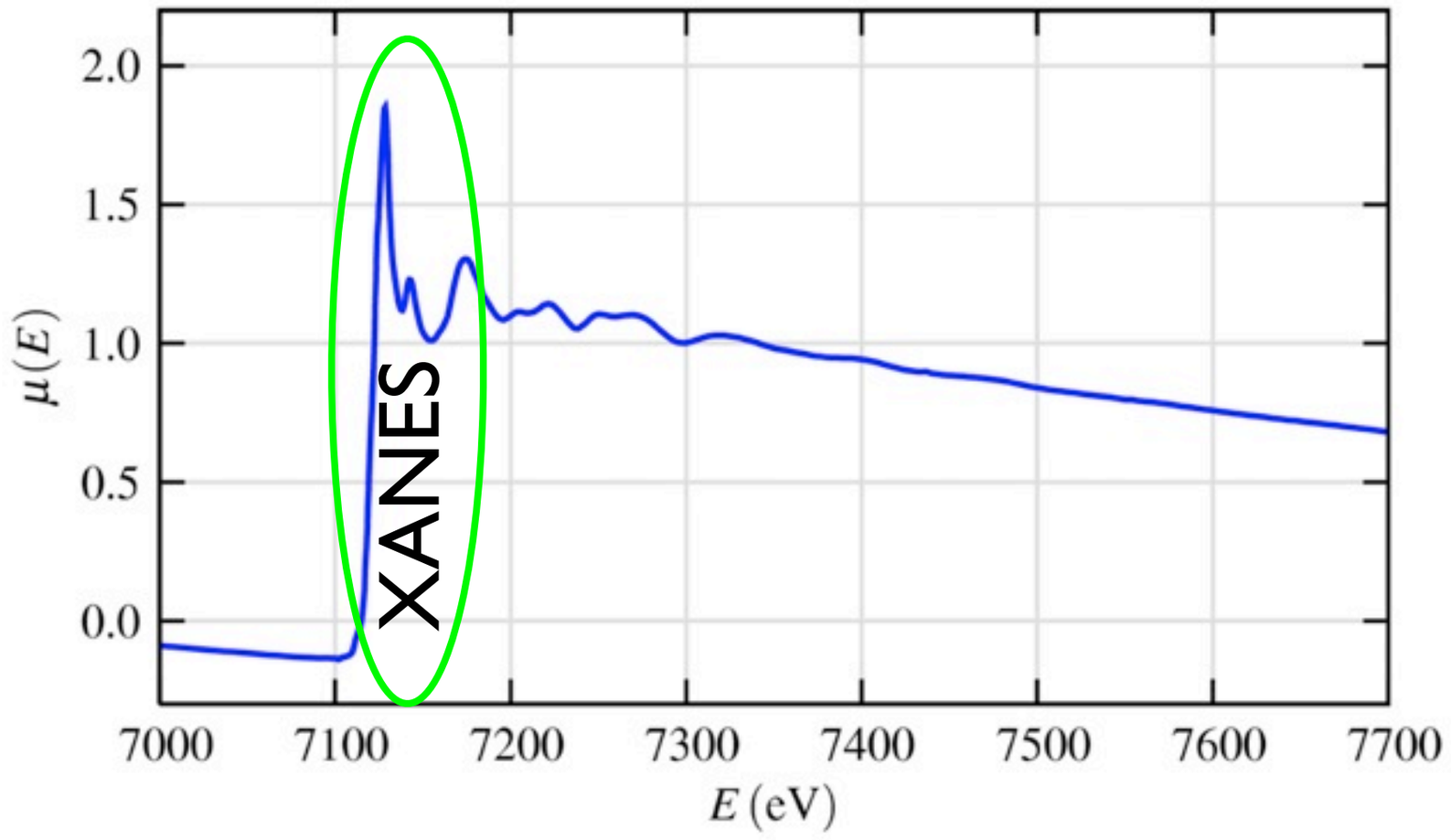

A typical (FeO) solid state k-edge spectrum.

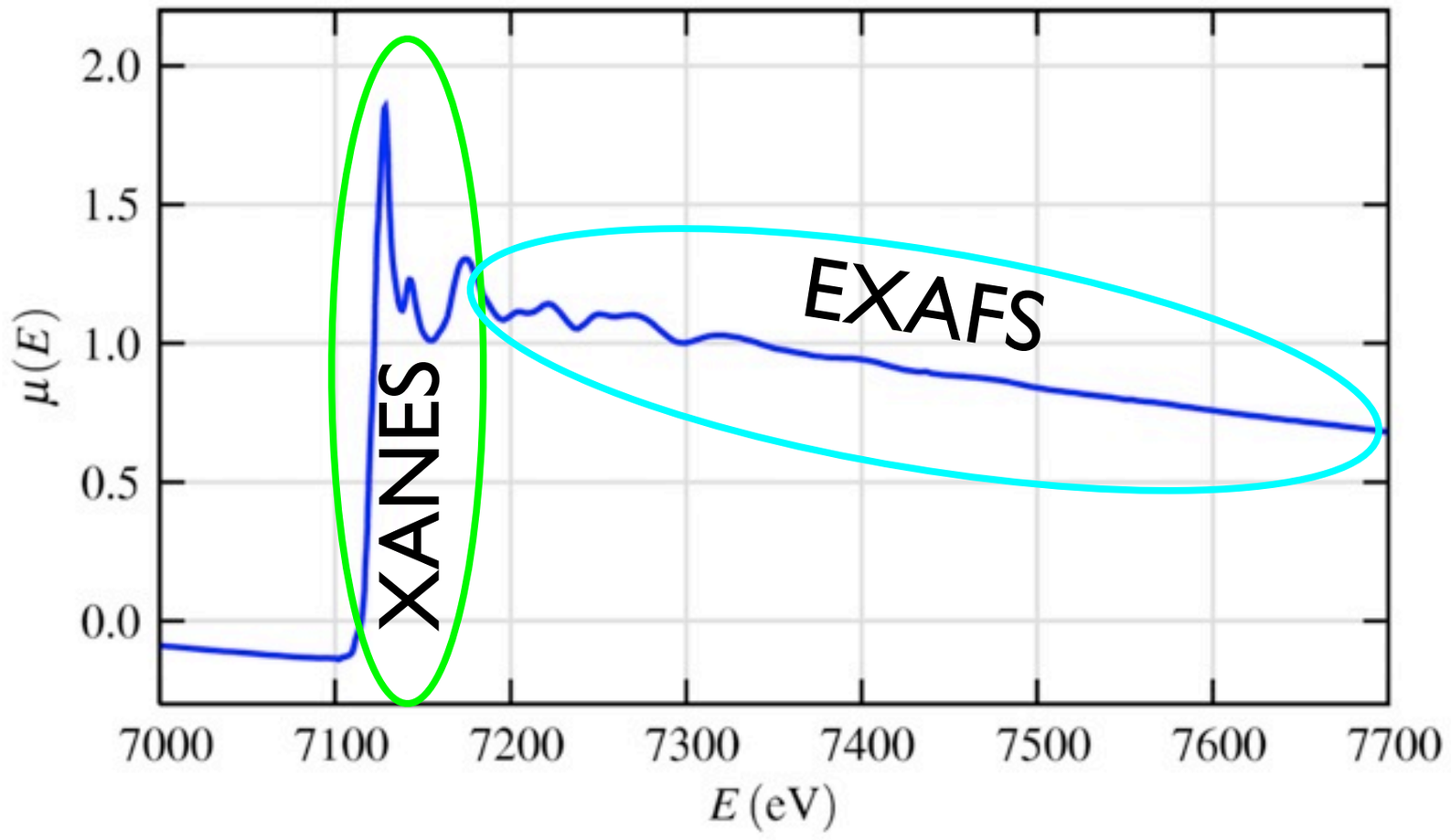

A typical (FeO) solid state k-edge spectrum.

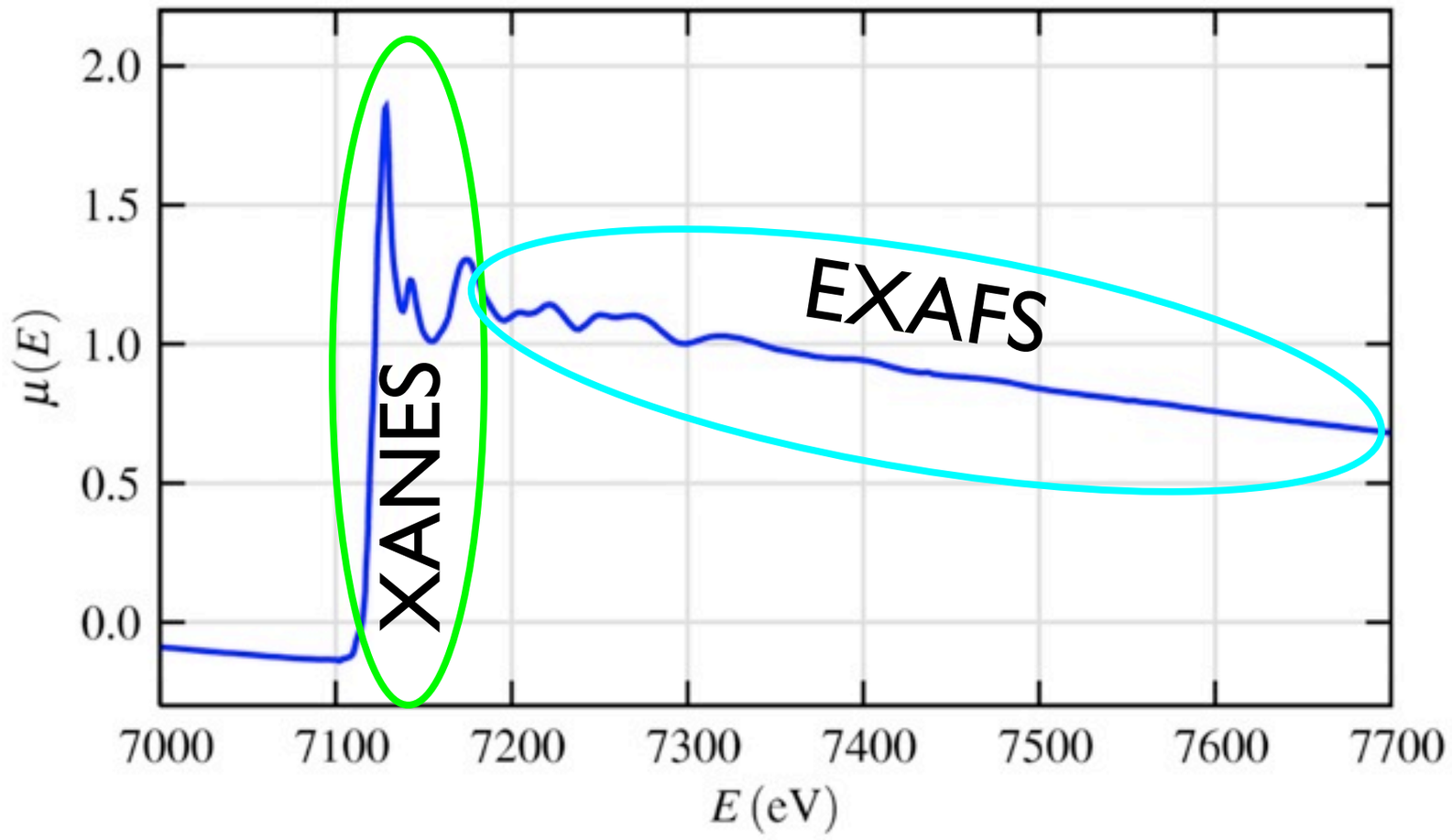

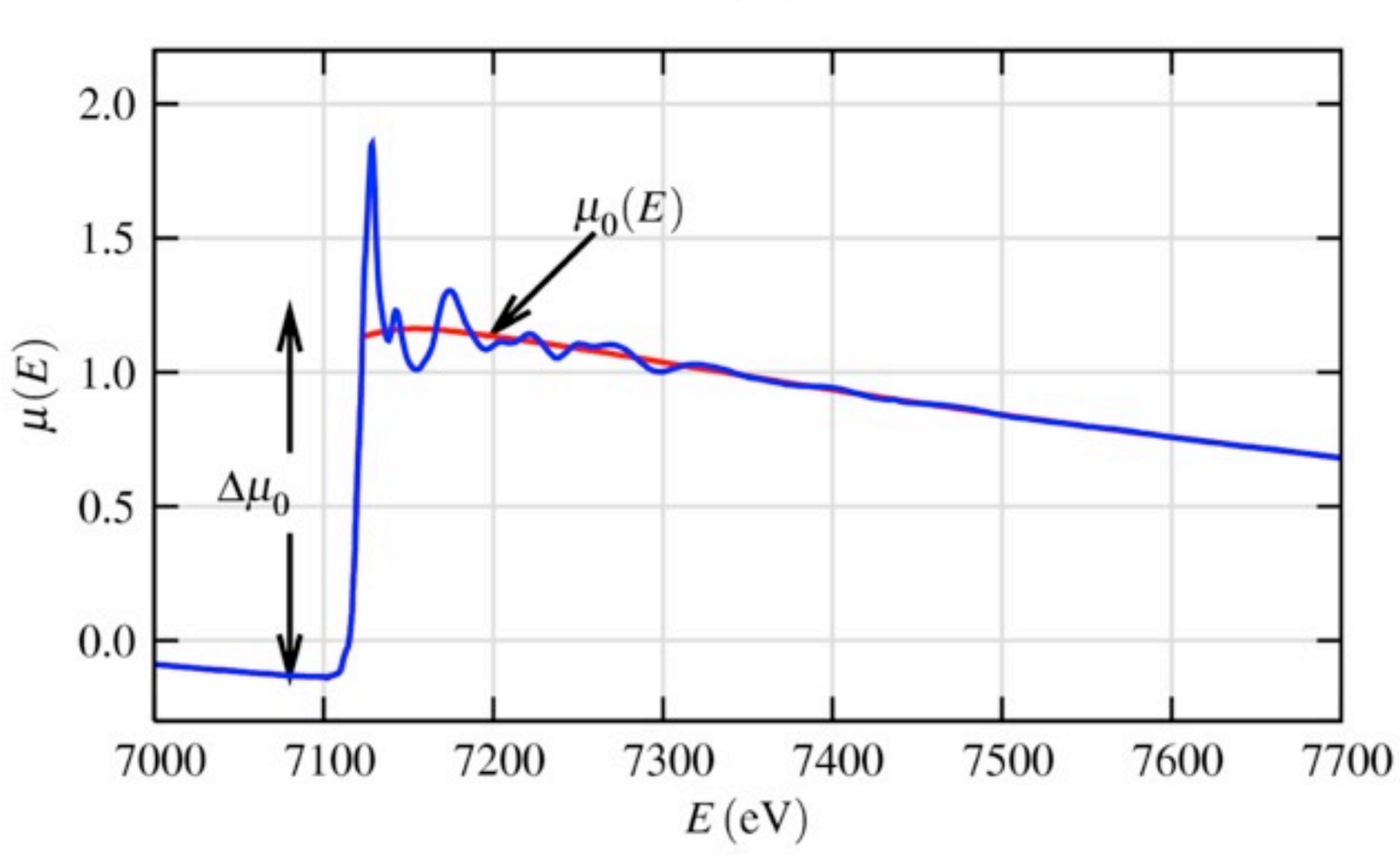

The absorption coefficient in the dipole approximation and for wavelengths >>r_0 is given by:

$$\mu(\hbar\omega) = \frac{4\pi^2 e^2}{nm^2 c\omega} \sum_{if} |\hat{e} \cdot \langle f| \vec{p} |i\rangle|^2 \delta(E_f - E_i - \hbar\omega)$$

For an isolated atom

$$\mu(\hbar\omega) = \frac{4\pi^2 e^2}{nm^2 c\omega} \sum_{if} |\hat{e} \cdot \langle f | \vec{p} | i \rangle|^2 \delta(E_f - E_i - \hbar\omega)$$

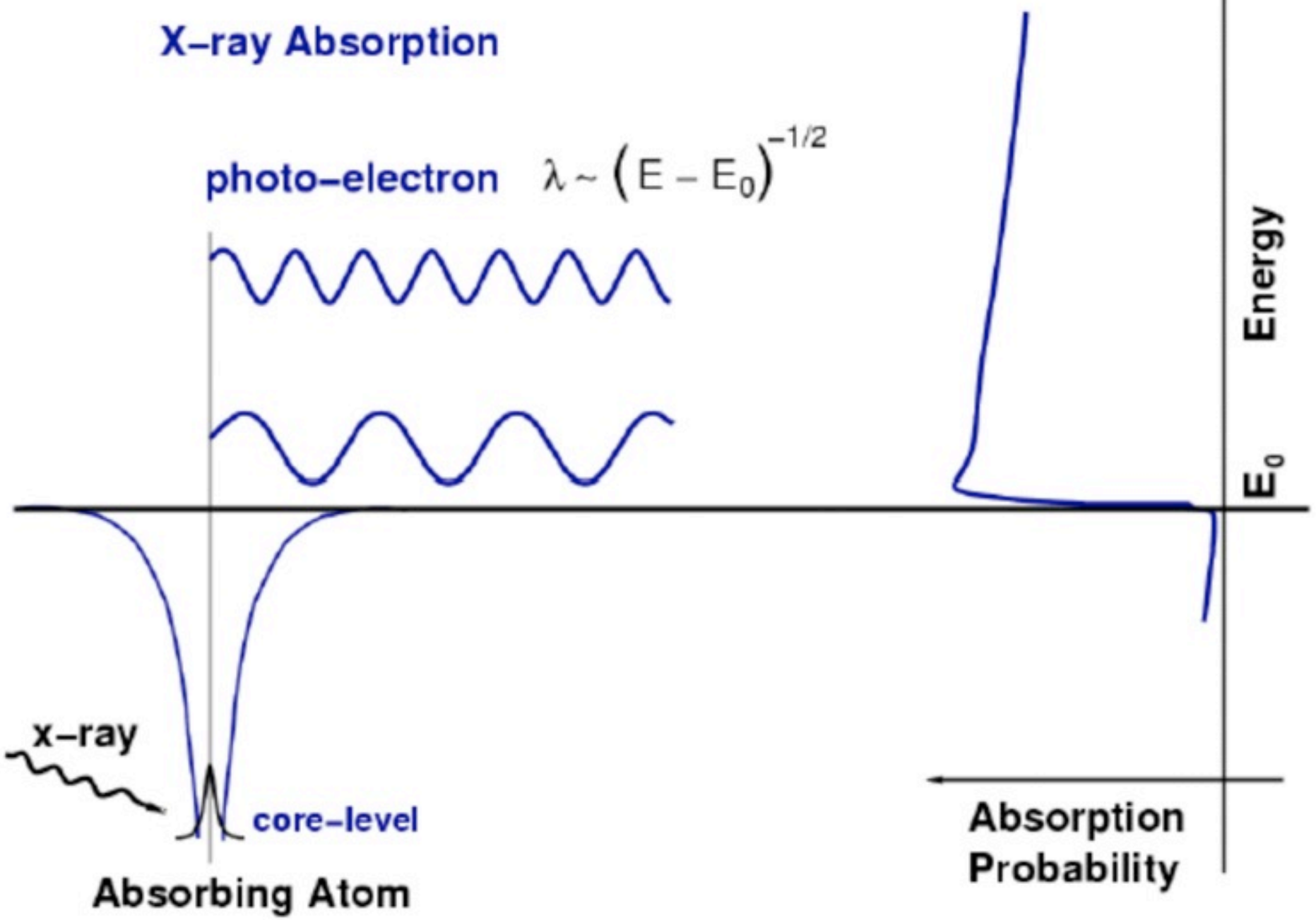

For an isolated atom

$$\mu(\hbar\omega) = \frac{4\pi^2 e^2}{nm^2 c\omega} \sum_{if} |\hat{e} \cdot \langle f | \vec{p} | i \rangle|^2 \delta(E_f - E_i - \hbar\omega)$$

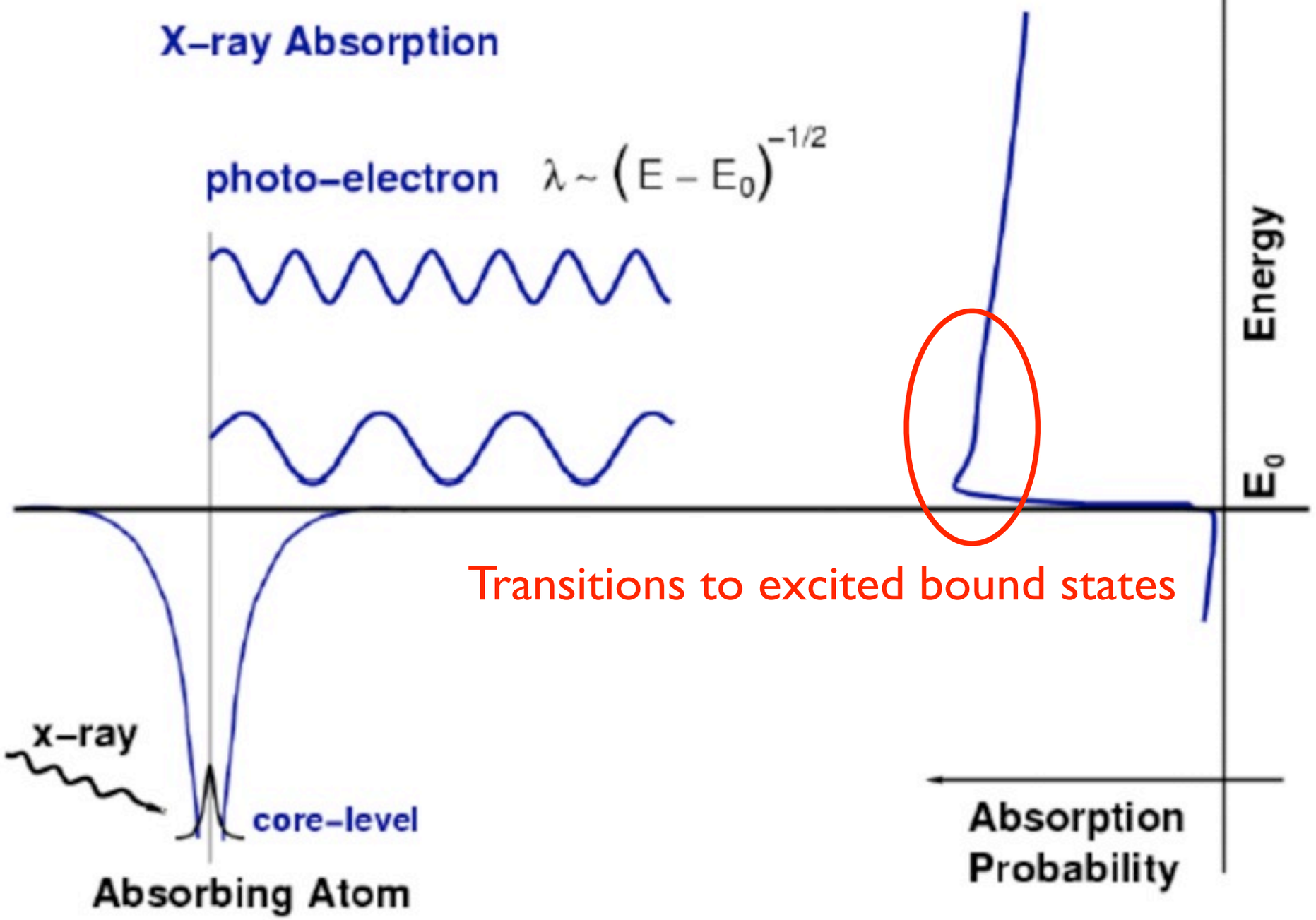

Isolated atoms: the Ne K-edge excitation

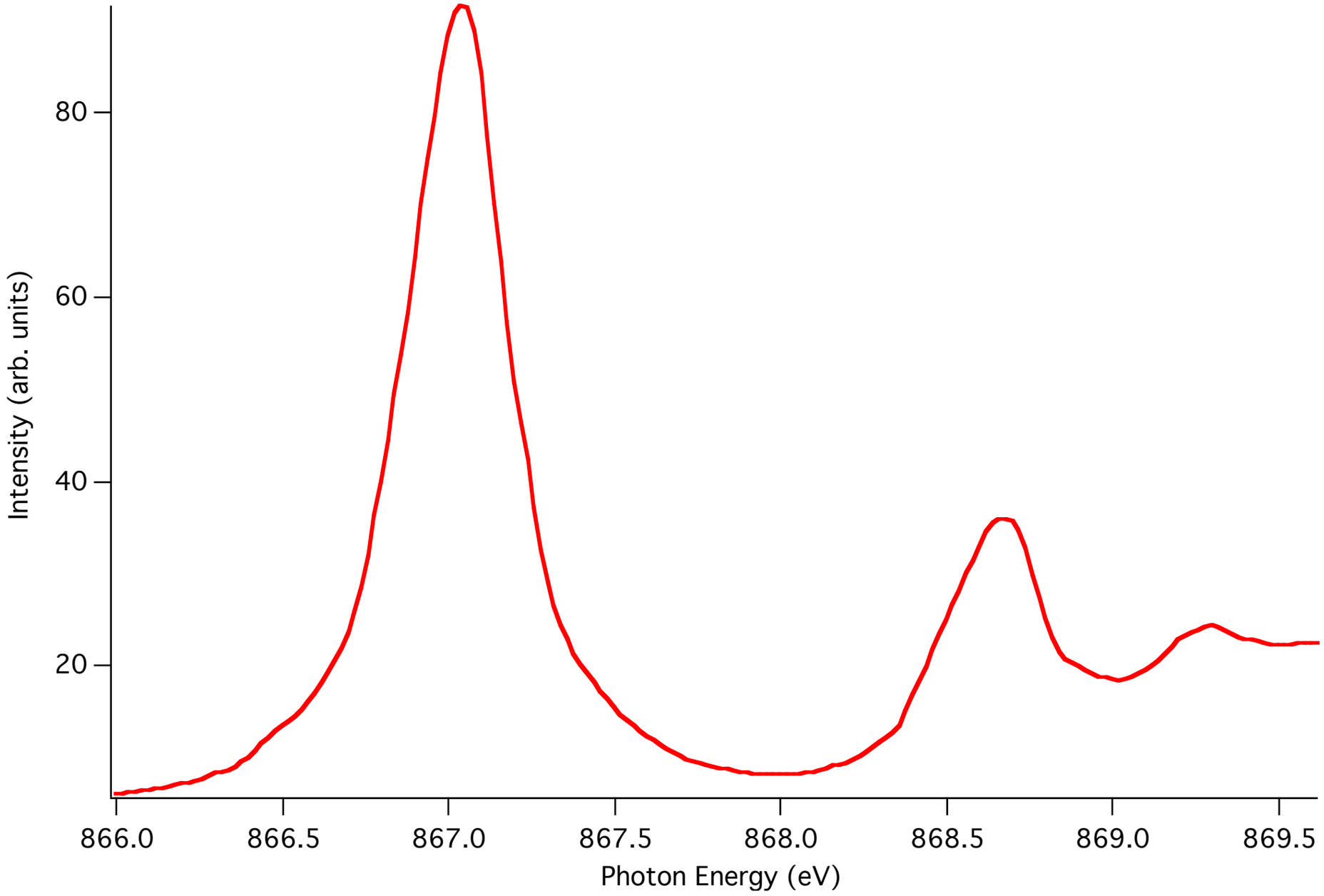

Internal wave source

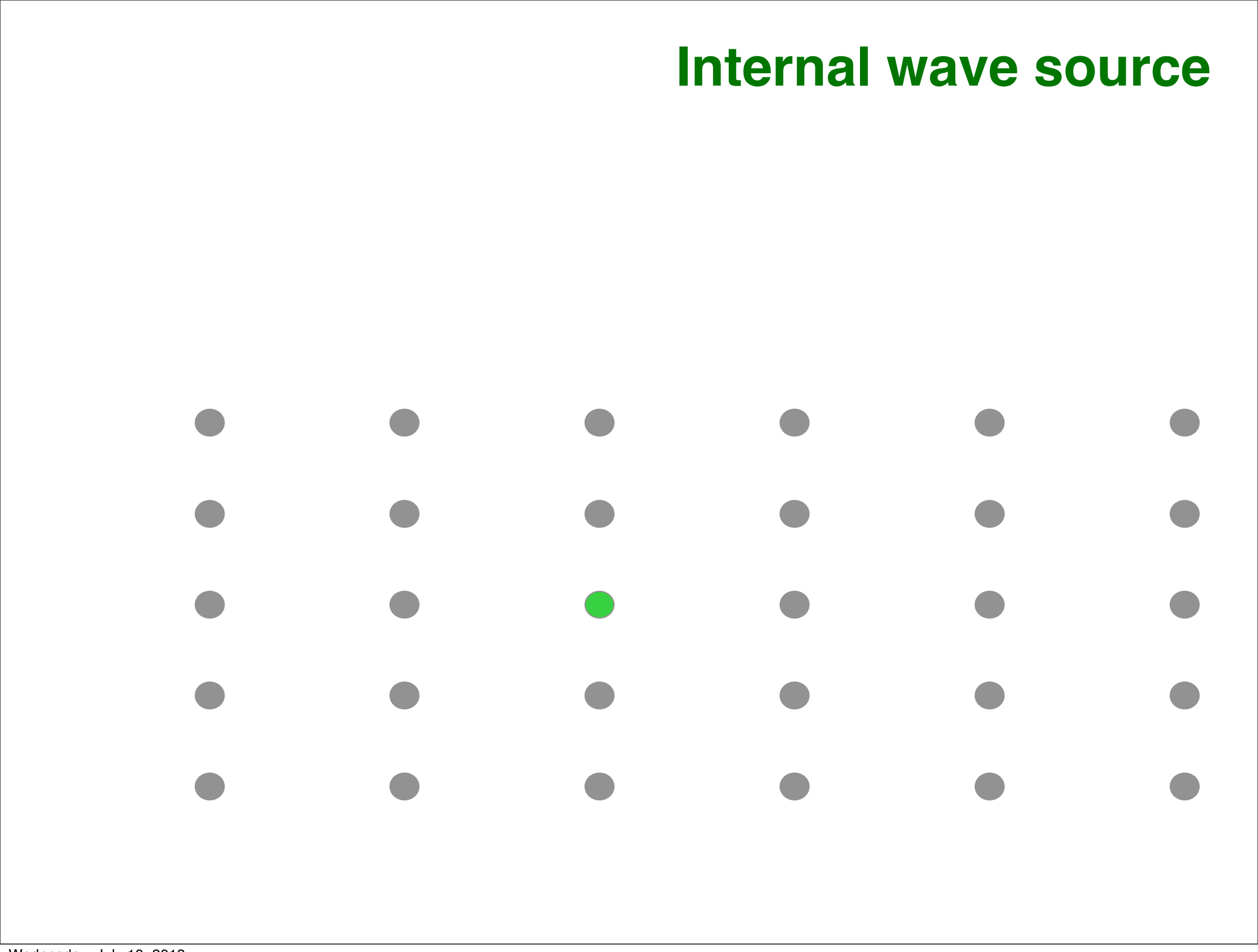

Internal wave source

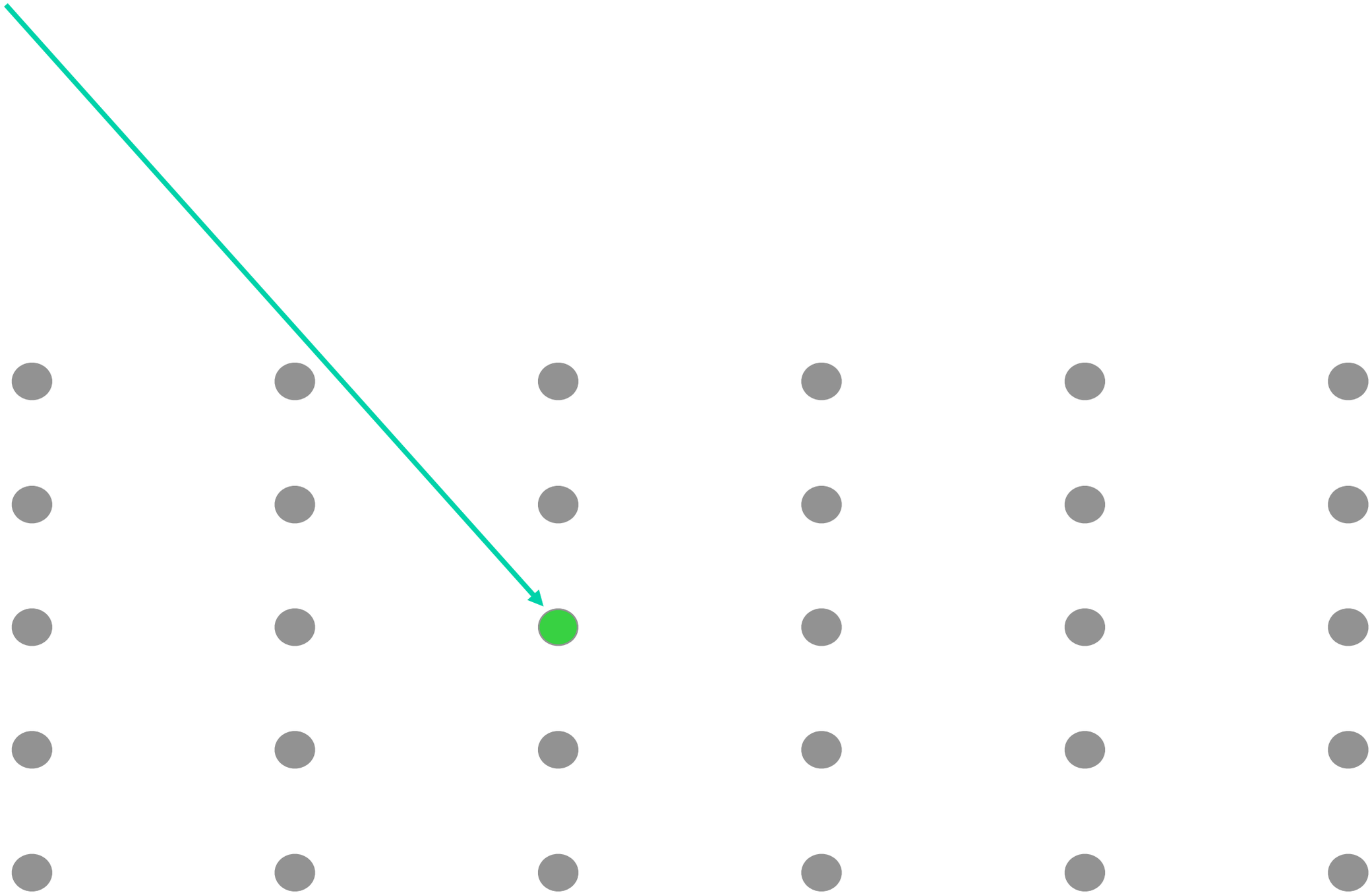

Internal wave source

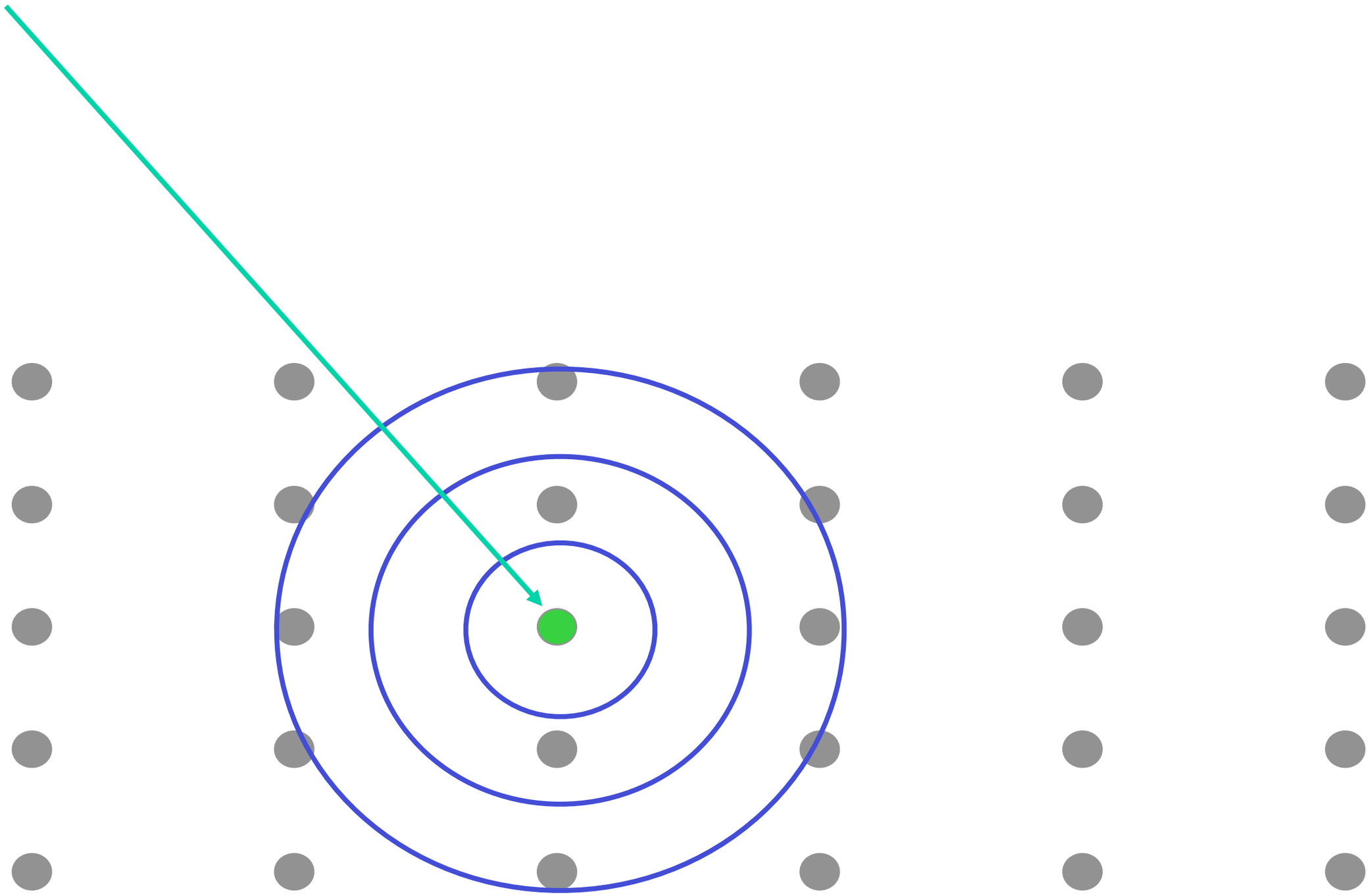

Internal wave source

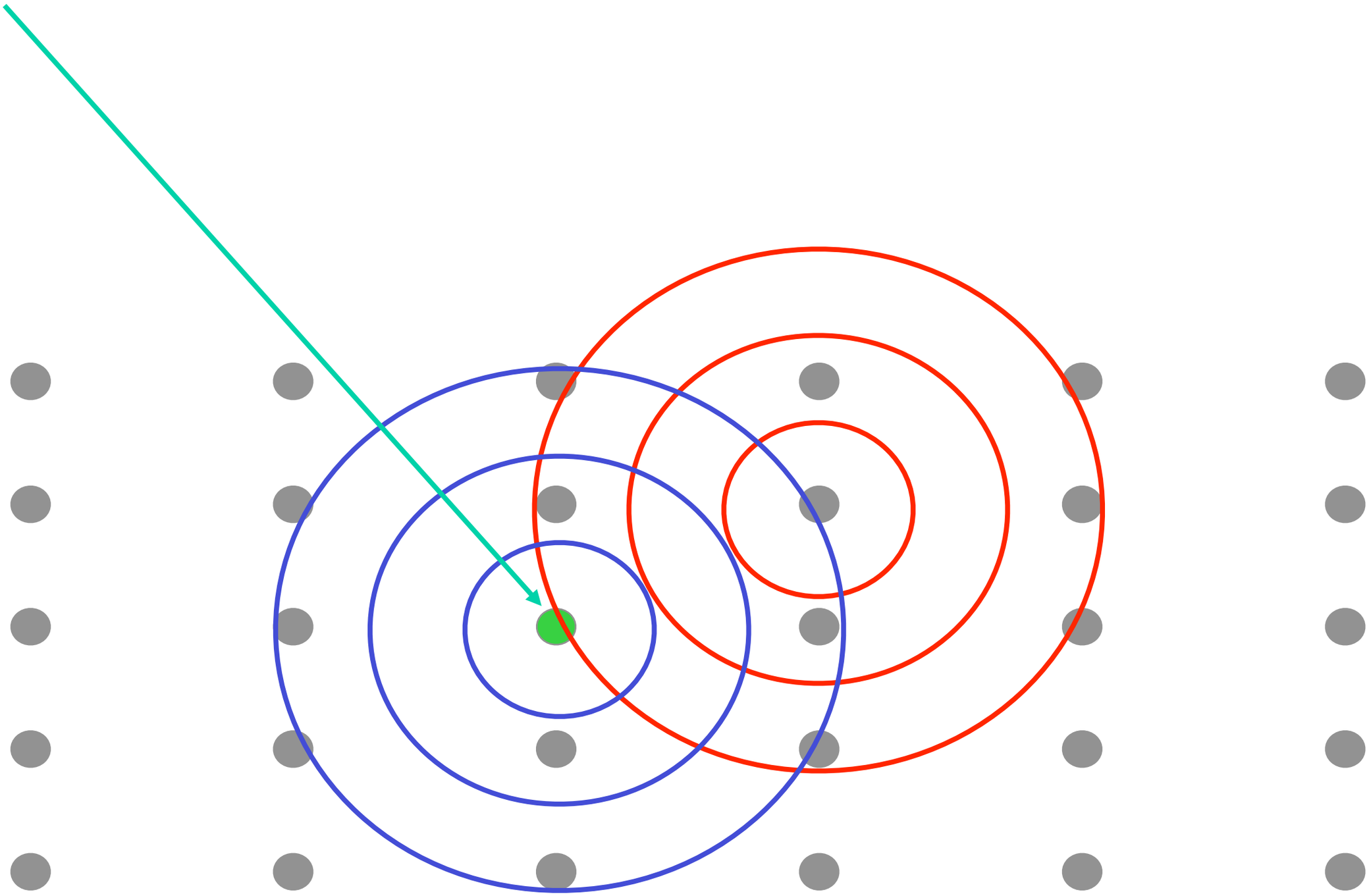

For a two atom system

$$\mu(\hbar\omega) = \frac{4\pi^2 e^2}{nm^2 c\omega} \sum_{if} |\hat{e} \cdot \langle f | \vec{p} | i \rangle|^2 \delta(E_f - E_i - \hbar\omega)$$

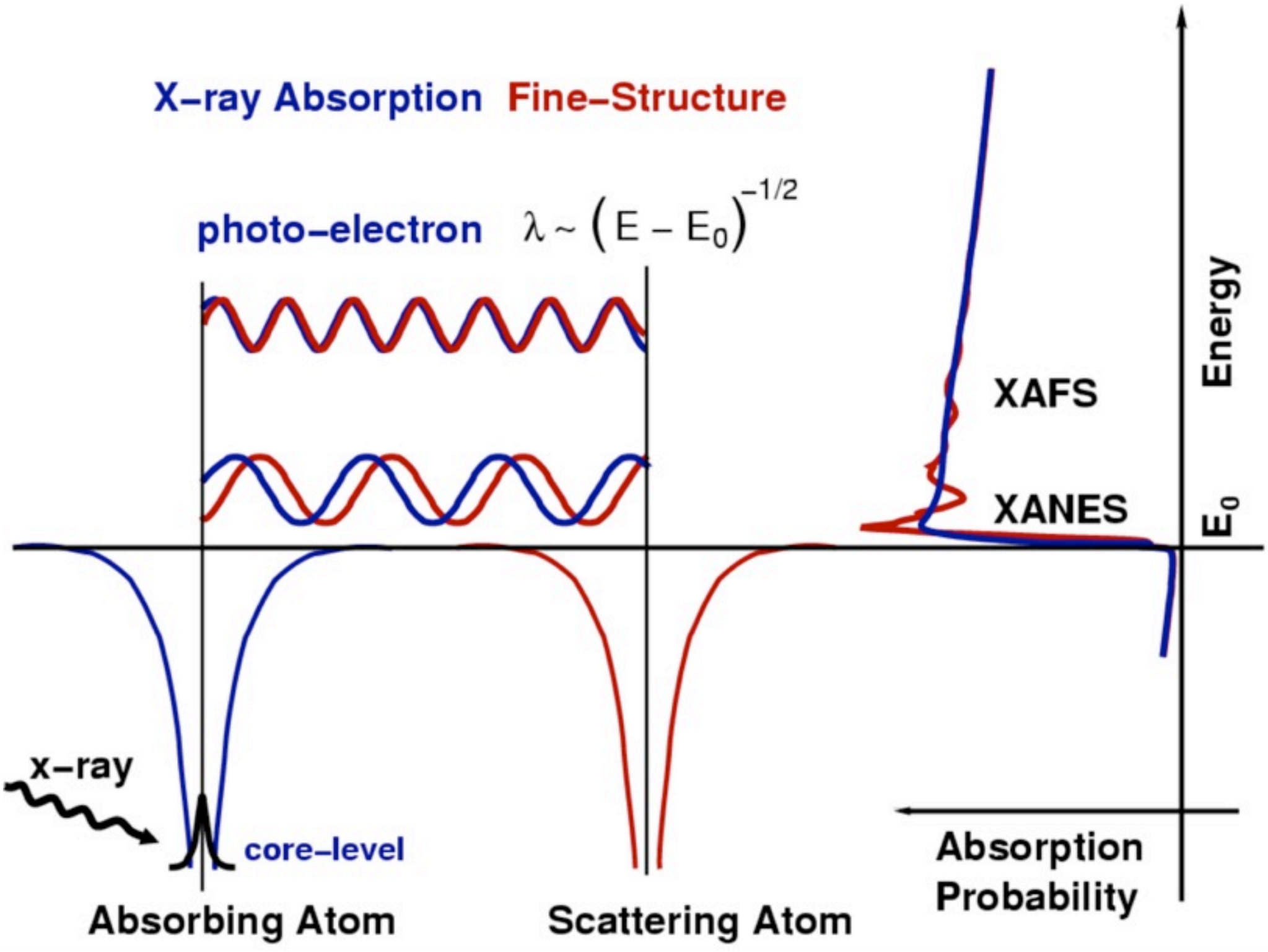

The EXAFS function

We define the function χ(k) as:

$$\chi(k) = \frac{\mu - \mu_0}{\mu_0}$$

in which, of course

$$k = \sqrt{\frac{2m}{\hbar^2}(\hbar\omega - E_b)}$$

and

$$\mu_0(\hbar\omega) \propto \left|\hat{e} \cdot \langle i| \vec{p} |f_0\rangle\right|^2$$

Multi-atom systems

$$\mu(\hbar\omega) = \frac{4\pi^2 e^2}{nm^2 c\omega} \sum_{if} \left| \hat{e} \cdot \langle f | \vec{p} | i \rangle \right|^2 \delta(E_f - E_i - \hbar\omega)$$

at high energy, the final wave function can be approximated by

$$|f\rangle \approx |f_0\rangle + |\delta f\rangle$$

in which |δf⟩ is the (small) perturbation to the single atom final state. So:

$$\mu(\hbar\omega) \propto \left| \hat{e} \cdot \left(\langle i | \vec{p} | f_0 \rangle + \langle i | \vec{p} | \delta f \rangle \right) \right|^2$$

Multi-atom systems

$$\mu(\hbar\omega) \propto \left|\hat{e}\cdot\left(\langle i|\vec{p}|f_0\rangle + \langle i|\vec{p}|\delta f\rangle\right)\right|^2$$

and by substituting and expanding:

$$\mu(\hbar\omega) \propto \left|\langle i|\hat{e}\cdot\vec{p}|f_0\rangle\right|^2\left[1+\langle i|\hat{e}\cdot\vec{p}|\delta f\rangle\frac{\langle f_0|\hat{e}\cdot\vec{p}|i\rangle^*}{\left|\langle i|\hat{e}\cdot\vec{p}|f_0\rangle\right|^2}+C.C.\right]$$

which means that

$$\chi(k) \propto \langle i|\hat{e}\cdot\vec{p}|\delta f\rangle$$

A two atom system

The electron photoemitted by atom A is back-scattered by atom B. For the potential we use the *muffin tin* approximation:

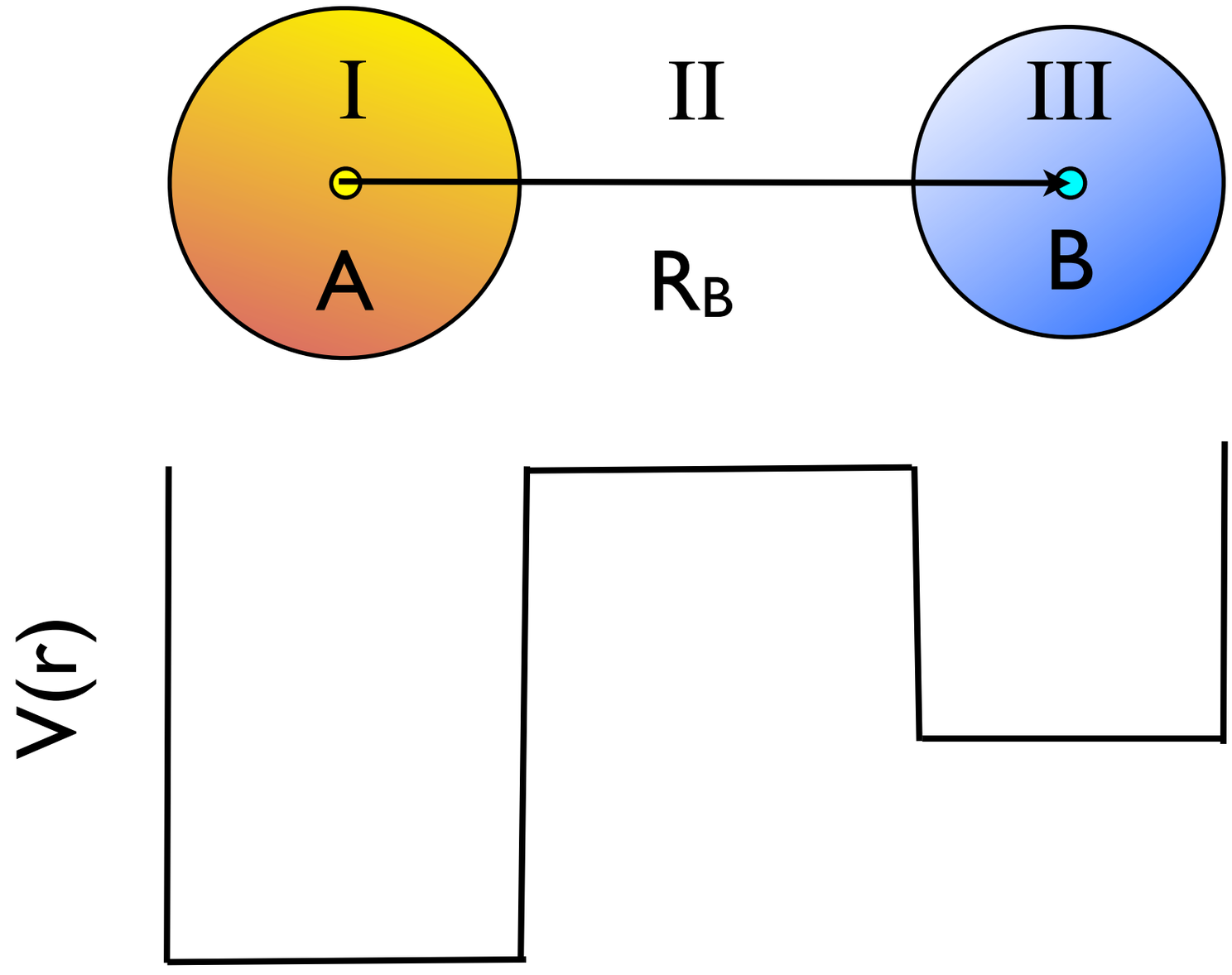

Two-atom systems

In region I, the *outgoing* wave is f_0.
In region II, the *outgoing* wave is modified into:

$$i\frac{e^{i(kr+\delta_1)}}{2kr}$$

in which δ_1 takes into account the matching of the waves.

At B we can assume the interaction occurs only with core electrons (if the energy is high enough) and therefore neglect the curvature. The amplitude of the back-scattered wave is:

$$f(k,\pi)=\frac{1}{k}\sum_{\ell=0}^{\infty}(-1)^{\ell}(2l+1)e^{i\delta_\ell}\sin\delta_\ell$$

Two-atom systems

f(k,π) is a particular case of:

$$f(k,\theta) = \frac{1}{k}\sum_{\ell=0}^{\infty}(2l+1)e^{i\delta_\ell}\sin\delta_\ell P_\ell(\cos\theta)$$

in which $P_\ell(\cos\theta)$ are Legendre polynomials

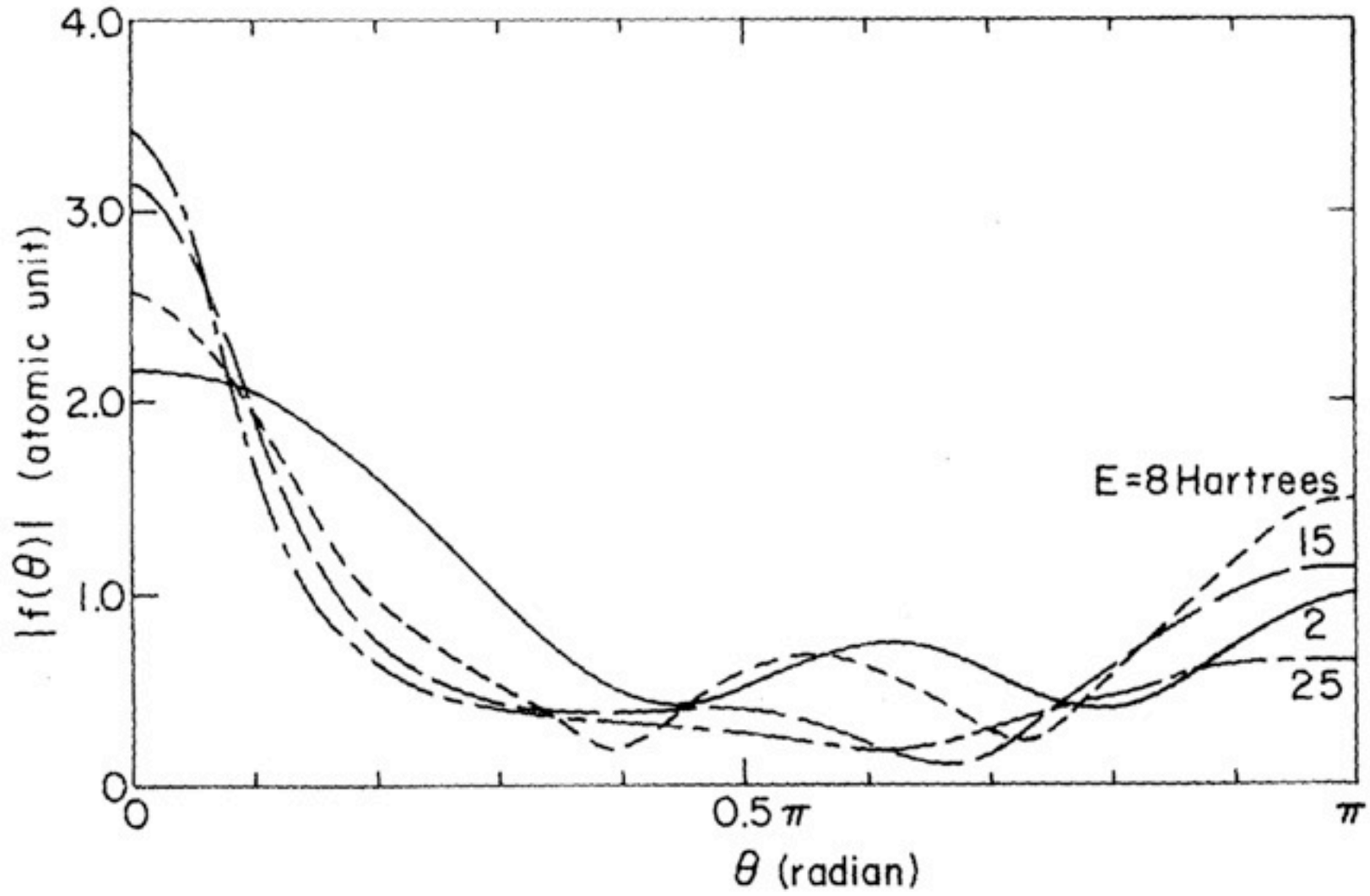

FIG. 5. Scattering amplitude $f(\theta)$ for energy $E=2, 8, 15, 25$ hartree (1 hartree = 27.2 eV).

Two-atom systems

phase shifts δ_l calculated for copper

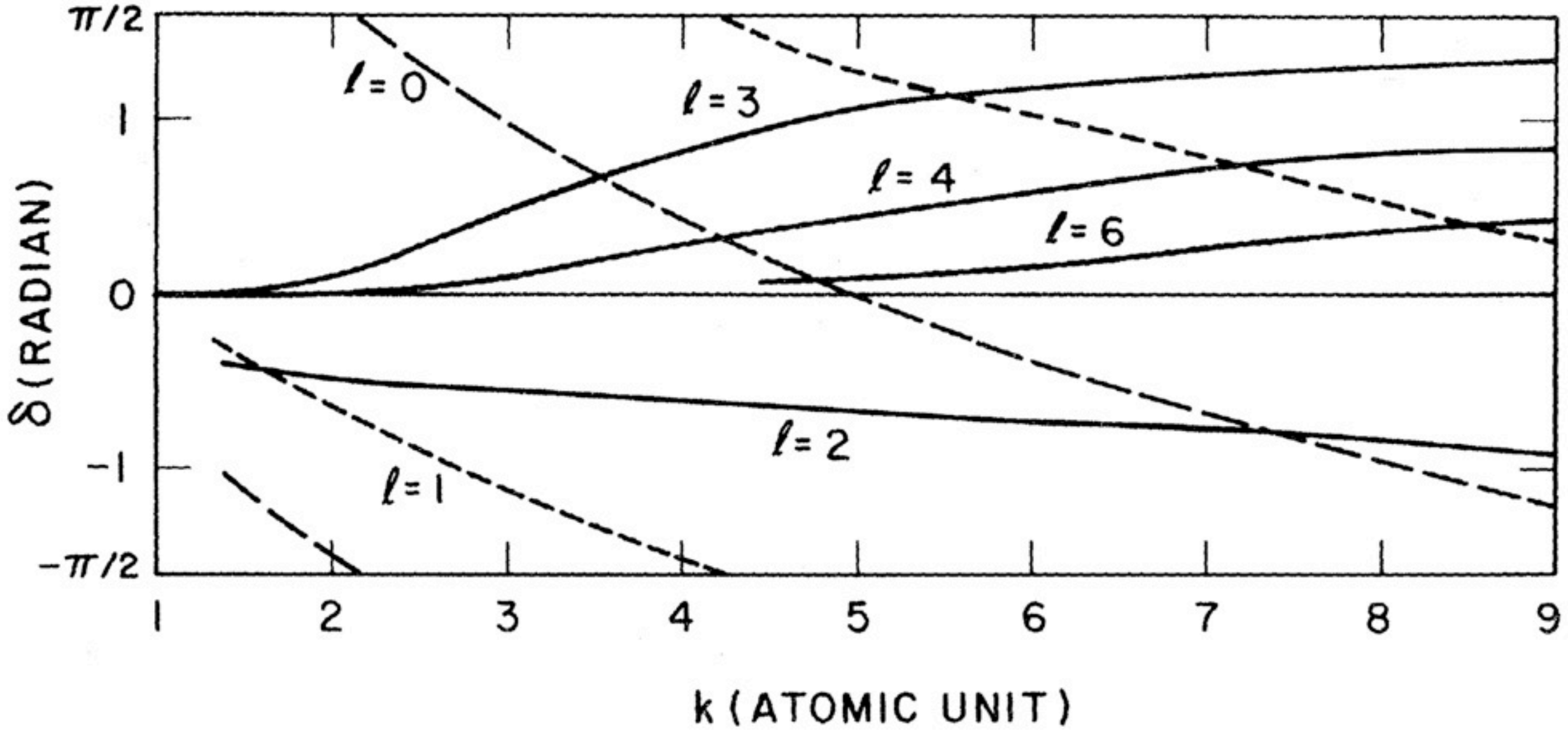

Two-atom systems

So, in region II, the *back-scattered* wave is:

$$i\frac{e^{i\left(kR_B+\delta_1\right)}}{2kR_B}f\left(k,\pi\right)i\frac{e^{i\left(kr'+\delta_1\right)}}{2r'}$$

and finally in region I for r´=R_B we get:

$$\delta\psi_f=\psi_f^0 if\left(k,\pi\right)i\frac{e^{2ikR_B}}{2kR_B^2}e^{2i\delta_1}$$

which inserted into the expression for χ gives:

$$\chi\left(k\right)=\frac{1}{kR_B^2}\mathrm{Im}\left\{f_B\left(k,\pi\right)e^{2i\left(kR_B+\delta_1\right)}\right\}$$

Two-atom systems

By separating modulus and phase of the complex back-scattering amplitude:

$$f_B(k,\pi)e^{2ik\delta_1} = \left|f_B(k,\pi)\right|e^{2i\phi}$$

we get:

$$\chi(k) = \frac{1}{kR_B^2}\left|f_B(k,\pi)\right|\sin\left[2kR_B + \phi(k)\right]$$

Extension to many-atom systems

By summing the contributions from all atoms surrounding atom A:

$$\chi(k) = \frac{1}{k}\sum_j \frac{1}{R_j^2}\,\mathrm{Im}\left\{ f_j(k,\pi)\, e^{2i(kR_j+\delta_1)} \right\}$$

Inelastic effects

Inelastic effects

- Intrinsic inelastic effects

Inelastic effects

- Intrinsic inelastic effects

  occur **at** the absorbing atoms (failing of the "frozen level" approximation) and reduce the coherent EXAFS signal by a factor 0.7 to 1.0

Inelastic effects

- Intrinsic inelastic effects

  occur **at** the absorbing atoms (failing of the "frozen level" approximation) and reduce the coherent EXAFS signal by a factor 0.7 to 1.0

- Extrinsic inelastic effects

Inelastic effects

- Intrinsic inelastic effects

  occur **at** the absorbing atoms (failing of the "frozen level" approximation) and reduce the coherent EXAFS signal by a factor 0.7 to 1.0

- Extrinsic inelastic effects

  occur **during** the path between absorber and scatterers (mean free path)

Inelastic effects

- Intrinsic inelastic effects

  occur **at** the absorbing atoms (failing of the "frozen level" approximation) and reduce the coherent EXAFS signal by a factor 0.7 to 1.0

- Extrinsic inelastic effects

  occur **during** the path between absorber and scatterers (mean free path)

$$\chi(k) = \frac{S_0^2}{k} \sum_j \frac{e^{\frac{-2R_j}{\lambda}}}{R_j^2} \mathrm{Im}\left\{ f_j(k,\pi) e^{2i(kR_j + \delta_1)} \right\}$$

Electron mean free path

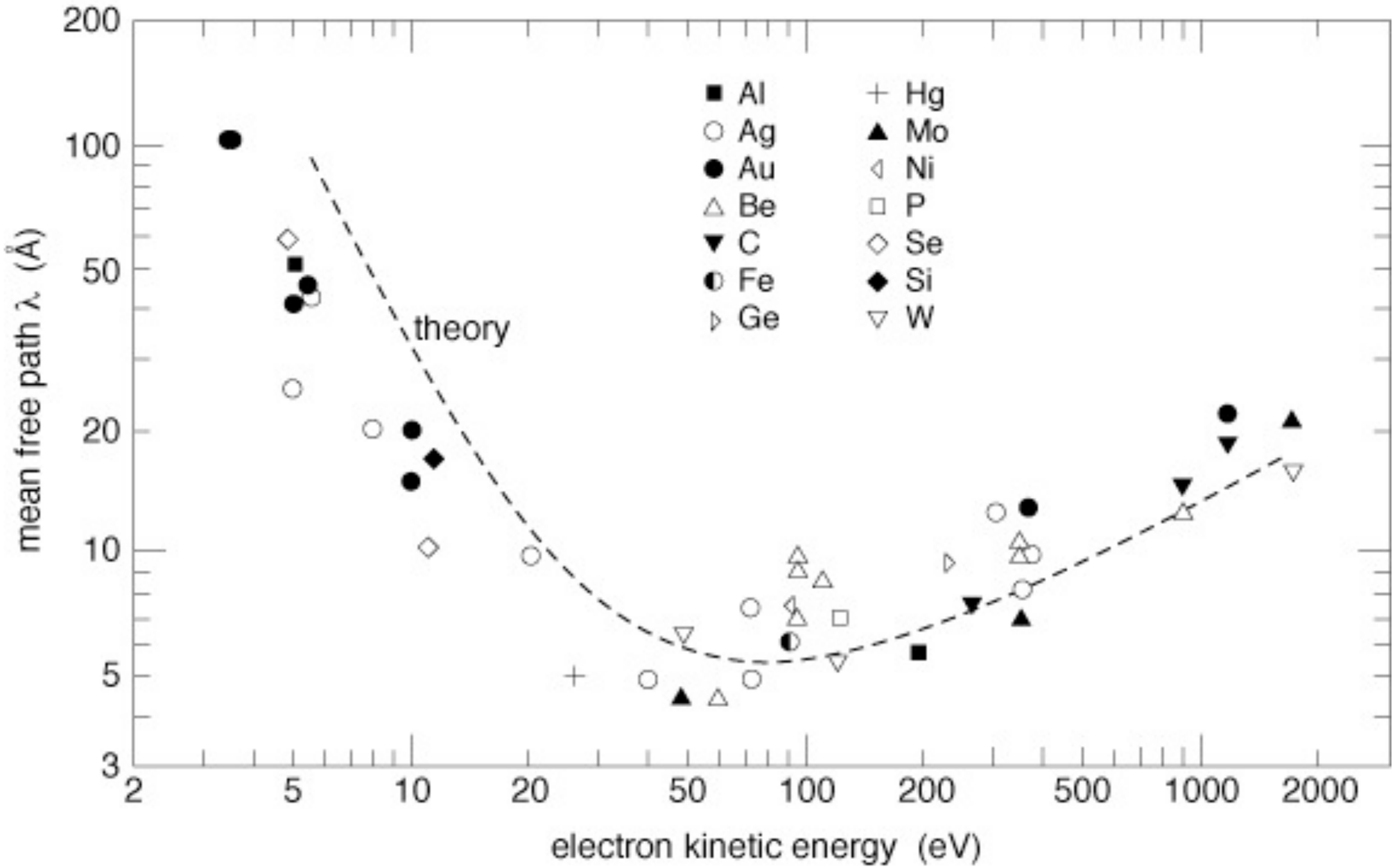

Coordination shells

A real system will have neighboring atoms at different distances and of different types. We can add all these contributions to get a slightly different version of the EXAFS equation:

$$\chi(k) = \frac{S_0^2}{k} \sum_s N_s \frac{e^{\frac{-2R_s}{\lambda}}}{R_s^2} \mathrm{Im}\left\{ f_s(k,\pi) e^{2i(kR_s + \delta_1)} \right\}$$

Disorder

We can identify three sources of disorder:

- thermal disorder
- structural disorder
- compositional disorder

We can take disorder into account by introducing a distribution function ρ(x) so that the EXAFS equation *for one shell* becomes:

$$\chi_s(k) = \frac{S_0^2}{k} N_s \,\mathrm{Im}\left\{ f_s(k,\pi) e^{2i\delta_1} \int_0^\infty \rho(r) e^{\frac{-2r}{\lambda}} \frac{e^{2ikr}}{r^2} dr \right\}$$

If we can assume that disorder has a harmonic behaviour we can write the so-called EXAFS standard formula:

$$\chi(k) = \frac{S_0^2}{k} \sum_s N_s \left| f_s(k,\pi) \right| \frac{e^{-2R_s/\lambda(k)} e^{-2k^2\sigma_s^2}}{R_s^2} \sin\left[2kR_s + \phi(k)\right]$$

One of the first EXAFS measurements (Sayers, Stern and Lytle) showing the effect of disorder in Ge

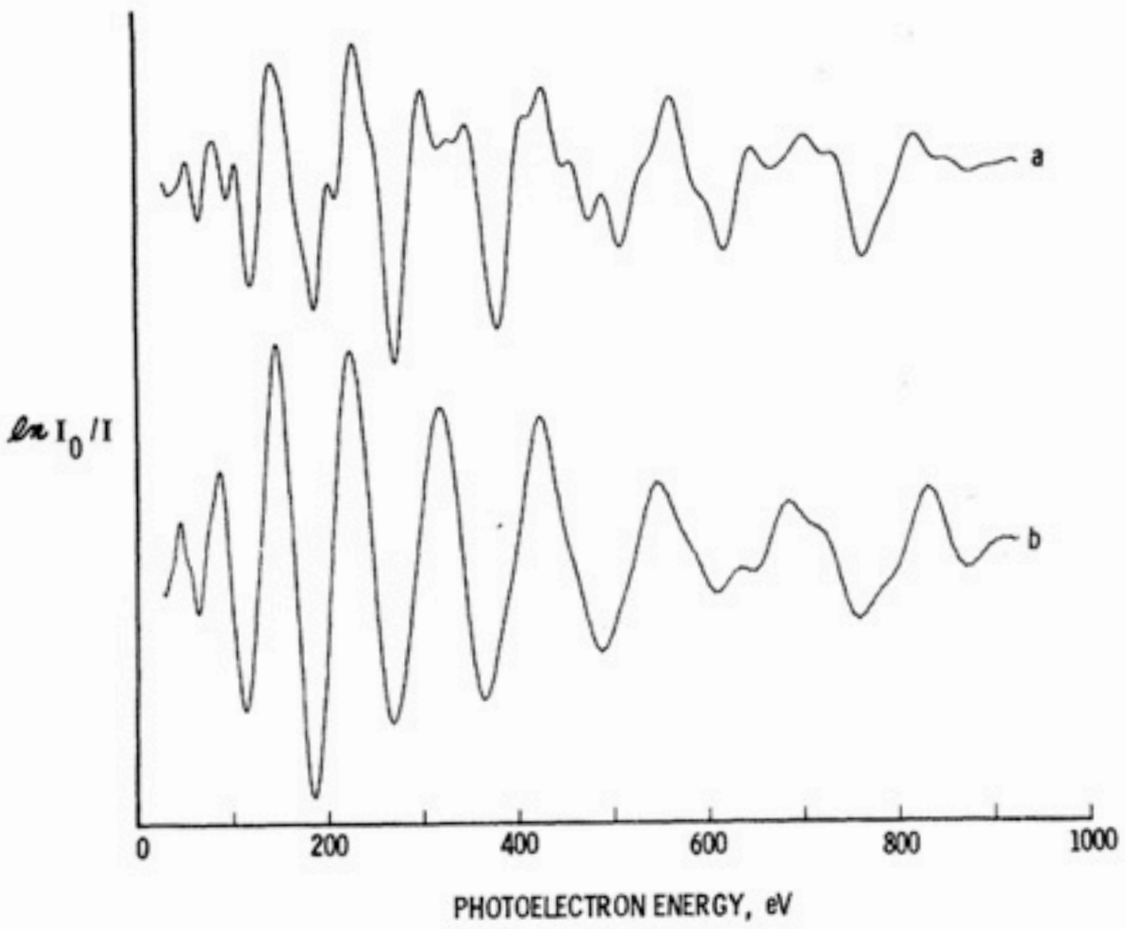

FIG. 1. Smoothed experimental EXAFS data for (a) crystalline and (b) amorphous Ge. Only the oscillatory part χ of the absorption edge is shown.

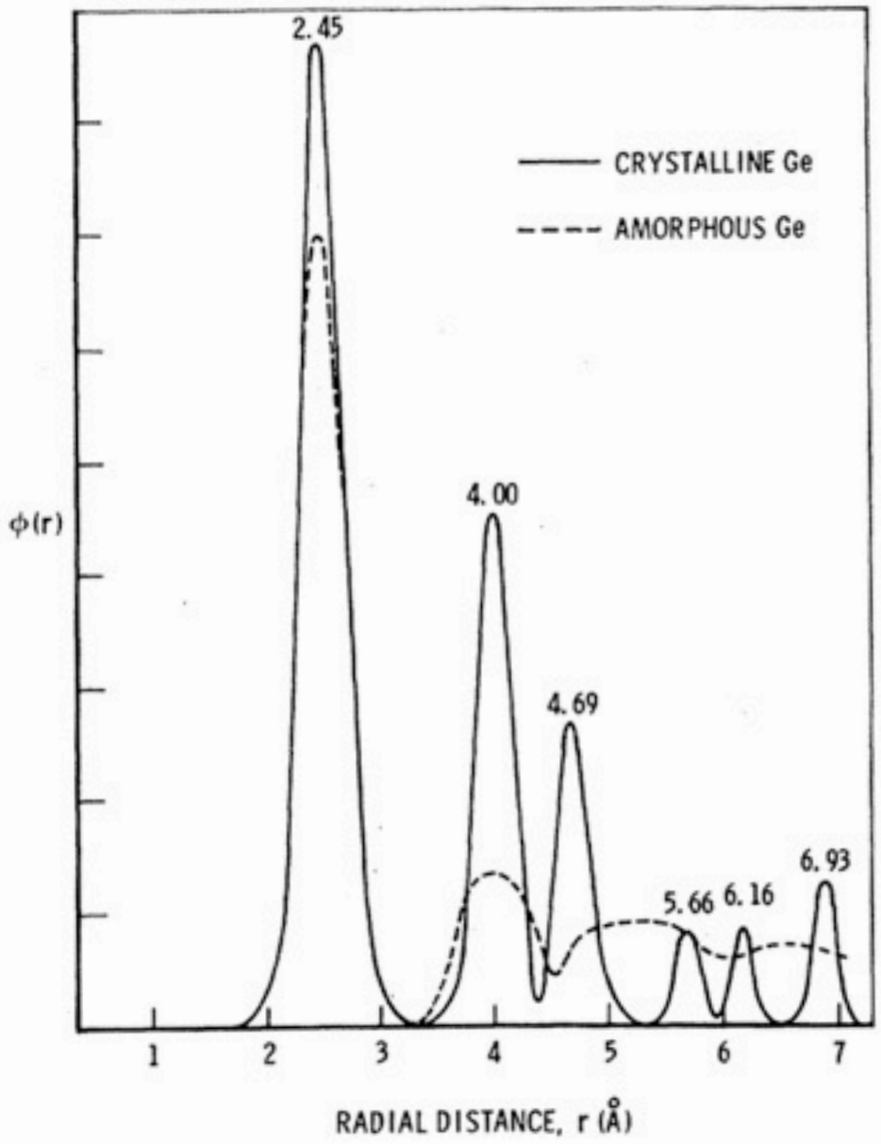

FIG. 2. Fourier transformation of the data of Fig. 1. $\varphi(r)$, a radial structure function, compares amorphous and crystalline Ge. Numbers over the peaks indicate the measured distances in Å.

Scattering amplitude and phase shift depend on the atomic number

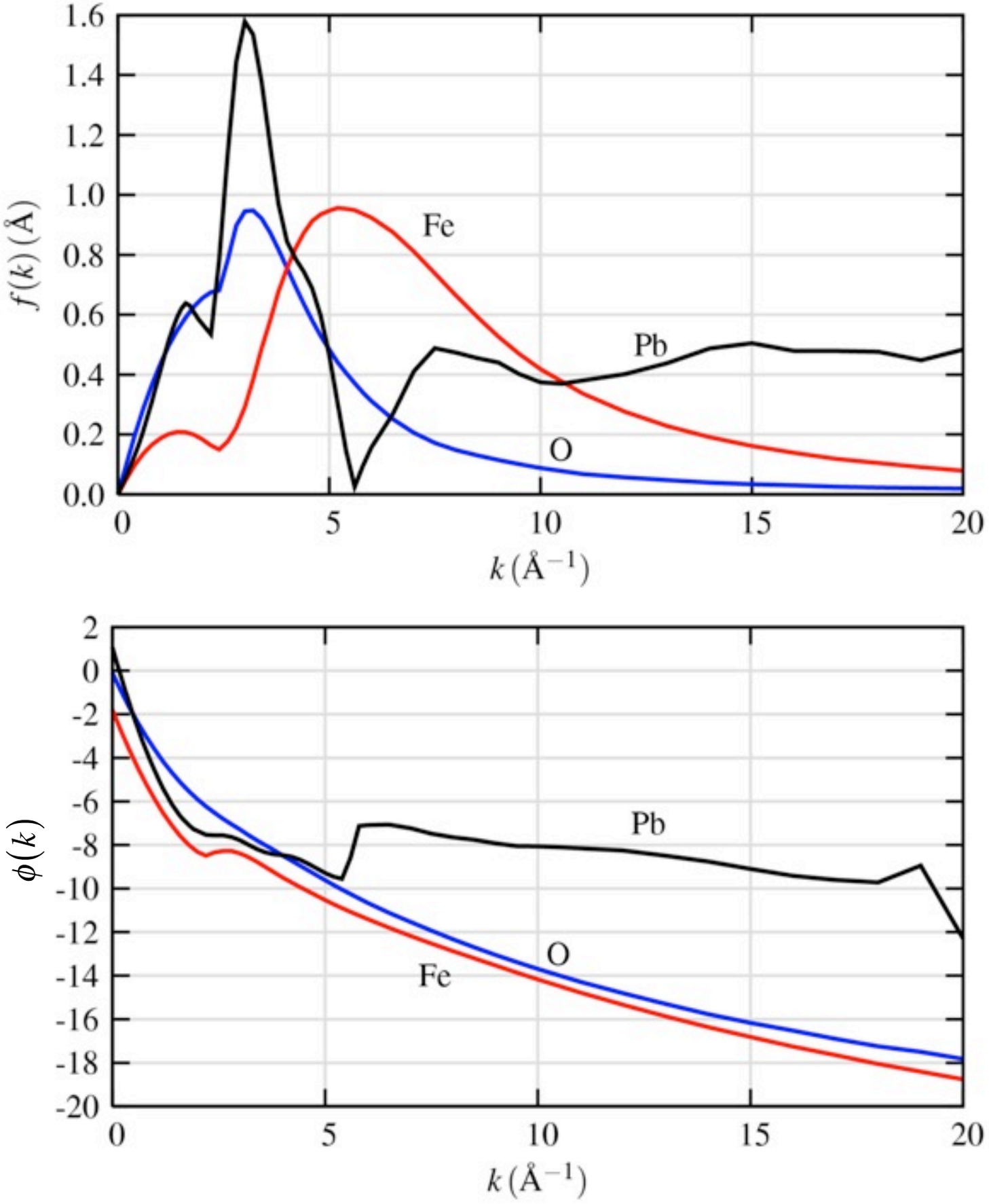

The scattering amplitude f(k) peaks at different k values and extends to higher-k for heavier elements. For very heavy elements, there are structures in f(k), associated with core level excitations, as the structures in ϕ(k)

EXAFS measurement scheme

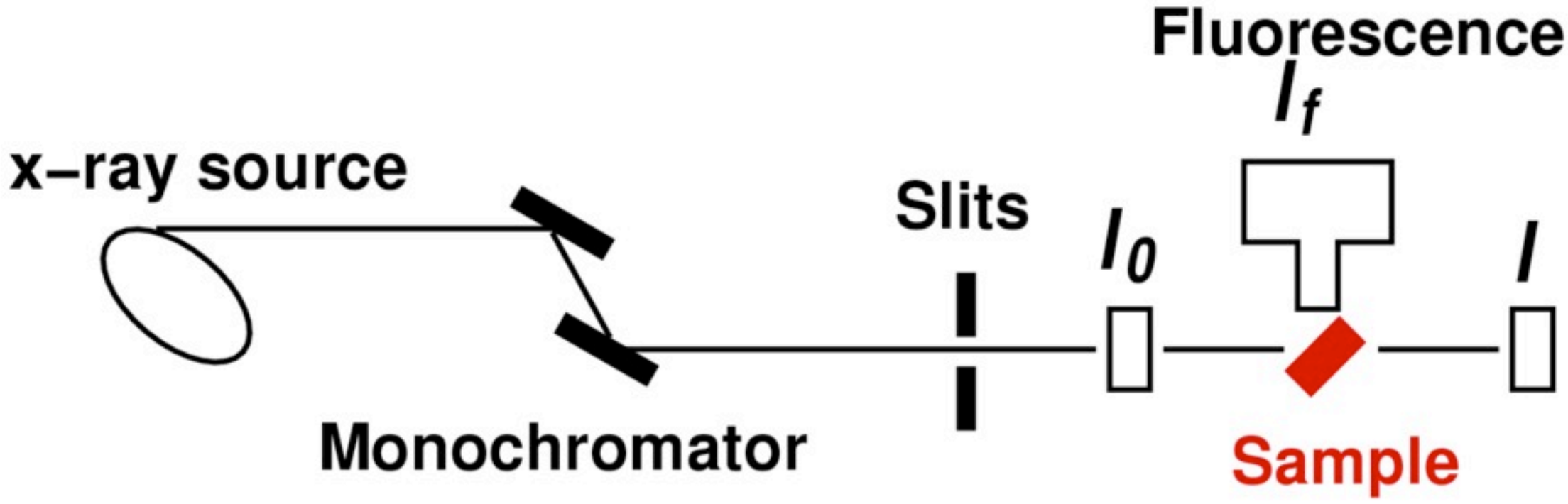

We want to measure the energy dependence of the x-ray absorption coefficient μ(E). It can be measured:

- Directly by measuring I and I_0:

$$\mu(E) = -\frac{1}{d}\ln\left[\frac{I}{I_0}\right]$$

- By measuring the signal from a recombination process of the core-hole, i.e. by measuring the fluorescence yield or the Auger yield. In this case:

$$\mu(E) \propto \frac{I_f}{I_0}$$

Core-hole recombination

Core-hole recombination

Fluorescence

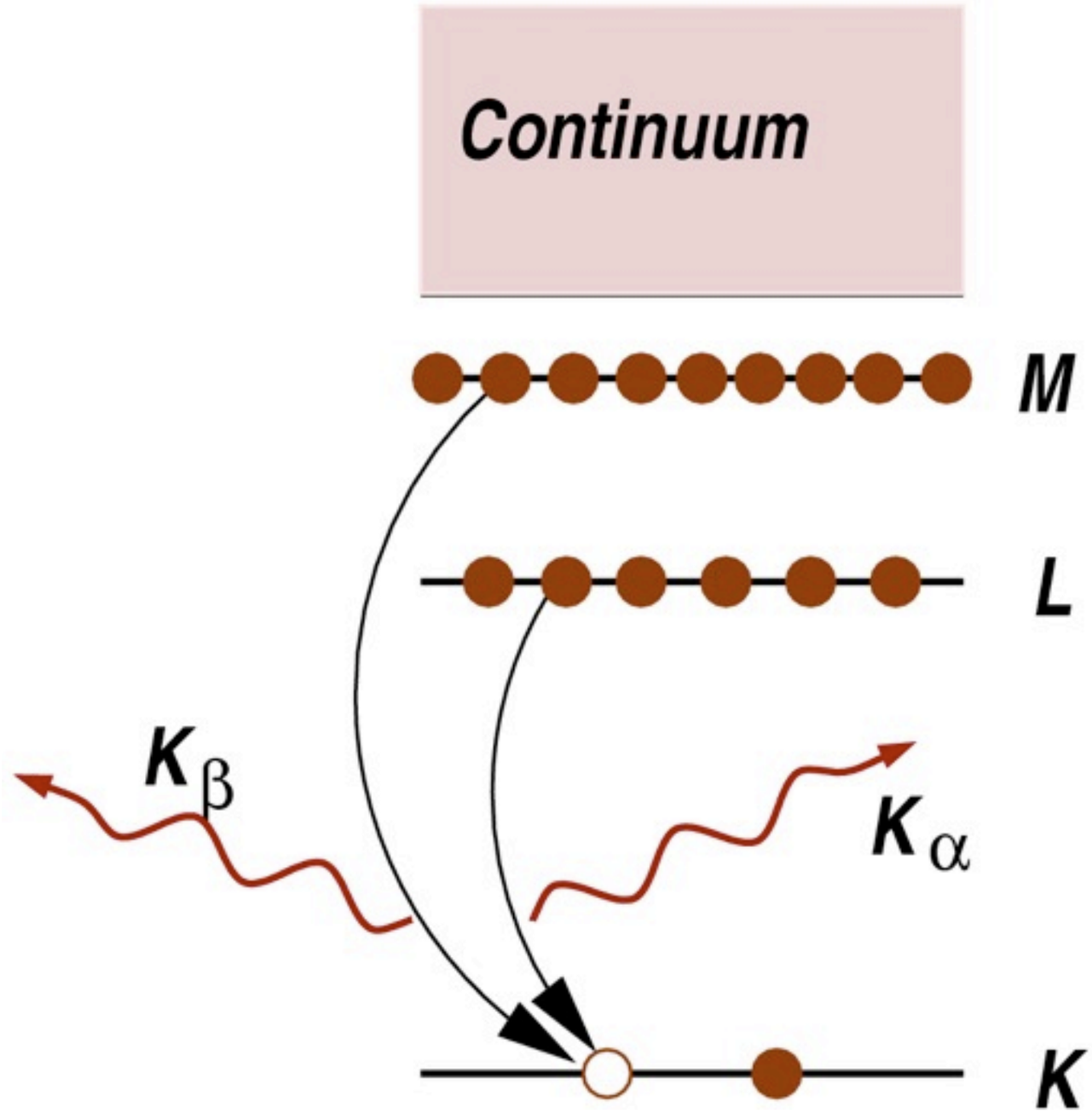

Core-hole recombination

Fluorescence

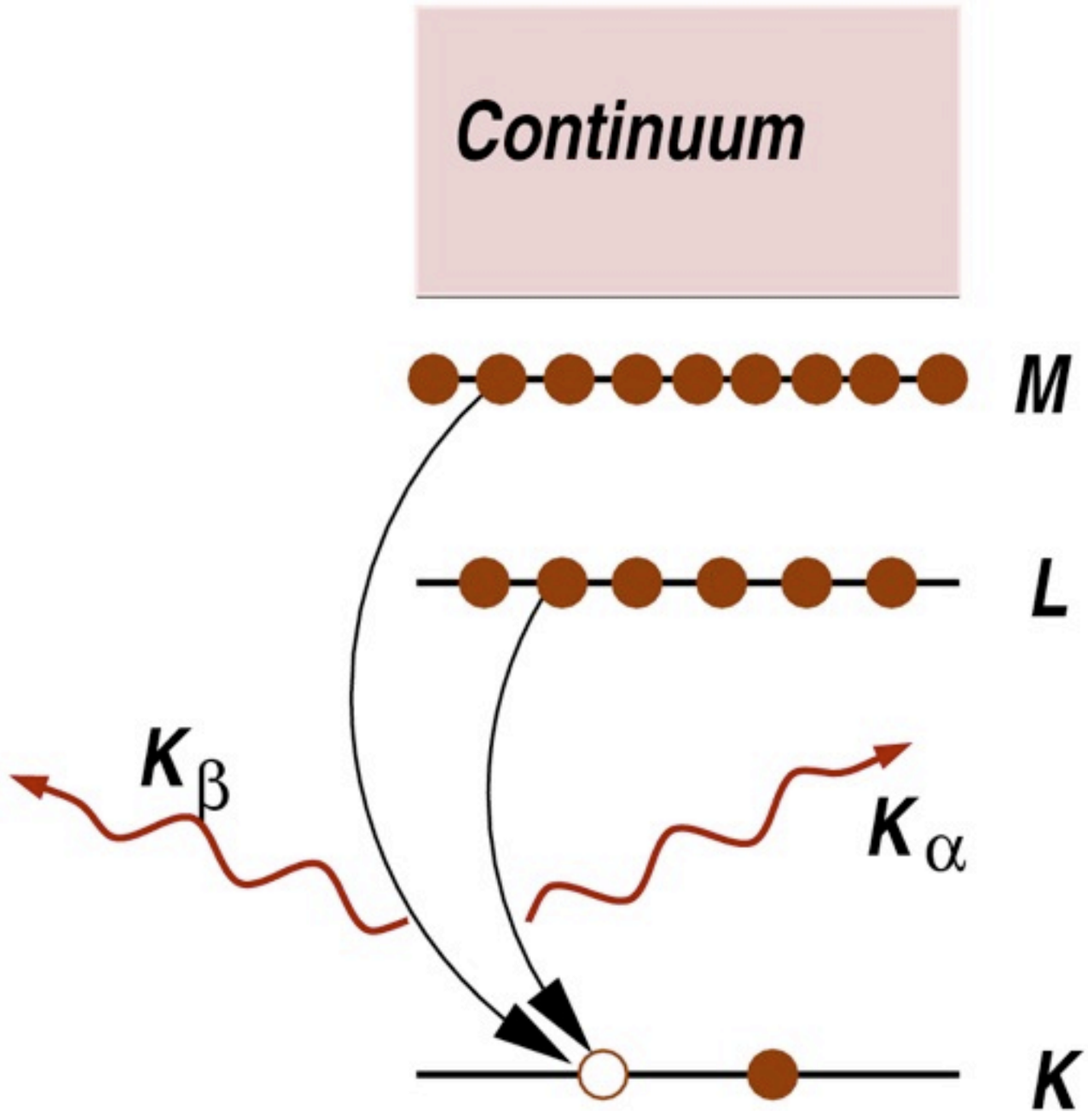

Auger

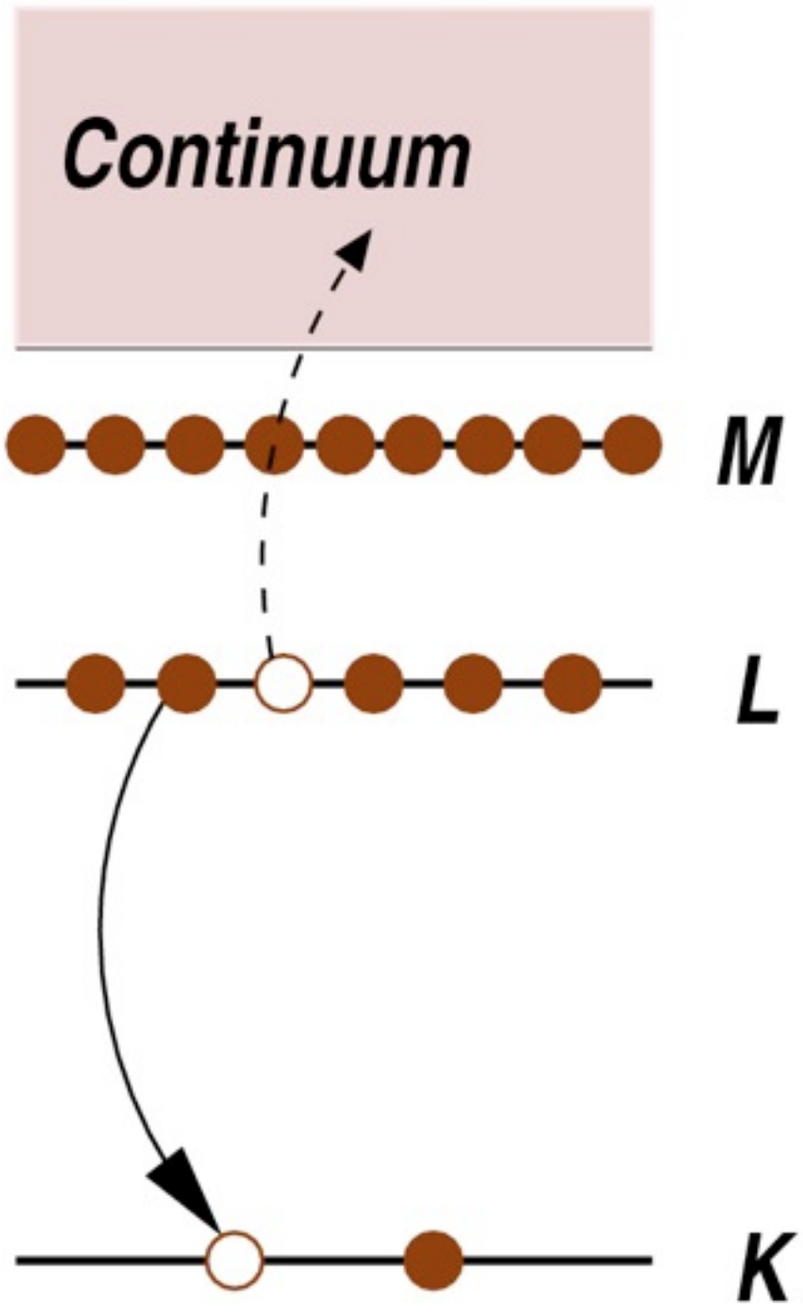

X-Ray Absorption Spectroscopy

Transmission

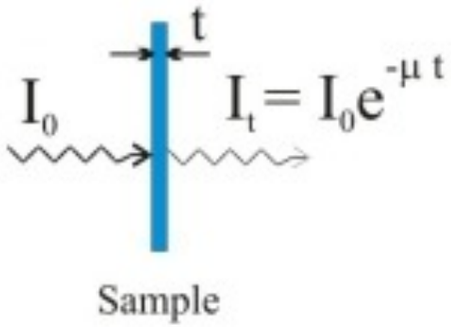

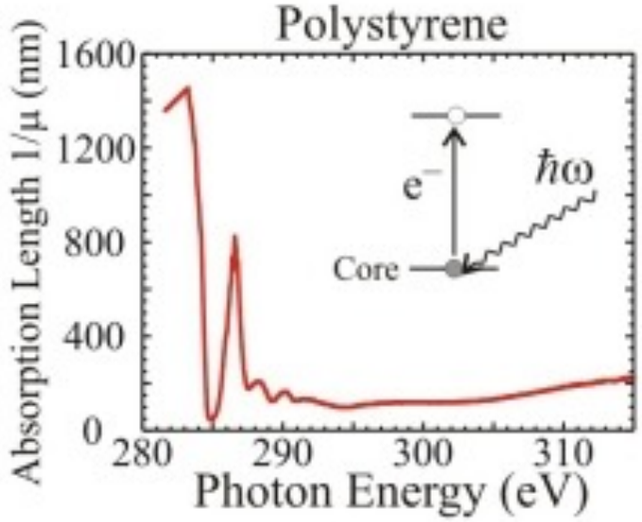

Electron Yield

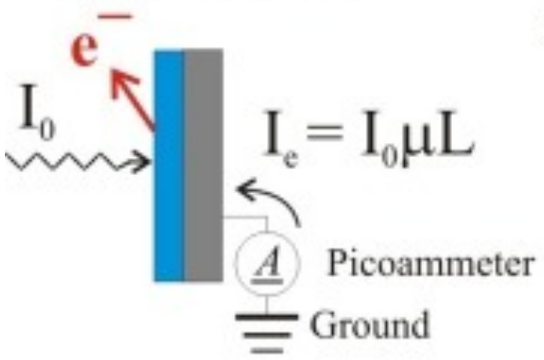

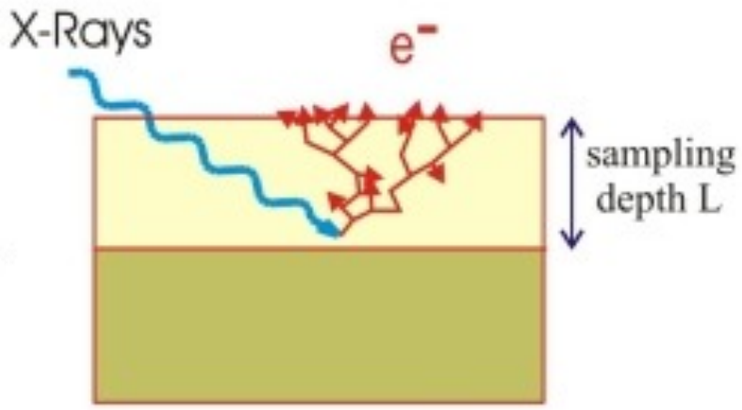

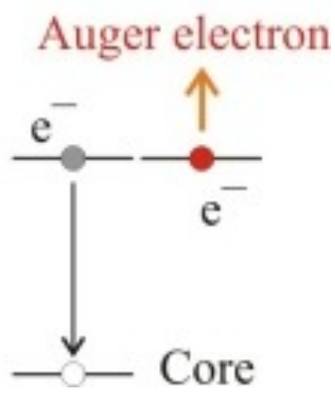

We want to measure the energy dependence of the x-ray absorption coefficient μ(E). It can be measured:

- Directly by measuring I and I_0:

$$\mu(E) = -\frac{1}{d}\ln\left[\frac{I}{I_0}\right]$$

- By measuring the signal from a recombination process of the core-hole, i.e. by measuring the fluorescence yield or the Auger yield. In this case:

$$\mu(E) \propto \frac{I_f}{I_0}$$

EXAFS data analysis

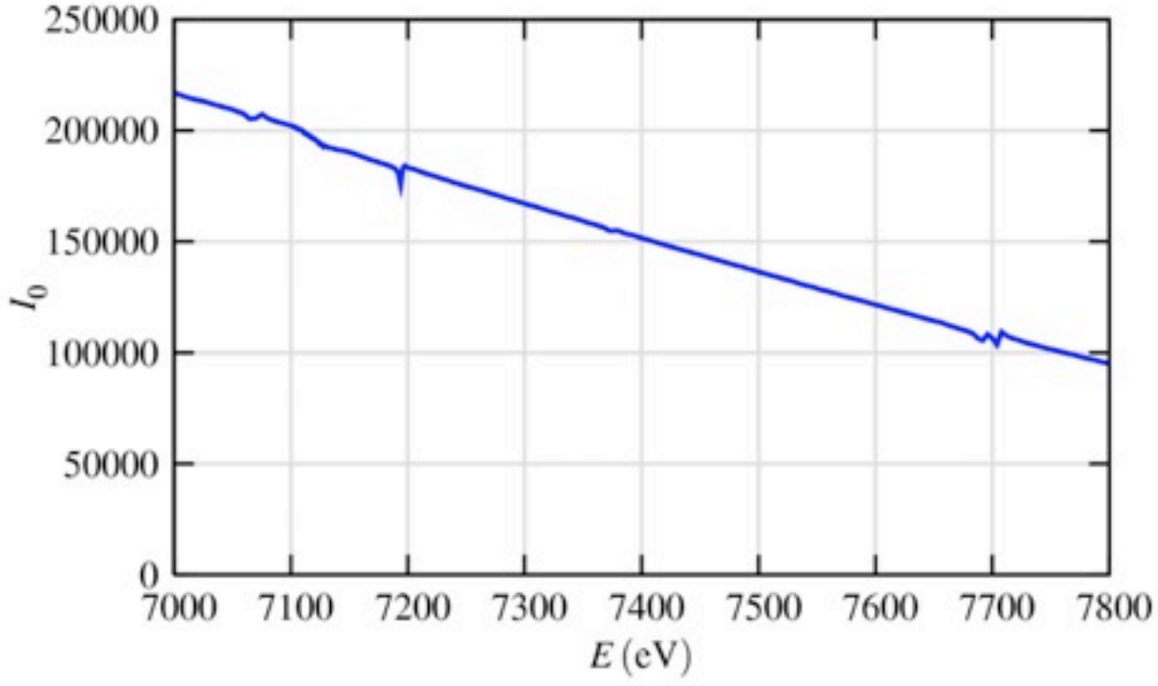

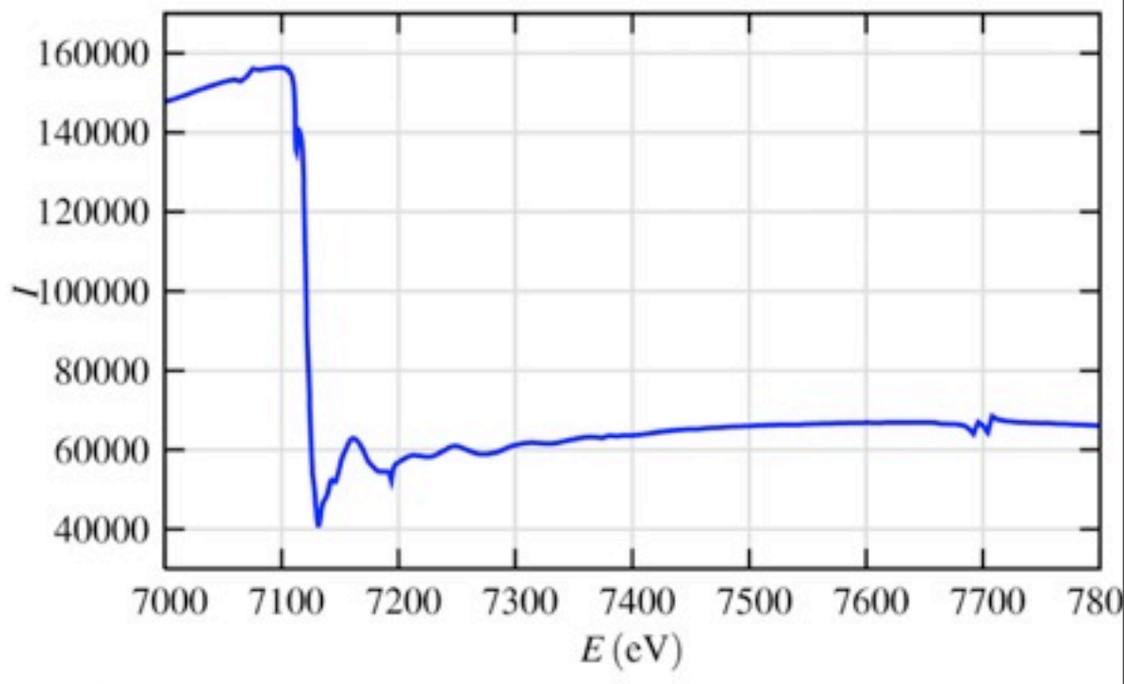

For Transmission XAFS

$$\mu(E) = -\frac{1}{d}\ln\left[\frac{I}{I_0}\right]$$

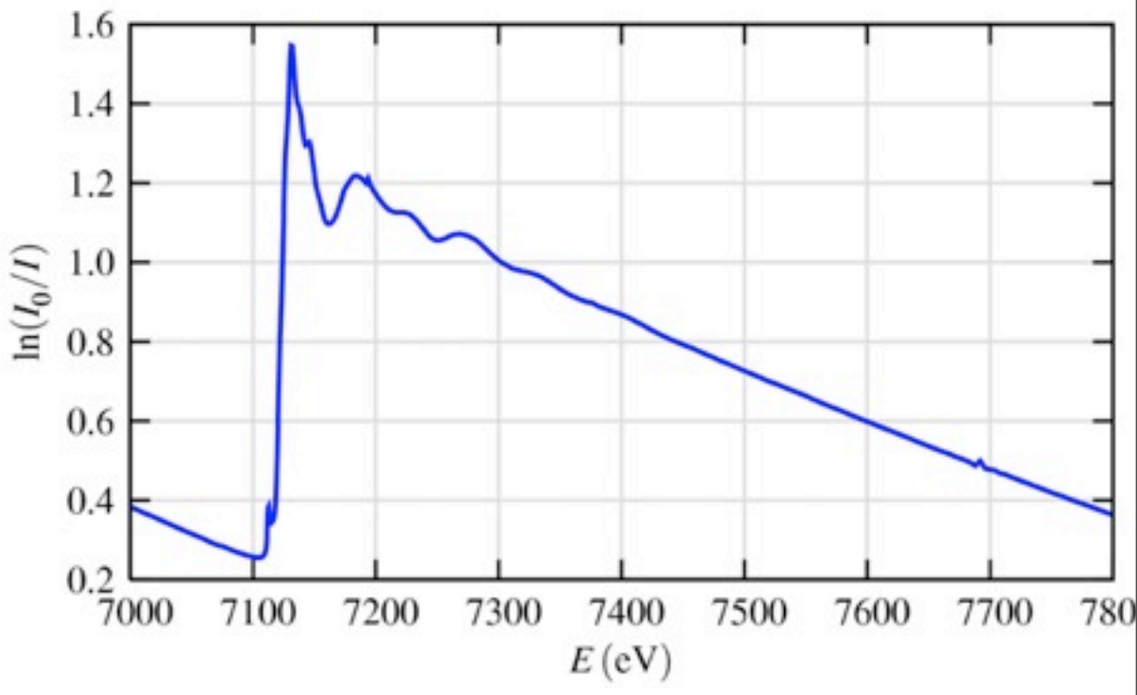

EXAFS data analysis

Pre-Edge Subtraction
We subtract away the background that fits the pre-edge region. This gets rid of the absorption due to other edges (say, the Fe L_{III} edge).

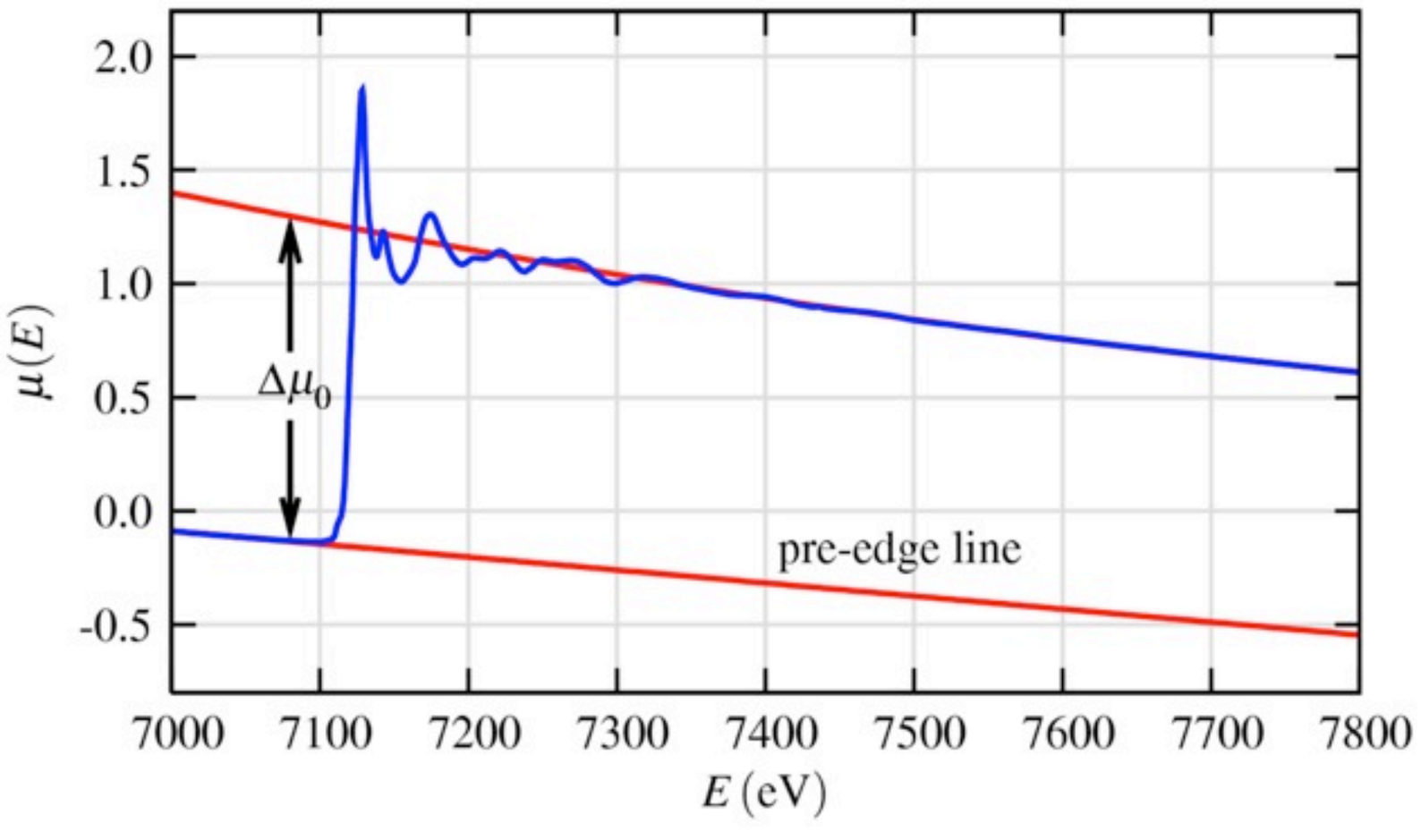

Normalization
We estimate the *edge step*, $\Delta\mu_0$ (E0) by extrapolating a simple fit to the above μ(E) to the edge. We normalize by this value to get the absorption from 1 x-ray.

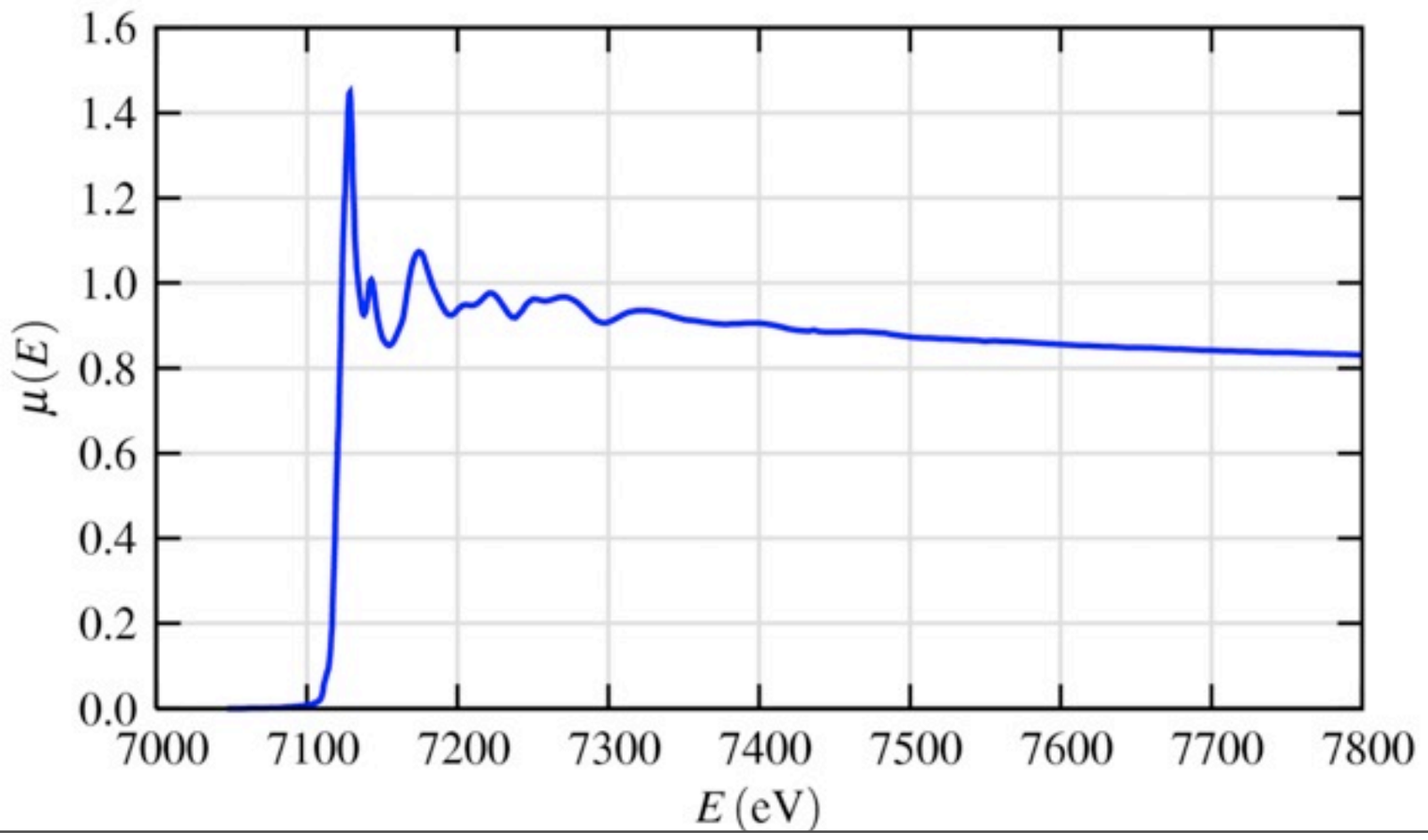

EXAFS data analysis

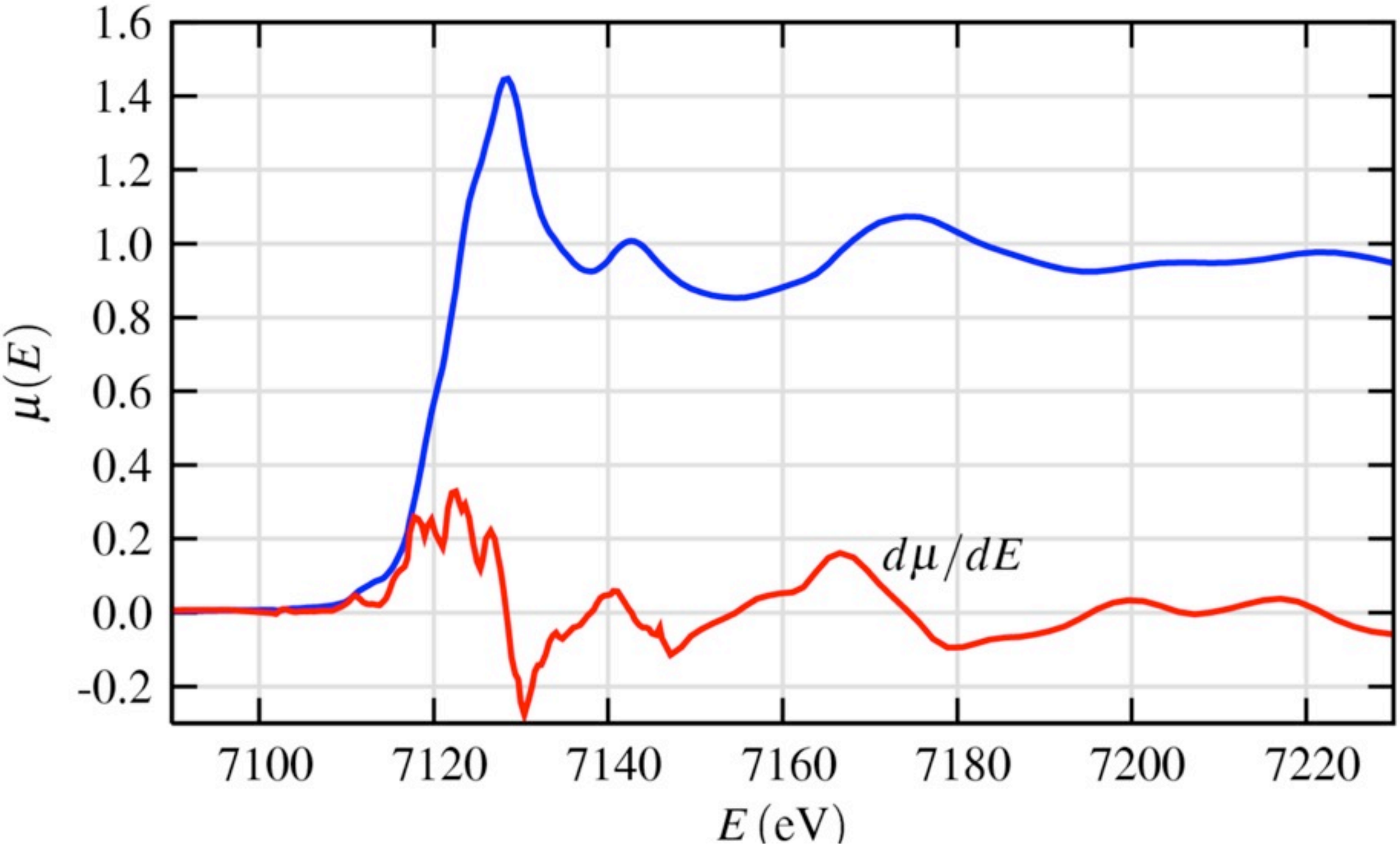

EXAFS data analysis

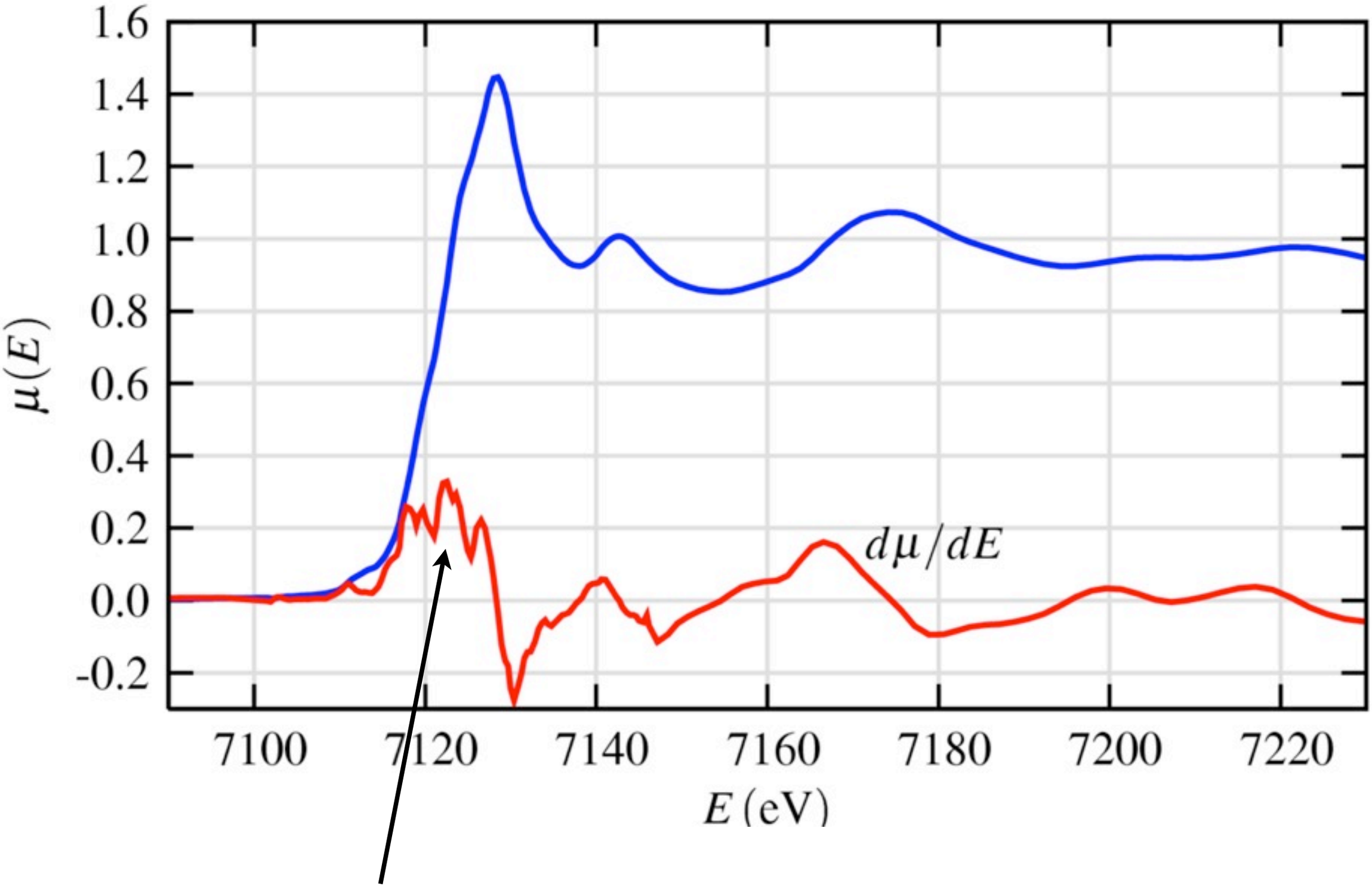

We set E_0 at the maximum slope of μ(E)

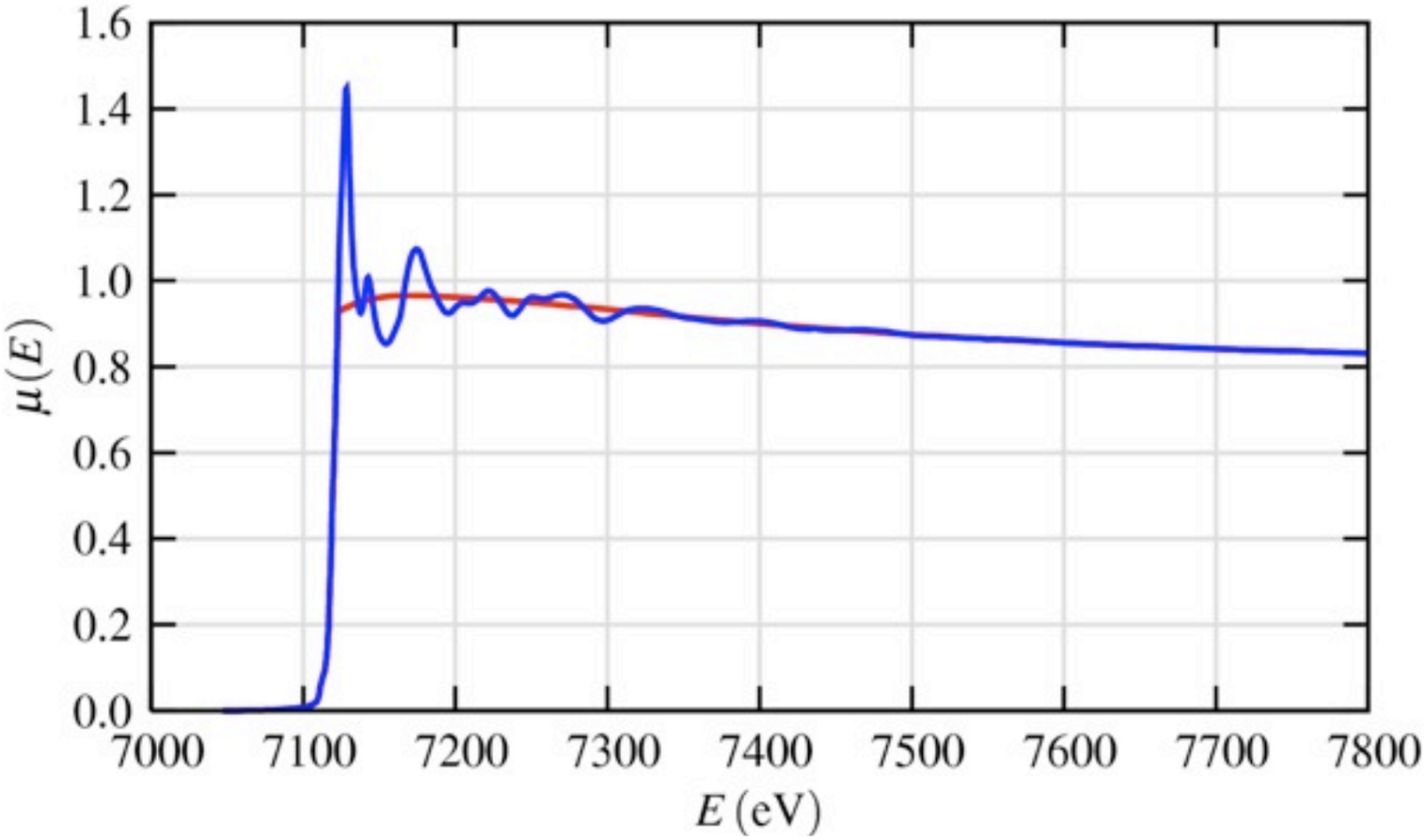

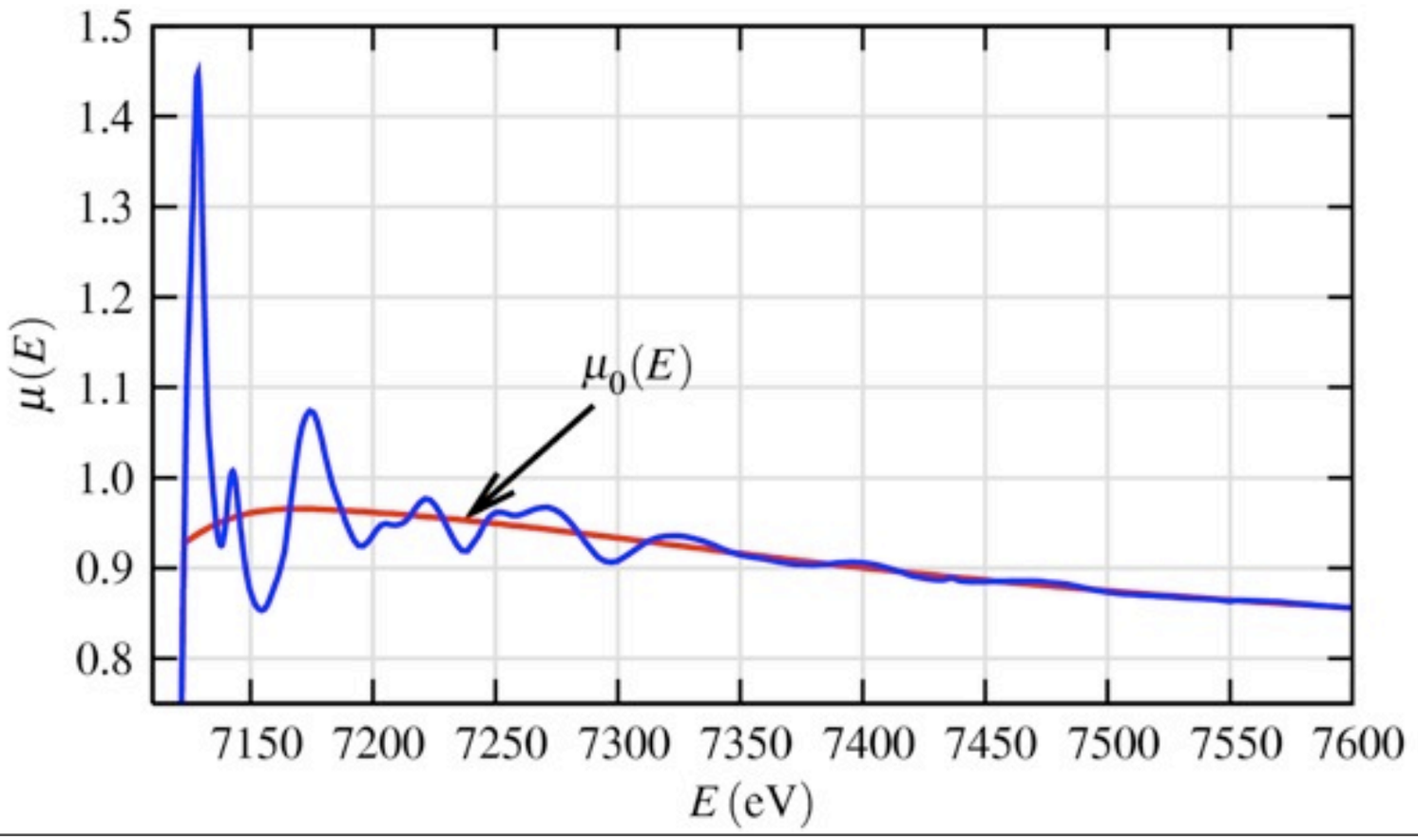

Background (μ_0...) removal

Extraction of χ(k)

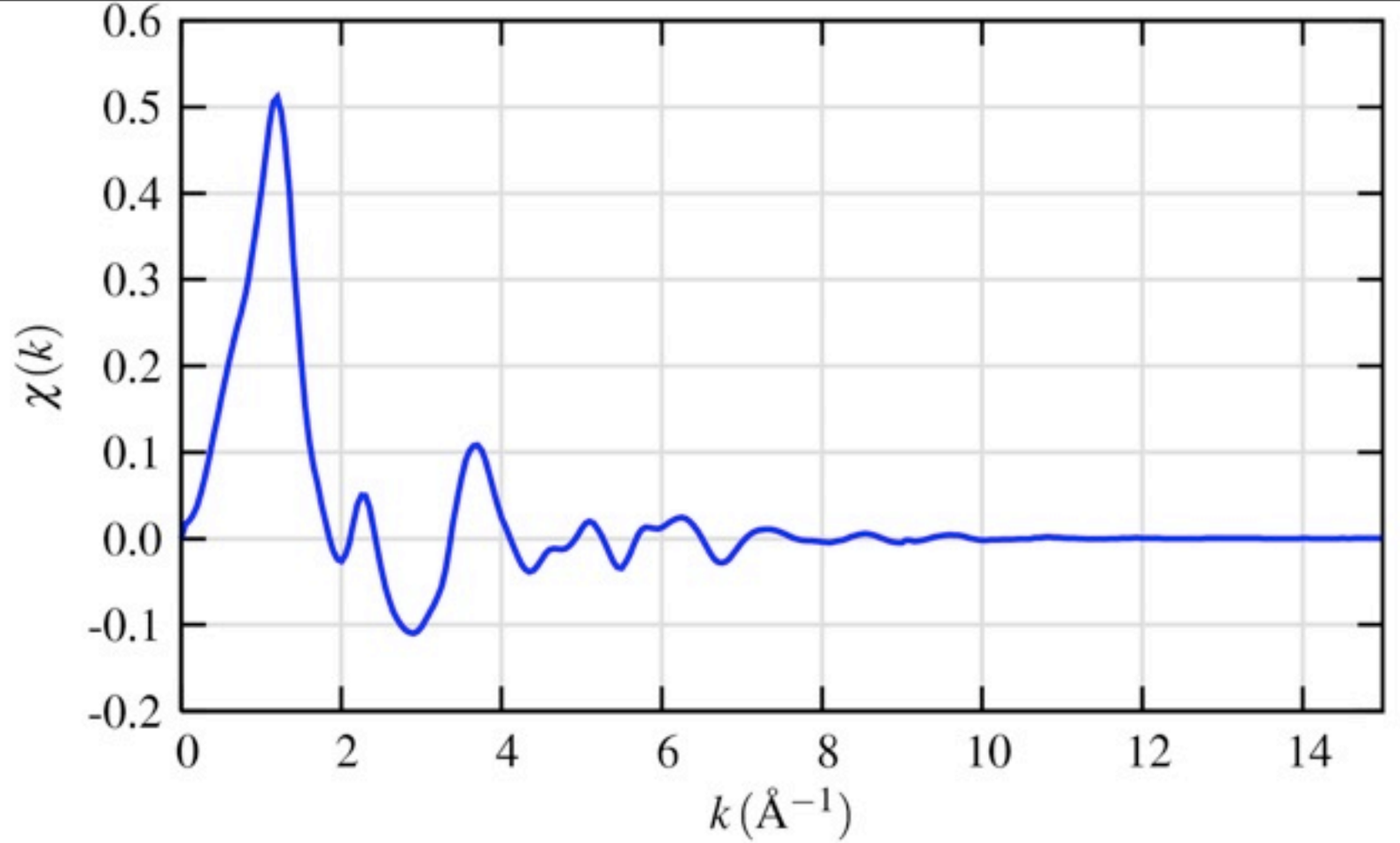

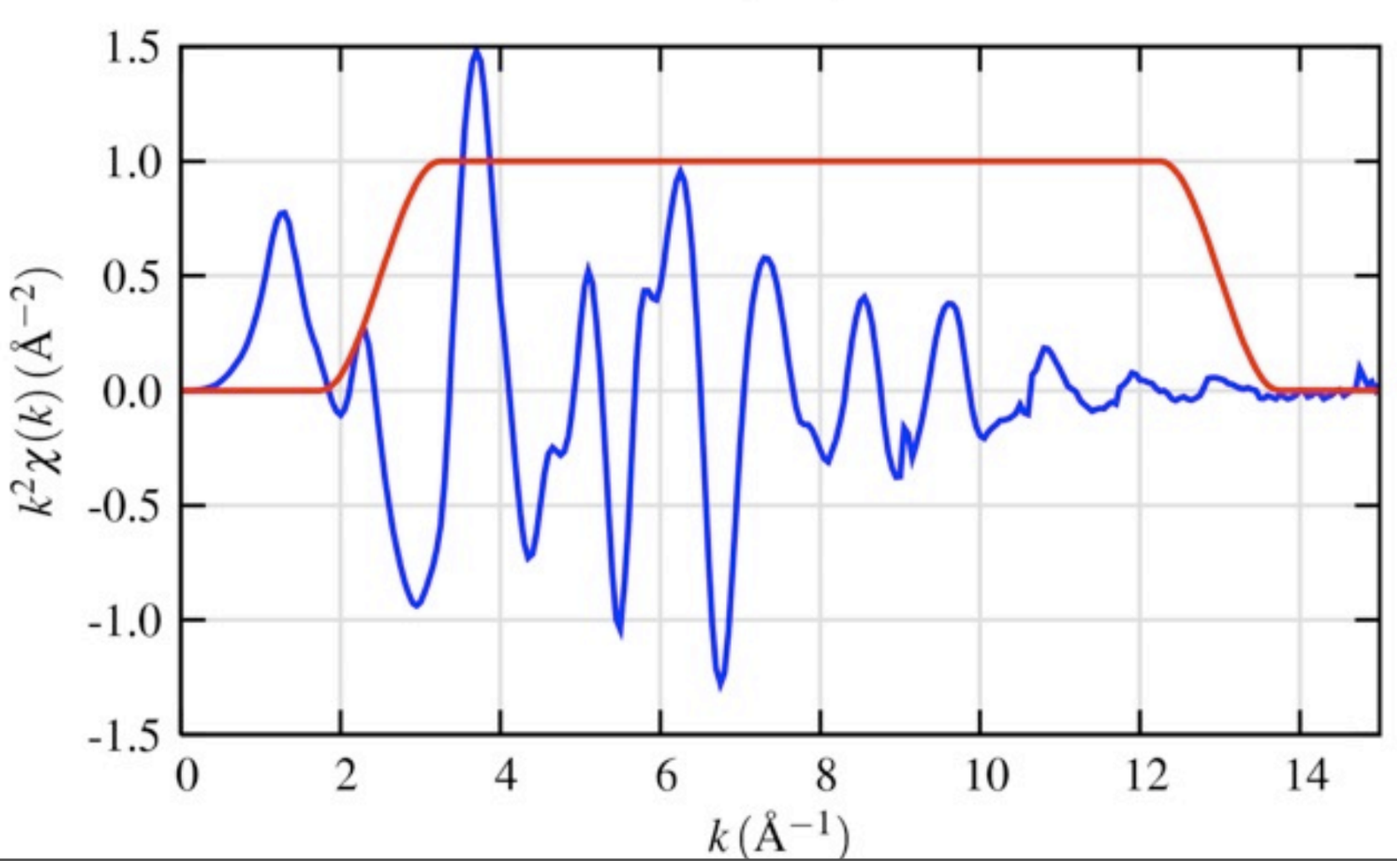

Extraction of χ(k)

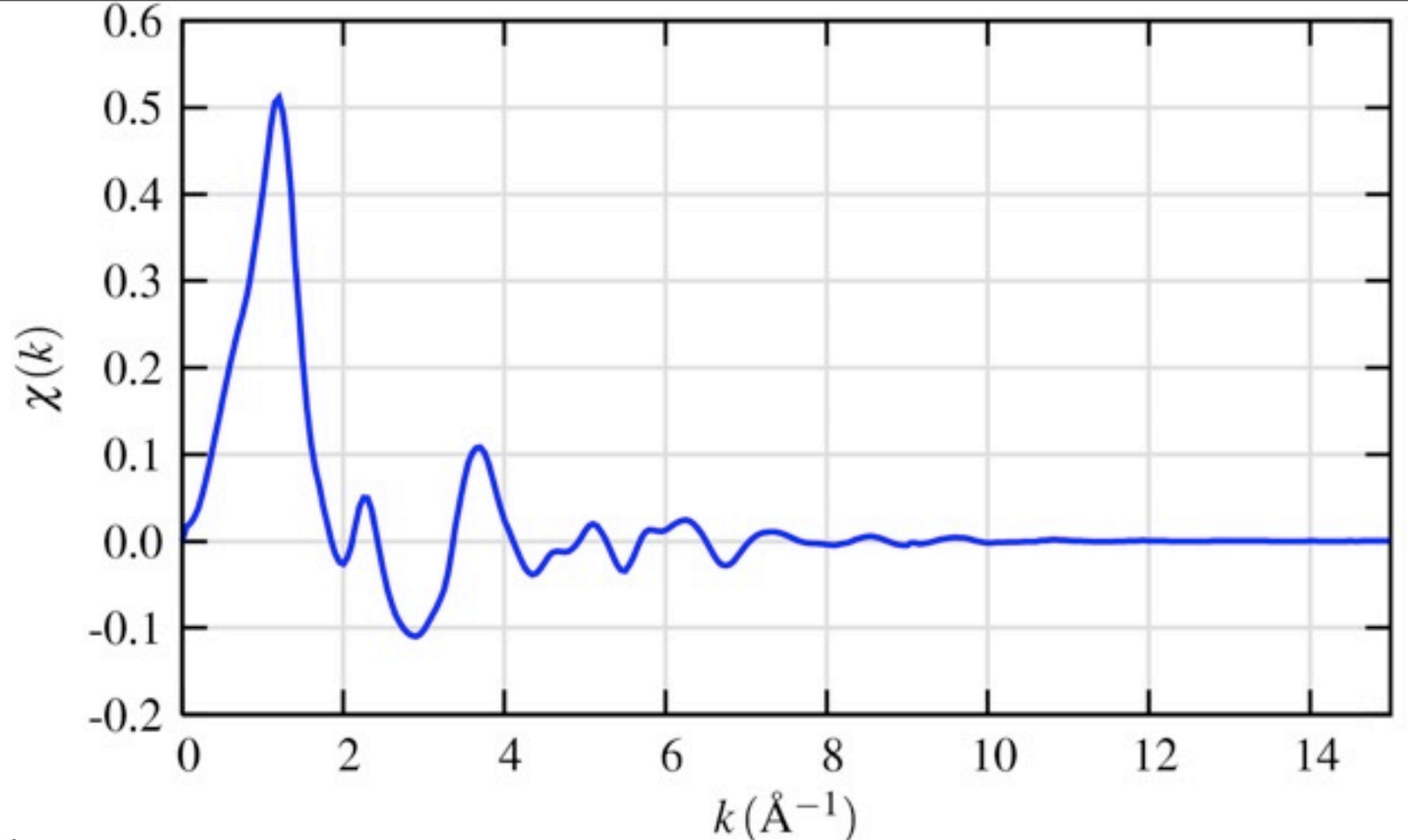

$$F(r) = \int_{k_{\min}}^{k_{\max}} \chi(k) W(k) k^n e^{2ikr} dk$$

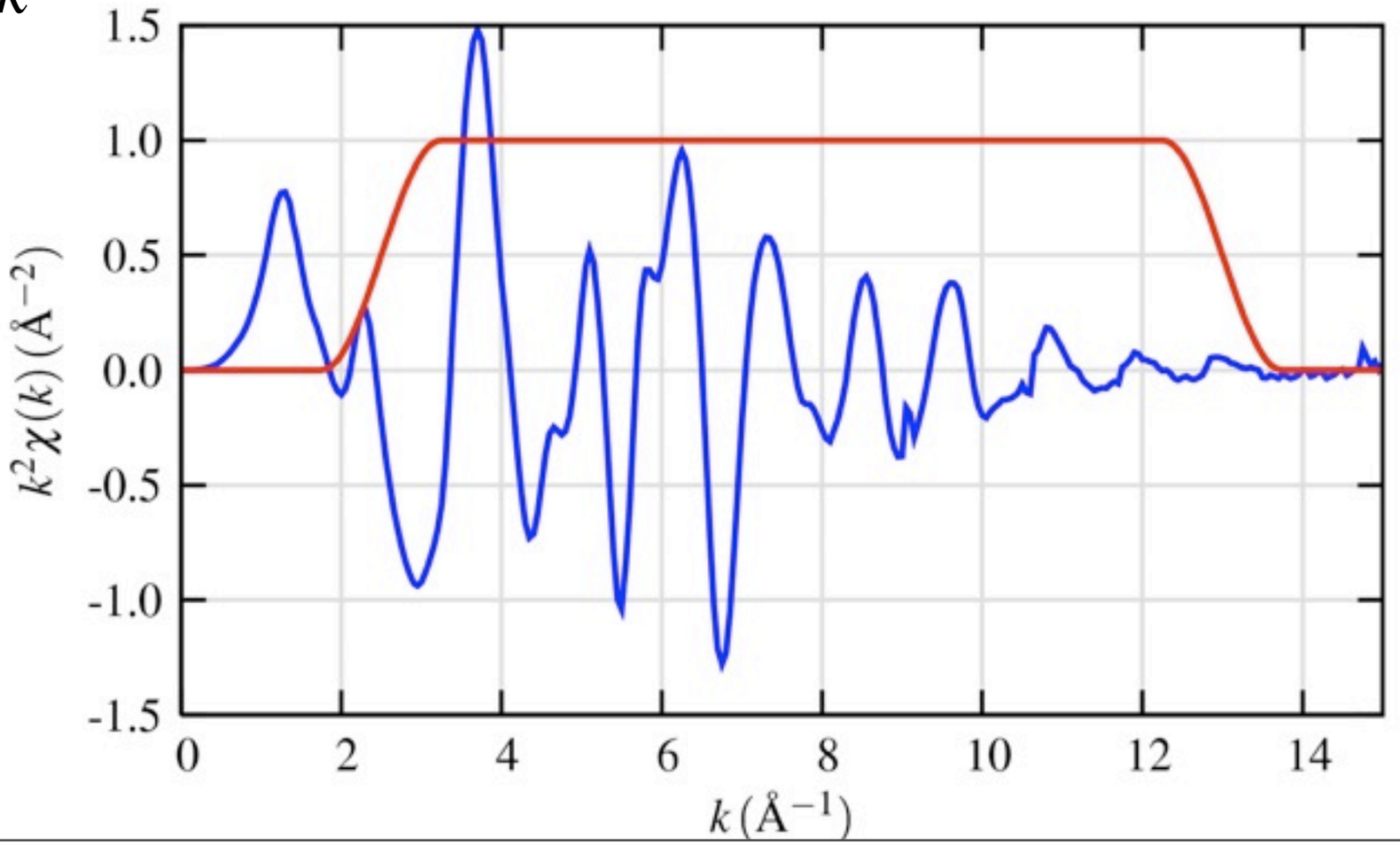

Extraction of χ(k)

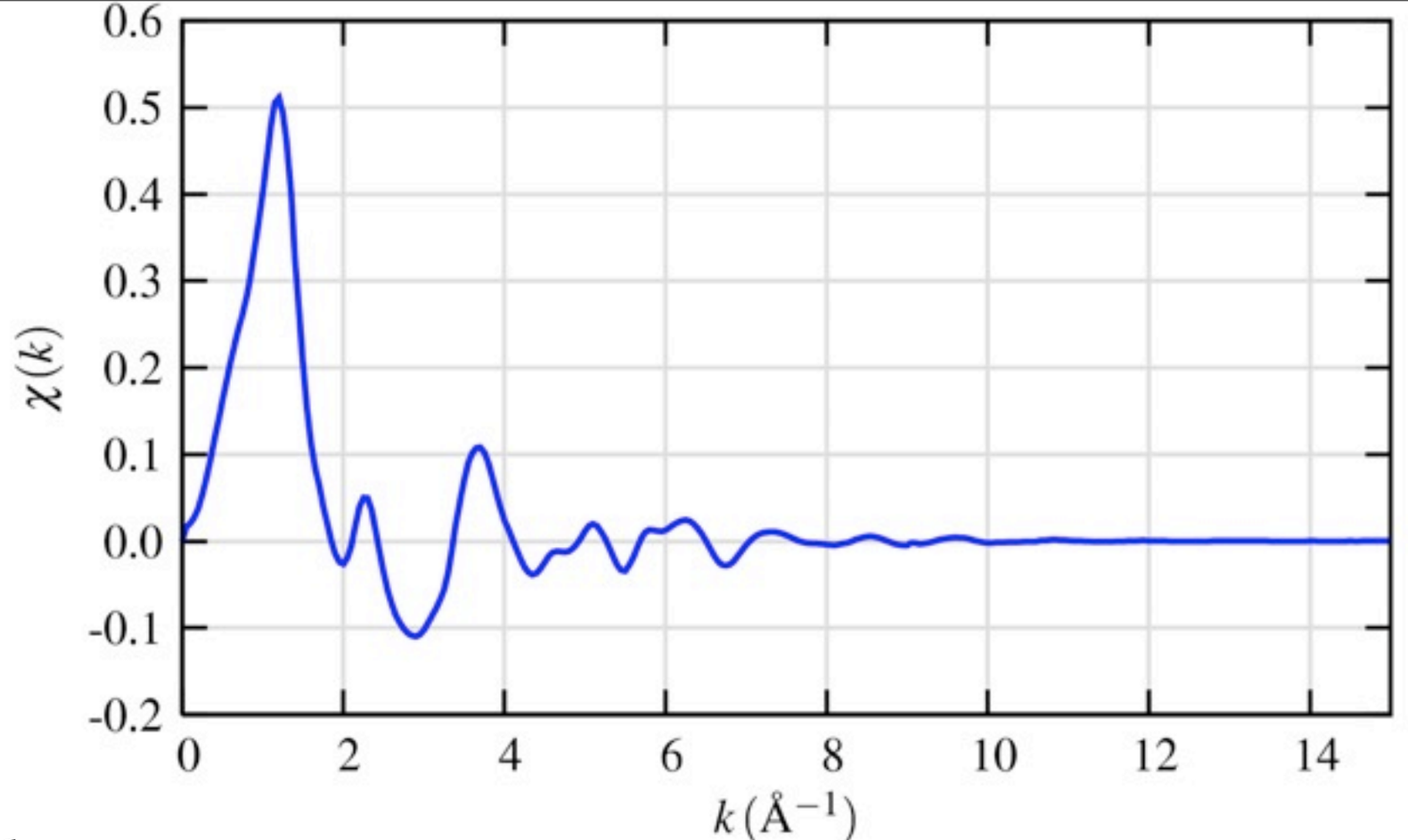

$$F(r) = \int_{k_{\min}}^{k_{\max}} \chi(k) W(k) k^n e^{2ikr} dk$$

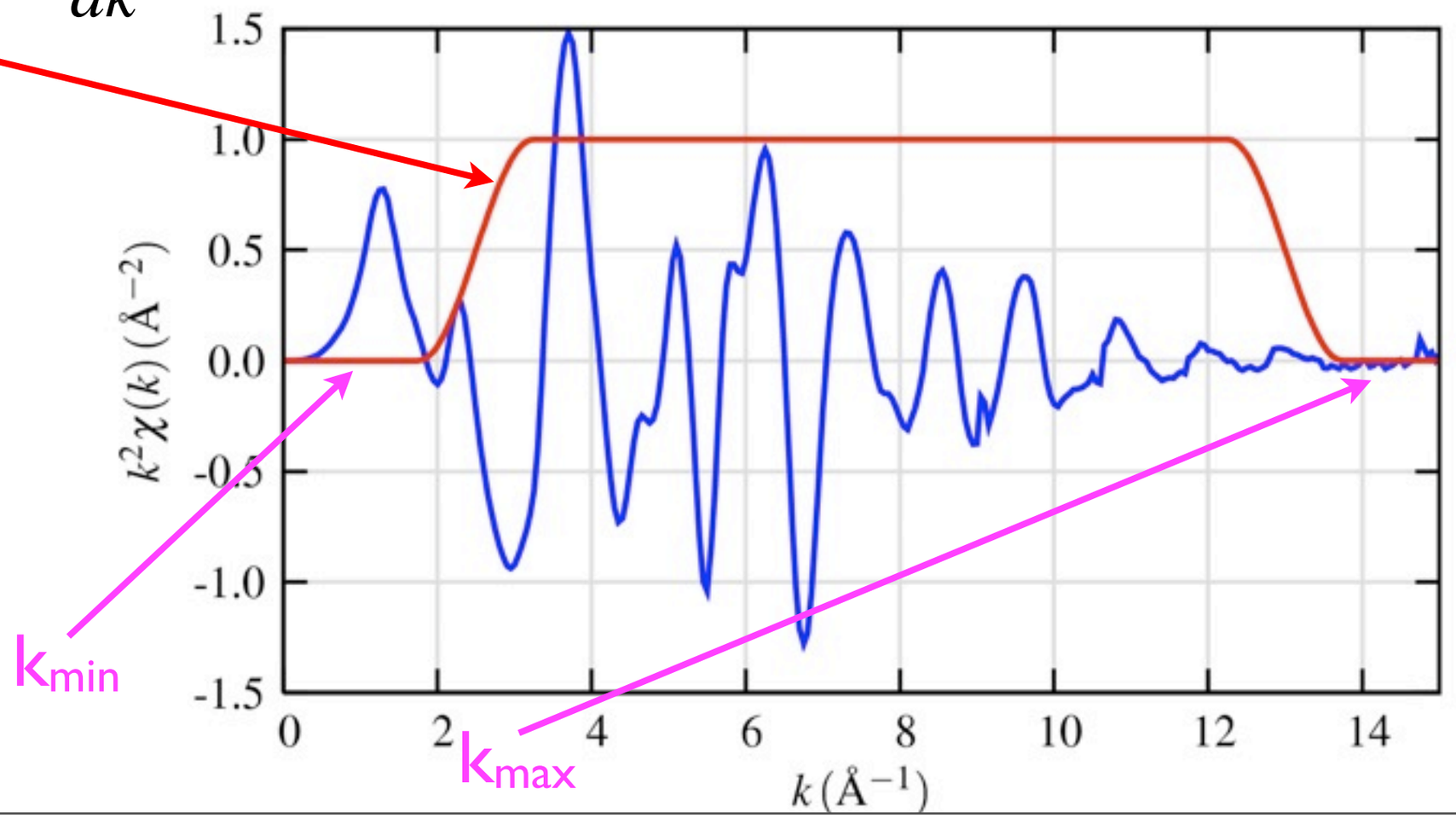

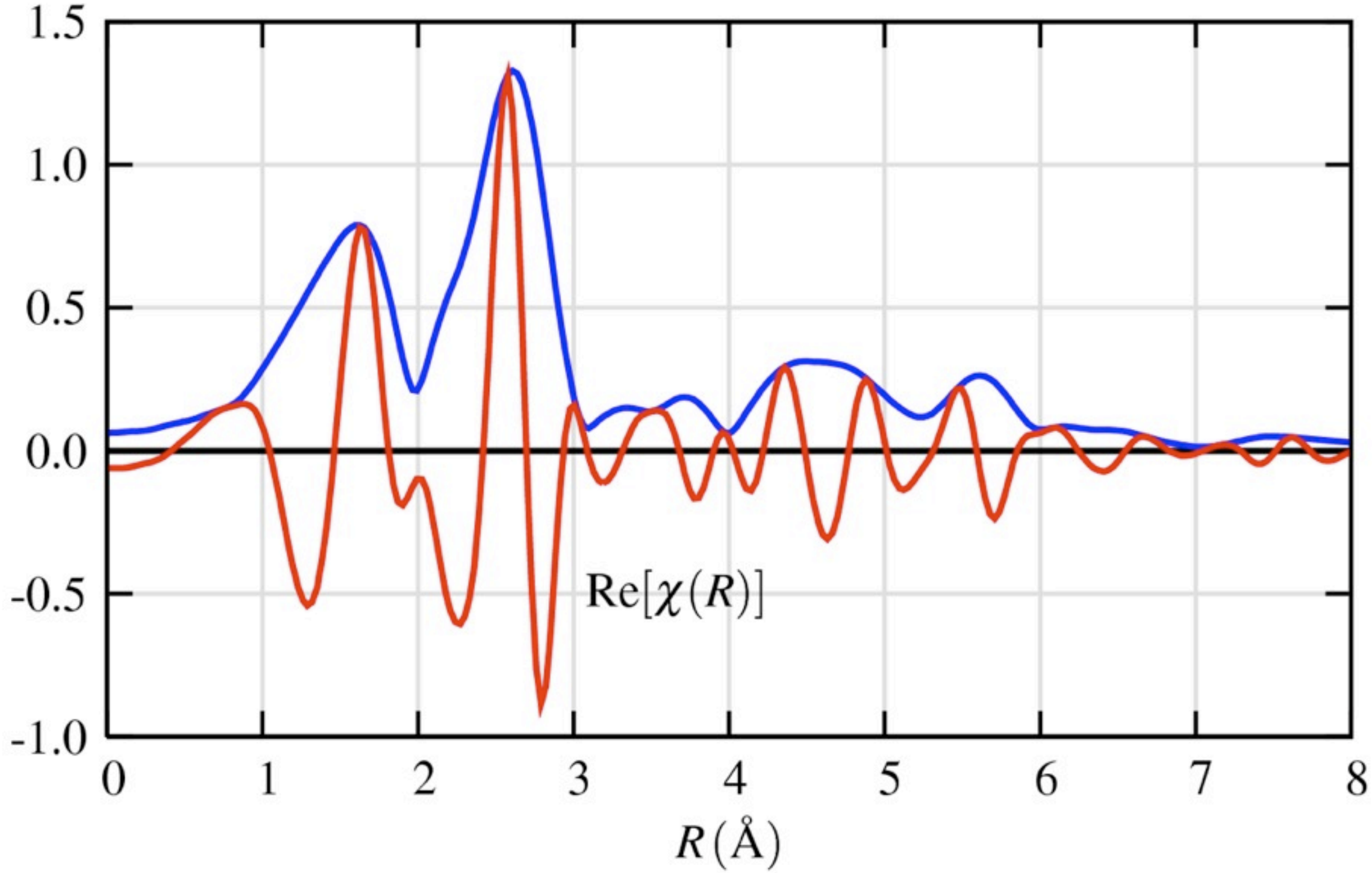

The Fourier Transform of $k^2\chi(k)$ has 2 main peaks, for the first 2 coordination shells: Fe-O and Fe-Fe. The Fe-O distance in FeO is 2.14Å, but the first peak is at 1.6Å. This shift in the first peak is due to the phase-shift, $\delta(k)$: $\sin[2kR+\delta(k)]$.

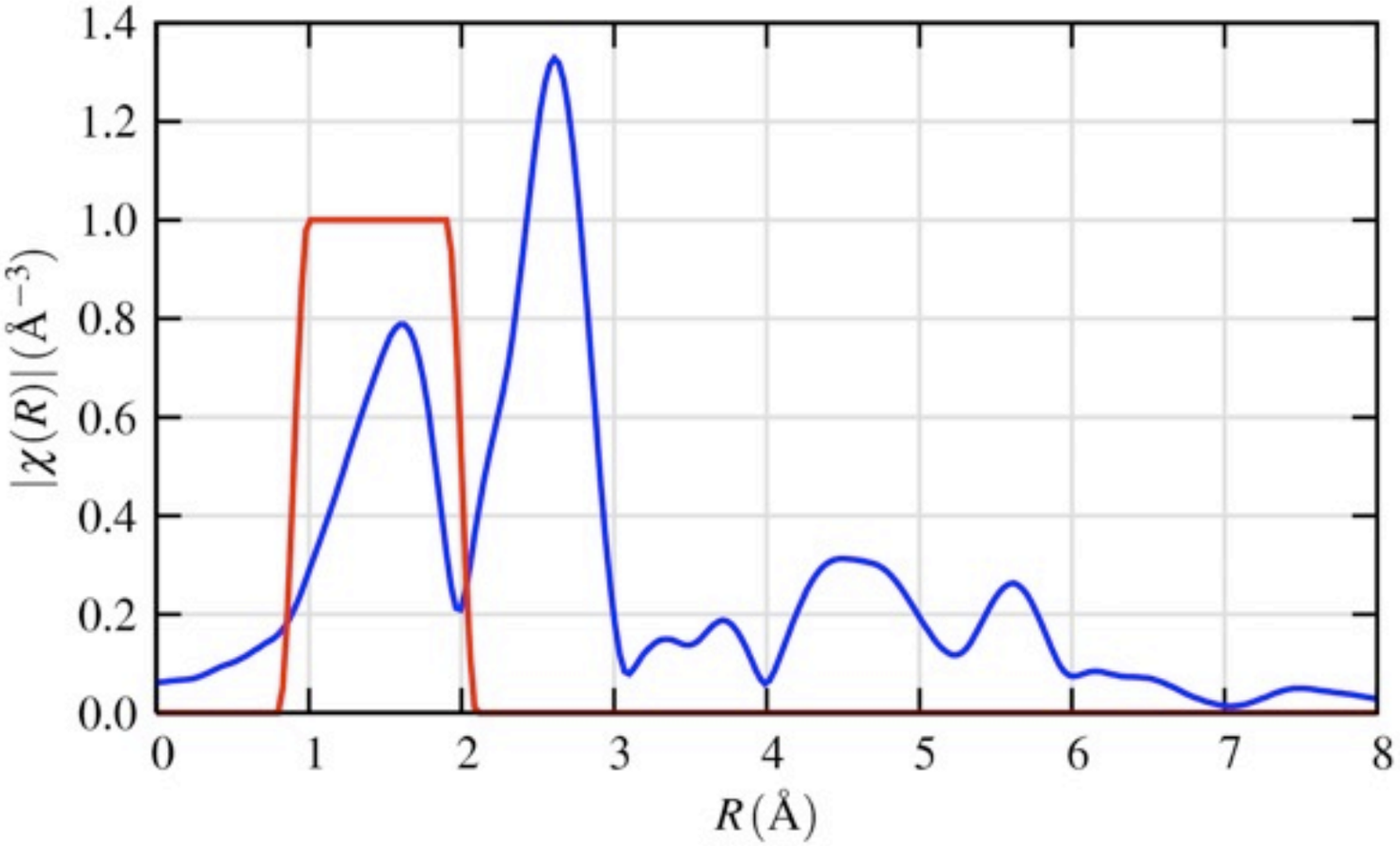

Isolating the contribution to the EXAFS signal of individual shells

$$\chi'(k) = \frac{2}{\pi}\int_{r_{\min}}^{r_{\max}} F(r)W'(r)e^{-2ikr}\,dr$$

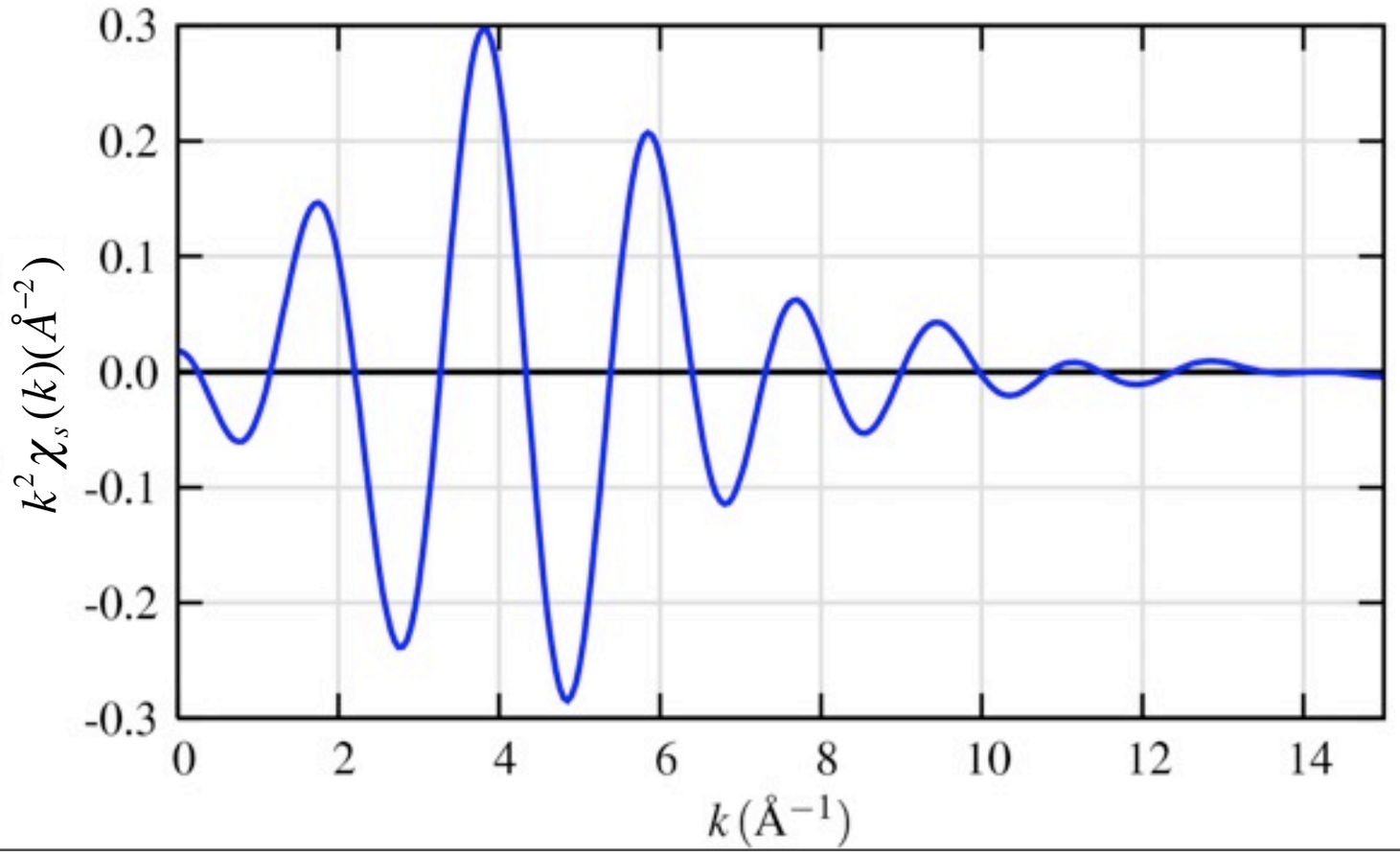

$$\chi_s(k) = \mathrm{Re}\left[\chi'(k)\right] = A_s(k)\sin\Phi_s(k)$$

Extracting structural parameters

Having singled out the contribution of each atomic shell, we can fit the data to get the structural information we look for by taking into account the atomic properties such as $|f_s(k,\pi)|$,ϕ_s, S_0^2 and λ which we can get from theory or from reference compounds.

Extracting structural parameters

Having singled out the contribution of each atomic shell, we can fit the data to get the structural information we look for by taking into account the atomic properties such as $|f_s(k,\pi)|$,ϕ_s, S_0^2 and λ which we can get from theory or from reference compounds.

The maximum number of independent parameters we can obtain is given by:

$$n_{ind} \simeq \frac{2\Delta k \Delta r}{\pi}$$

in which Δk and Δr are the ranges of the direct and inverse Fourier transforms. Typically $\Delta k \approx 9 Å^{-1}$ and $\Delta R \approx 1.5 Å$, so $n_{ind} \approx 9$

Extracting structural parameters

Having singled out the contribution of each atomic shell, we can fit the data to get the structural information we look for by taking into account the atomic properties such as $|f_s(k,\pi)|$,ϕ_s, S_0^2 and λ which we can get from theory or from reference compounds.

The maximum number of independent parameters we can obtain is given by:

$$n_{ind} \simeq \frac{2\Delta k \Delta r}{\pi}$$

in which Δk and Δr are the ranges of the direct and inverse Fourier transforms. Typically $\Delta k \approx 9 Å^{-1}$ and $\Delta R \approx 1.5 Å$, so $n_{ind} \approx 9$

Cautions:

- check distortions introduced by Fourier filtering;
- check multiple scattering events for shells beyond the first one.

EXAFS Analysis: Modeling the 1st Shell of FeO

FeO has a rock-salt structure.

To model the FeO EXAFS, we calculate the scattering amplitude $\mathbf{f(k)}$ and phase-shift $\boldsymbol{\delta(k)}$, based on a guess of the structure, with Fe-O distance $\mathbf{R = 2.14}$ Å (a regular octahedral coordination).

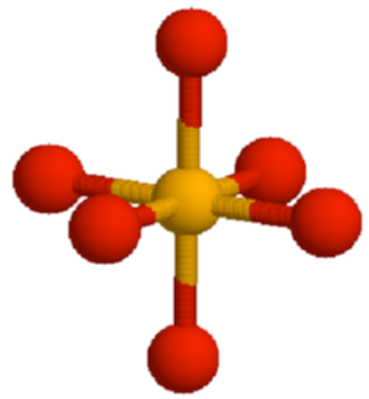

We'll use these functions to *refine* the values $\mathbf{R}$, $\mathbf{N}$, $\boldsymbol{\sigma^2}$, and $\mathbf{E_0}$ so our model EXAFS function matches our data.

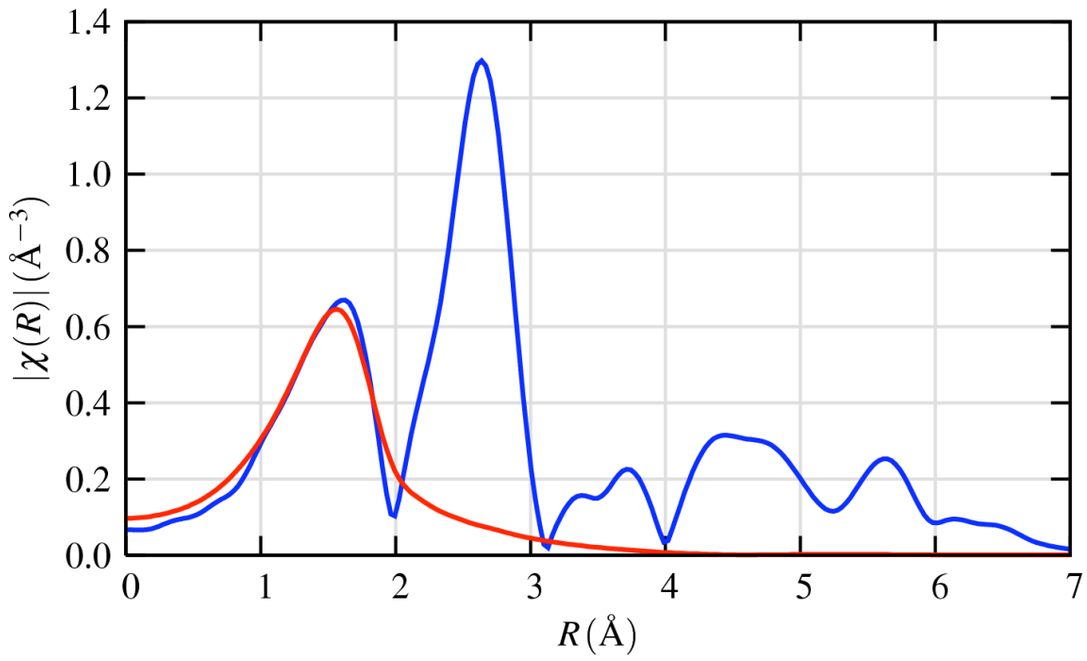

$|\chi(\mathbf{R})|$ **for FeO (blue), and a 1st shell fit (red).**

Fit results:

$\mathbf{N}$	**= 5.8 ± 1.8**
$\mathbf{R}$	**= 2.10 ± 0.02Å**
$\mathbf{\Delta E_0}$	**= -3.1 ± 2.5 eV**
$\boldsymbol{\sigma^2}$	**= 0.015 ± 0.005 Å^2.**

EXAFS Analysis: 1st Shell of FeO

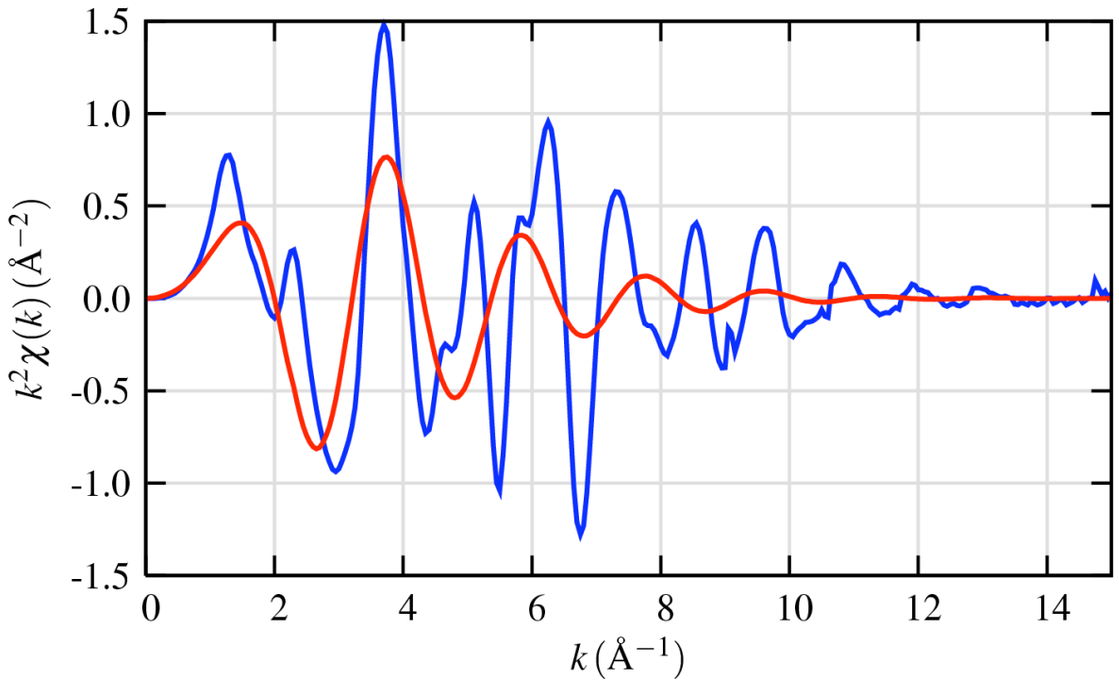

1^{st} shell fit in k space.

The 1^{st} shell fit to FeO in k space.

There is clearly another component in the XAFS!

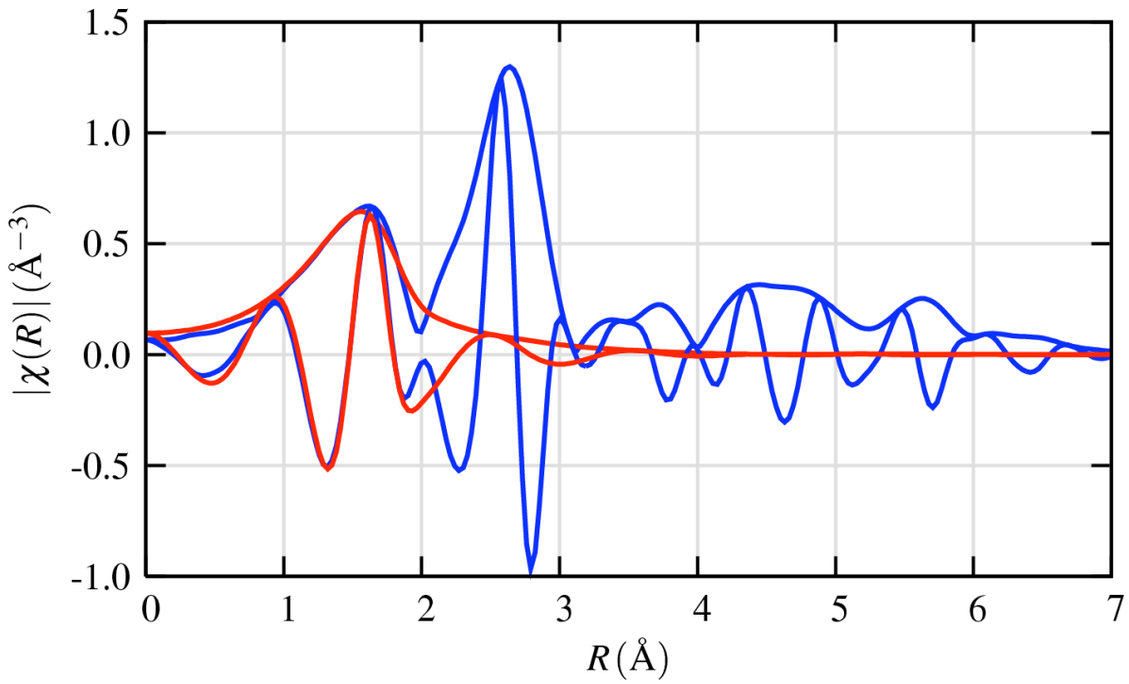

1^{st} shell fit in R space.

$|\chi(R)|$ and Re$[\chi(R)]$ for FeO (blue), and a 1^{st} shell fit (red).

Though the fit to the magnitude didn't look great, the fit to Re$[\chi(R)]$ looks very good.

EXAFS Analysis: Second Shell of FeO

To add the second shell Fe to the model, we use calculation for $\mathbf{f(k)}$ and $\boldsymbol{\delta}\mathbf{(k)}$ based on a guess of the Fe-Fe distance, and refine the values $\mathbf{R}$, $\mathbf{N}$, $\boldsymbol{\sigma}^{\mathbf{2}}$.
Such a fit gives a result like this:

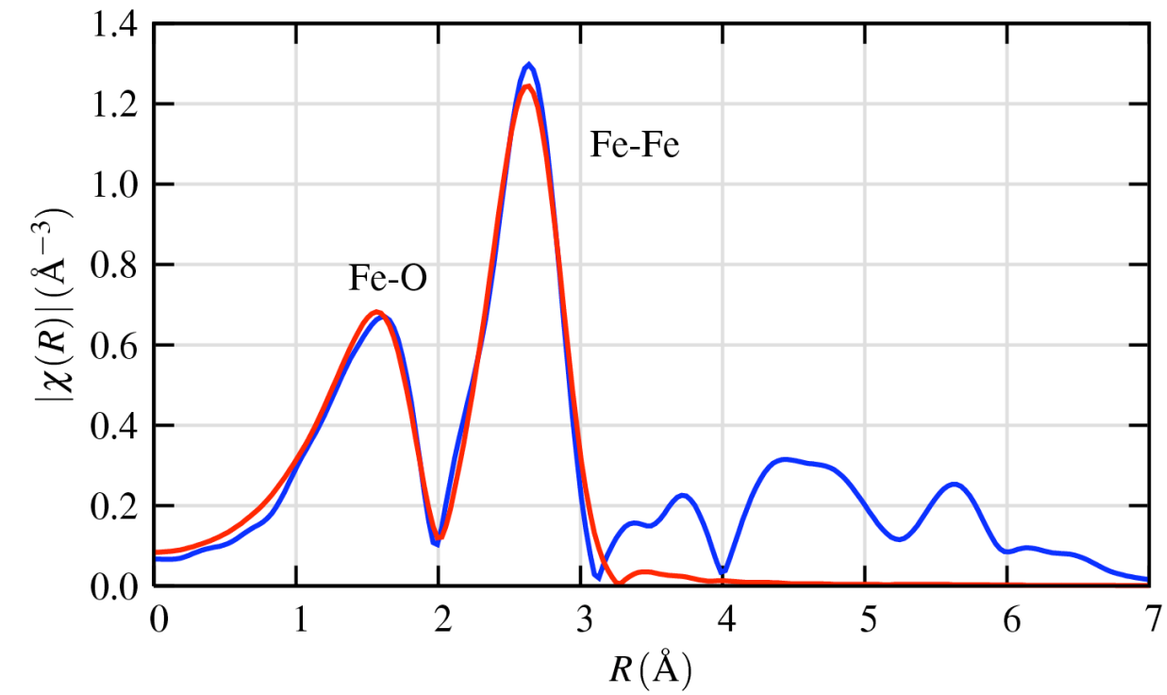

$|\chi(\mathbf{R})|$ **data for FeO (blue), and fit of 1st and 2nd shells (red).**
The results are fairly consistent with the known values for crystalline FeO:
6 O at 2.13Å, 12 Fe at 3.02Å.

Fit results (uncertainties in parentheses):

Shell	$\mathbf{N}$	$\mathbf{R}$ (Å)	$\boldsymbol{\sigma}^{\mathbf{2}}$ (Å^2)	$\boldsymbol{\Delta E_0}$ (eV)
Fe-O	6.0(1.0)	2.10(.02)	0.015(.003)	-2.1(0.8)
Fe-Fe	11.7(1.3)	3.05(.02)	0.014(.002)	-2.1(0.8)

EXAFS Analysis: Second Shell of FeO

Other views of the data and two-shell fit:

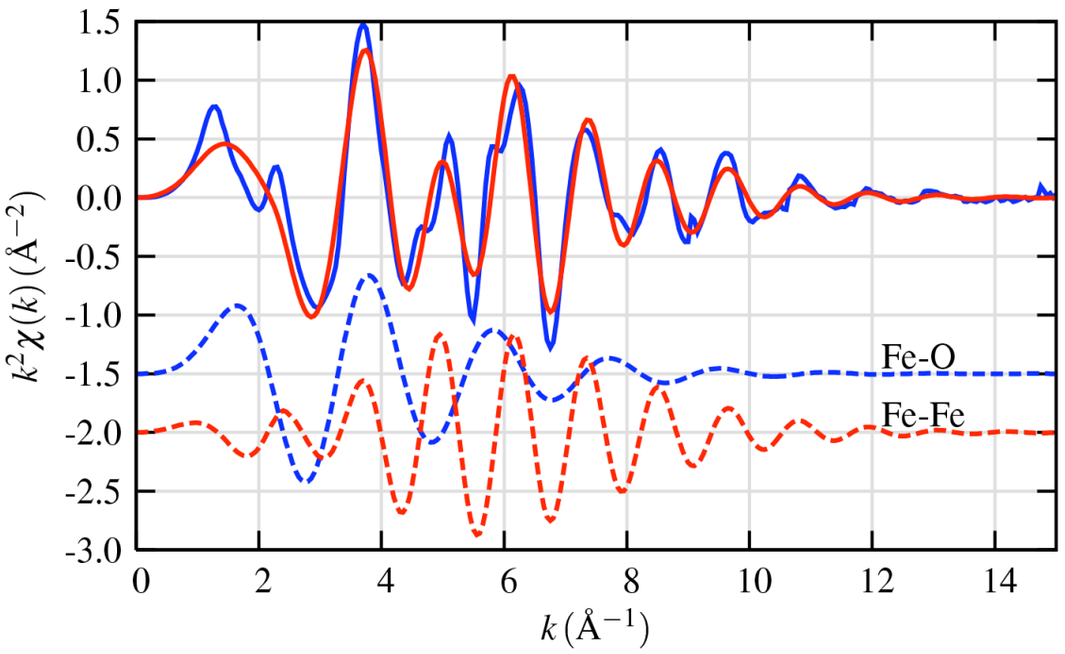

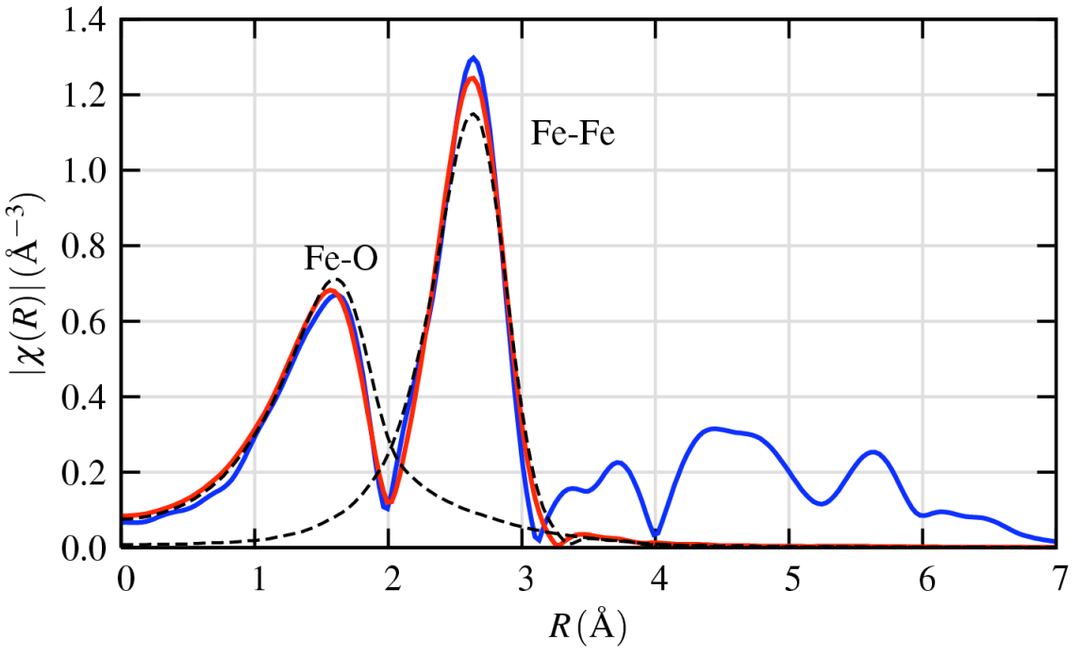

The Fe-Fe EXAFS extends to higher-k than the Fe-O EXAFS.

Even in this simple system, there is some *overlap* of shells in R-space.

The agreement in Re$[\chi(R)]$ look especially good – this is how the fits are done.

Of course, the modeling can get more complicated than this!

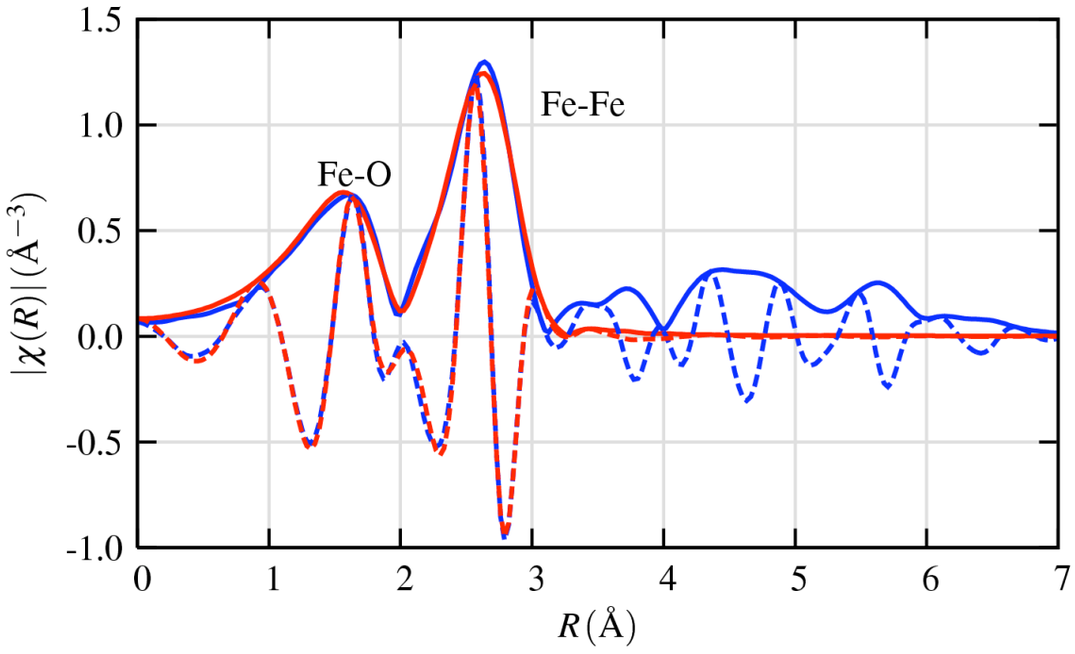

XANES

XANES Analysis: Oxidation State and Coordination Chemistry

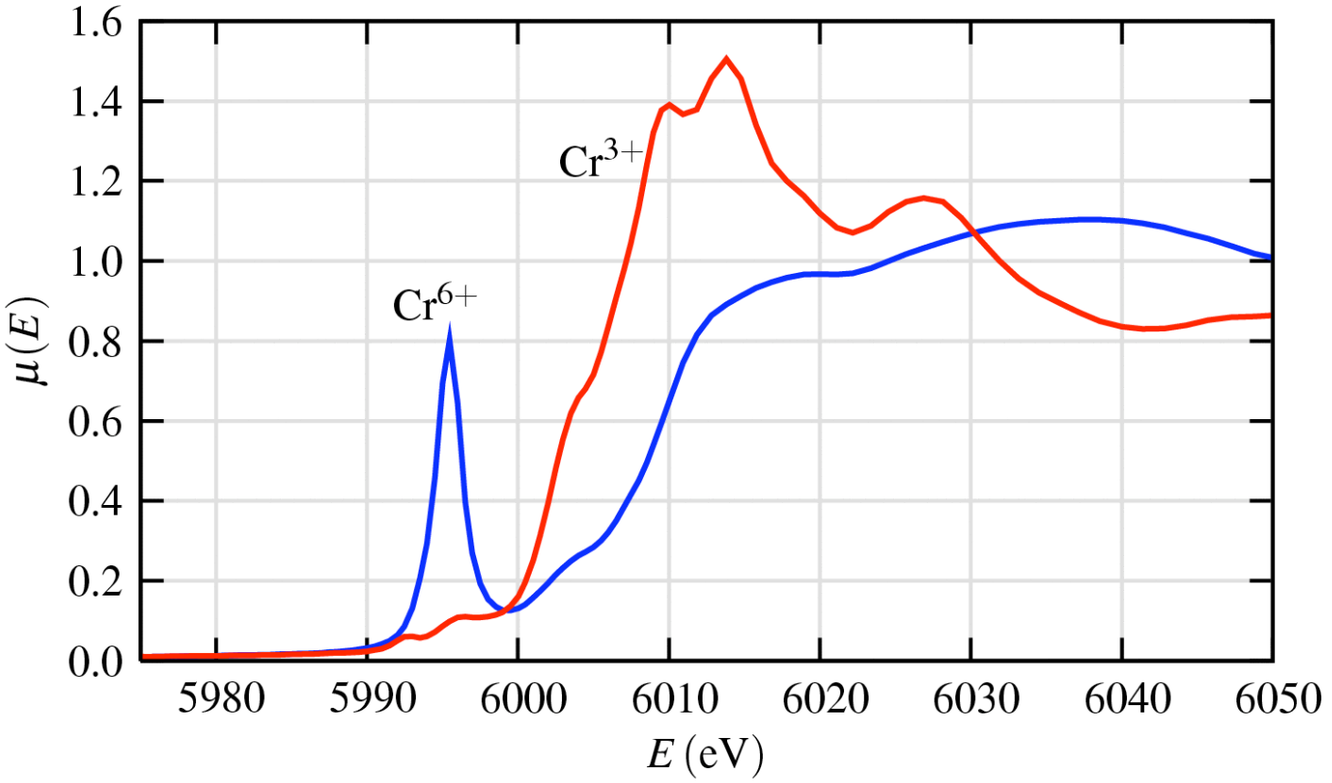

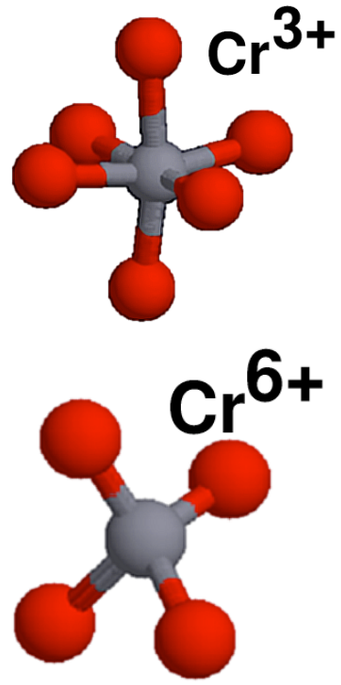

The XANES of Cr^{3+} and Cr^{6+} shows a dramatic dependence on oxidation state and coordination chemistry.

For ions with partially filled d shells, the p-d hybridization changes dramatically as *regular octahedra* distort, and is very large for *tetrahedral* coordination.

This gives a dramatic *pre-edge peak* – absorption to a localized electronic state.

XANES Interpretation

The EXAFS Equation breaks down at low-k, and the mean-free-path goes up.
This complicates XANES interpretation:

We do not have a simple equation for XANES.

XANES can be described *qualitatively* (and nearly *quantitatively*) in terms of

coordination chemistry	**regular, distorted octahedral, tetrahedral, . . .**
molecular orbitals	**p-d orbital hybridization, crystal-field theory, . . .**
band-structure	**the density of available electronic states.**
multiple-scattering	**multiple bounces of the photo-electron.**

These chemical and physical interpretations are all related, of course:

What electronic states can the photo-electron fill?

XANES calculations are becoming reasonably accurate and simple. These can help explain what *bonding orbitals* and/or *structural characteristics* give rise to certain spectral features.

Quantitative XANES analysis using first-principles calculations are still rare, but becoming possible...

Edge Shifts and Pre-edge Peaks in Fe oxides

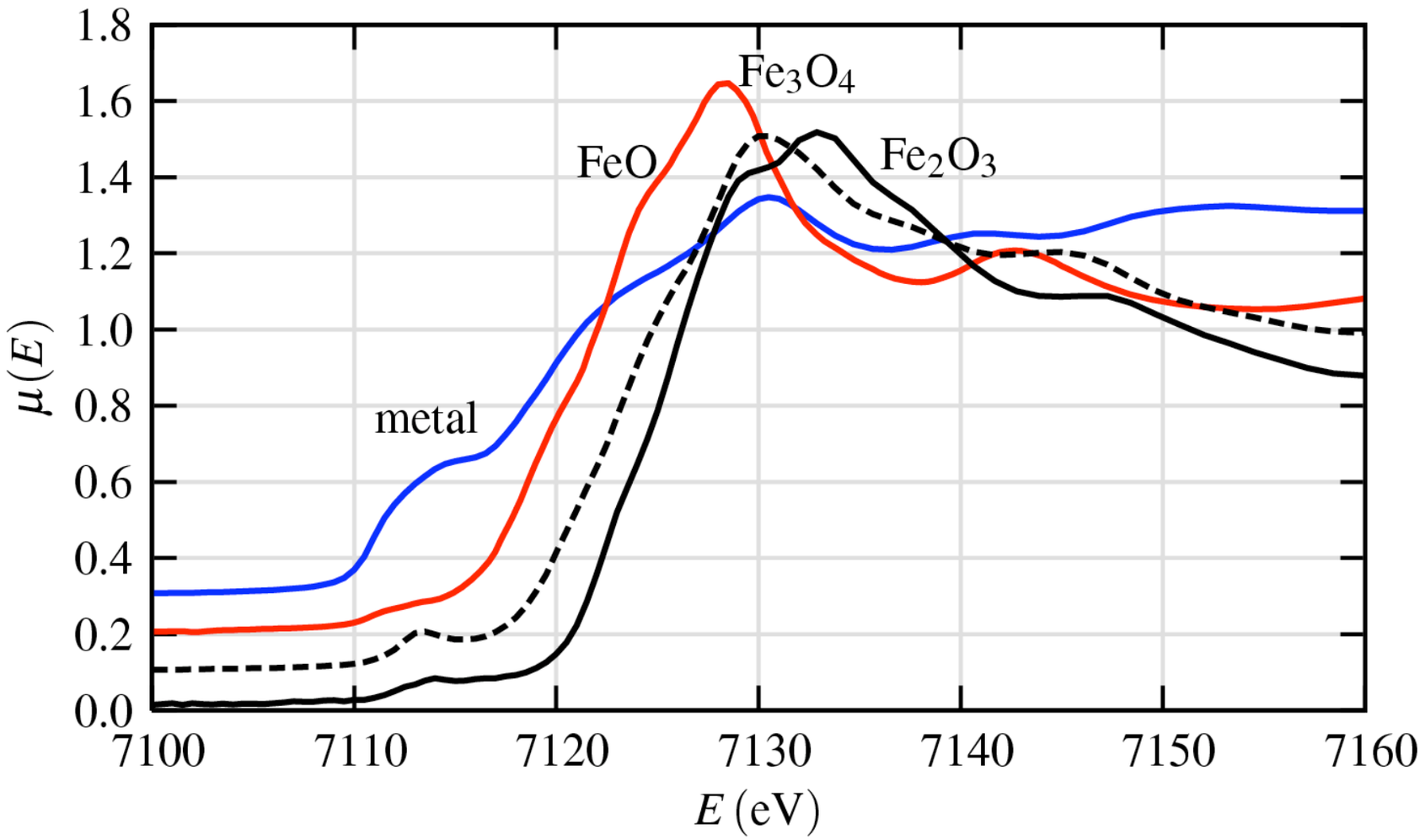

XANES for Fe oxides and metal. **The shift of the edge position can be used to determine the valence state.**

The heights and positions of pre-edge peaks can also be reliably used to determine Fe^{3+}/Fe^{2+} ratios (and similar ratios for many cations).

XANES Analysis: Oxidation State

The Normalized XANES from several Fe compounds:

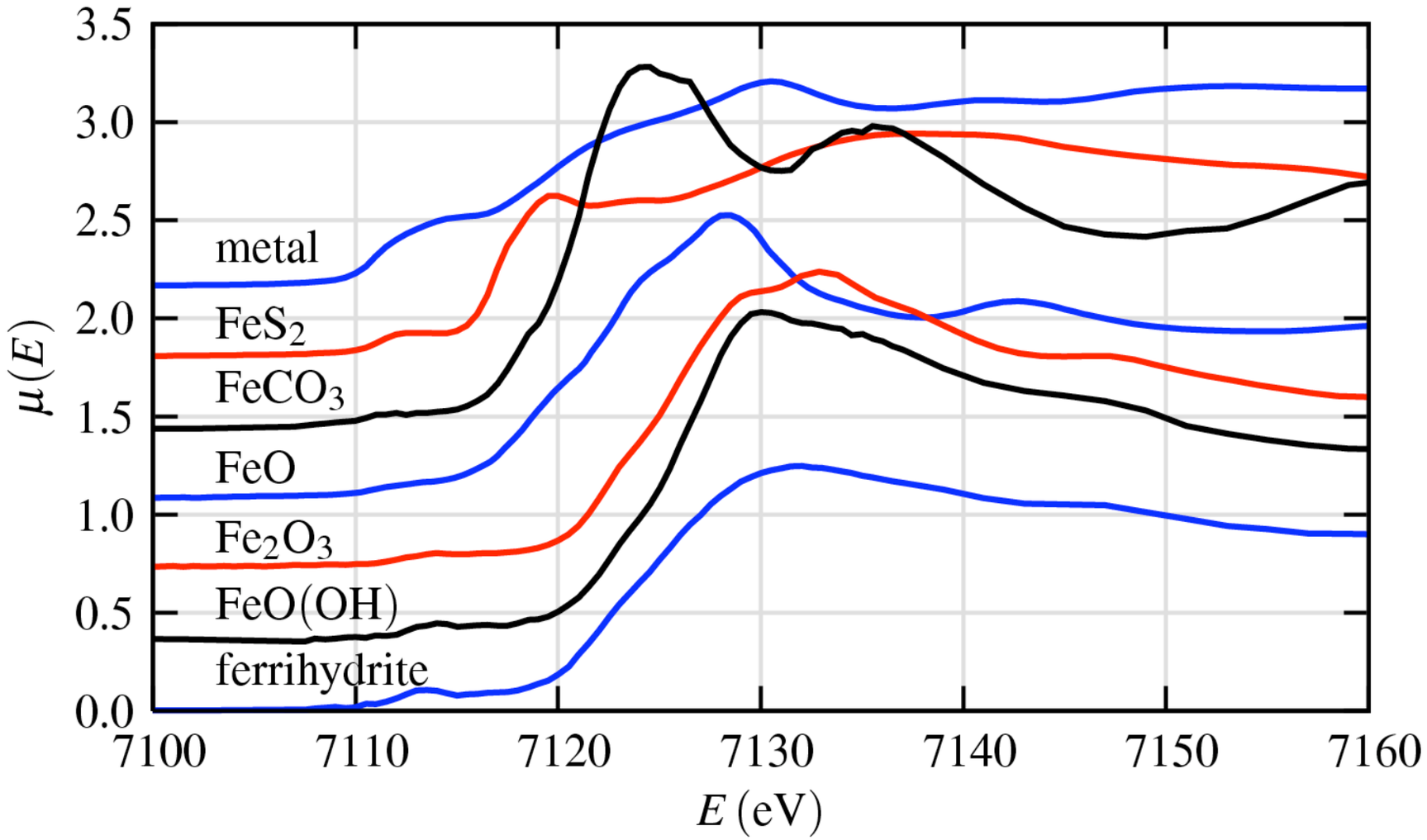

XANES can be used simply as a fingerprint of phases and oxidation state.

XANES Analysis can be as simple as making linear combinations of "known" spectra to get compositional fraction of these components.

XANES Analysis: Oxidation State

The Normalized XANES from several Fe compounds:

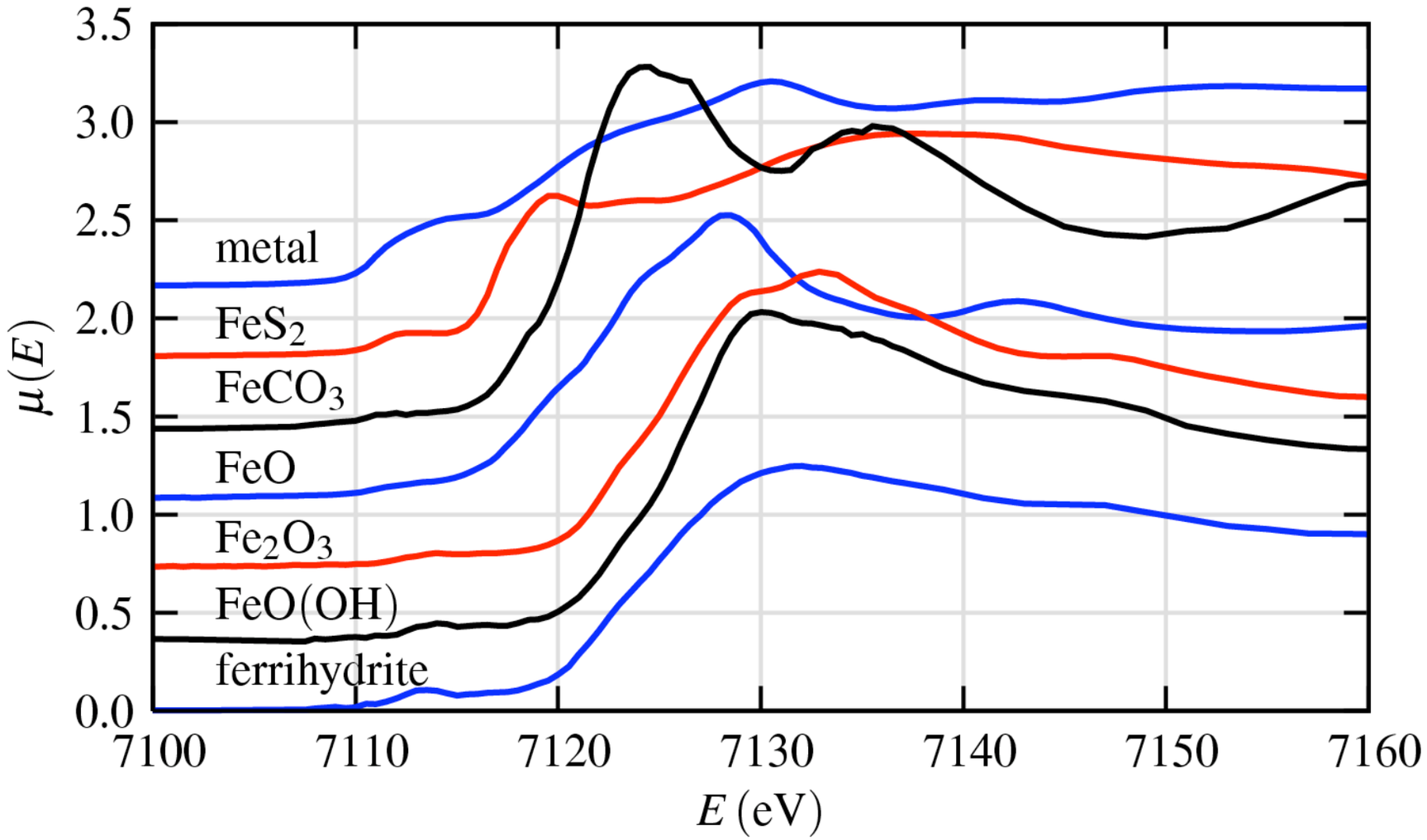

XANES can be used simply as a fingerprint of phases and oxidation state.

XANES Analysis can be as simple as making linear combinations of "known" spectra to get compositional fraction of these components.

XANES: Conclusions

XANES is a much larger signal than EXAFS

XANES can be done at lower concentrations, and less-than-perfect sample conditions.

XANES is easier to crudely interpret than EXAFS

For many systems, the XANES analysis based on linear combinations of known spectra from "model compounds" is sufficient.

XANES is harder to fully interpret than EXAFS

The exact physical and chemical interpretation of all spectral features is still difficult to do accurately, precisely, and reliably.

This situation is improving, so stay tuned to the progress in XANES calculations . . . .

Anal. Chem. **2008,** *80,* 6436–6442

Visualization of a Lost Painting by Vincent van Gogh Using Synchrotron Radiation Based X-ray Fluorescence Elemental Mapping

Joris Dik,[*,†] Koen Janssens,[‡] Geert Van Der Snickt,[‡] Luuk van der Loeff,[§] Karen Rickers,[∥] and Marine Cotte[⊥,⊗]

Department of Materials Science, Delft University of Technology, Mekelweg 2, 2628CD Delft, The Netherlands, Centre for Micro- and Trace Analysis, Department of Chemistry, Universiteit Antwerpen, Universiteitsplein 1, 2610 Antwerp, Belgium, Kröller-Müller Museum, Houtkampweg 6, P.O. Box 1, 6730 AA Otterlo, The Netherlands, Deutsches Elektronen-Synchrotron (DESY), Notkestrasse 85, 22603 Hamburg, Germany, Centre of Research and Restoration of the French Museums, UMR-171-CNRS, Palais du Louvre, Porte des Lions, 14 quai François Mitterrand, 75001 Paris, France, and European Synchrotron Radiation Facility BP220, 38043 Grenoble Cedex, France

X-Ray absorption and magnetism

X-ray absorption spectra of a wedge sample, revealing the composition at various points along the wedge. The Fe signal increases from bottom to top because of the increasing Fe layer thickness and the Ni signal decreases because of the limited electron escape depth of the total electron yield signal used to record the spectra. The Cu signal is constant, reflecting its constant 1nm thickness.

X-rays can pick materials apart: layer-by-layer

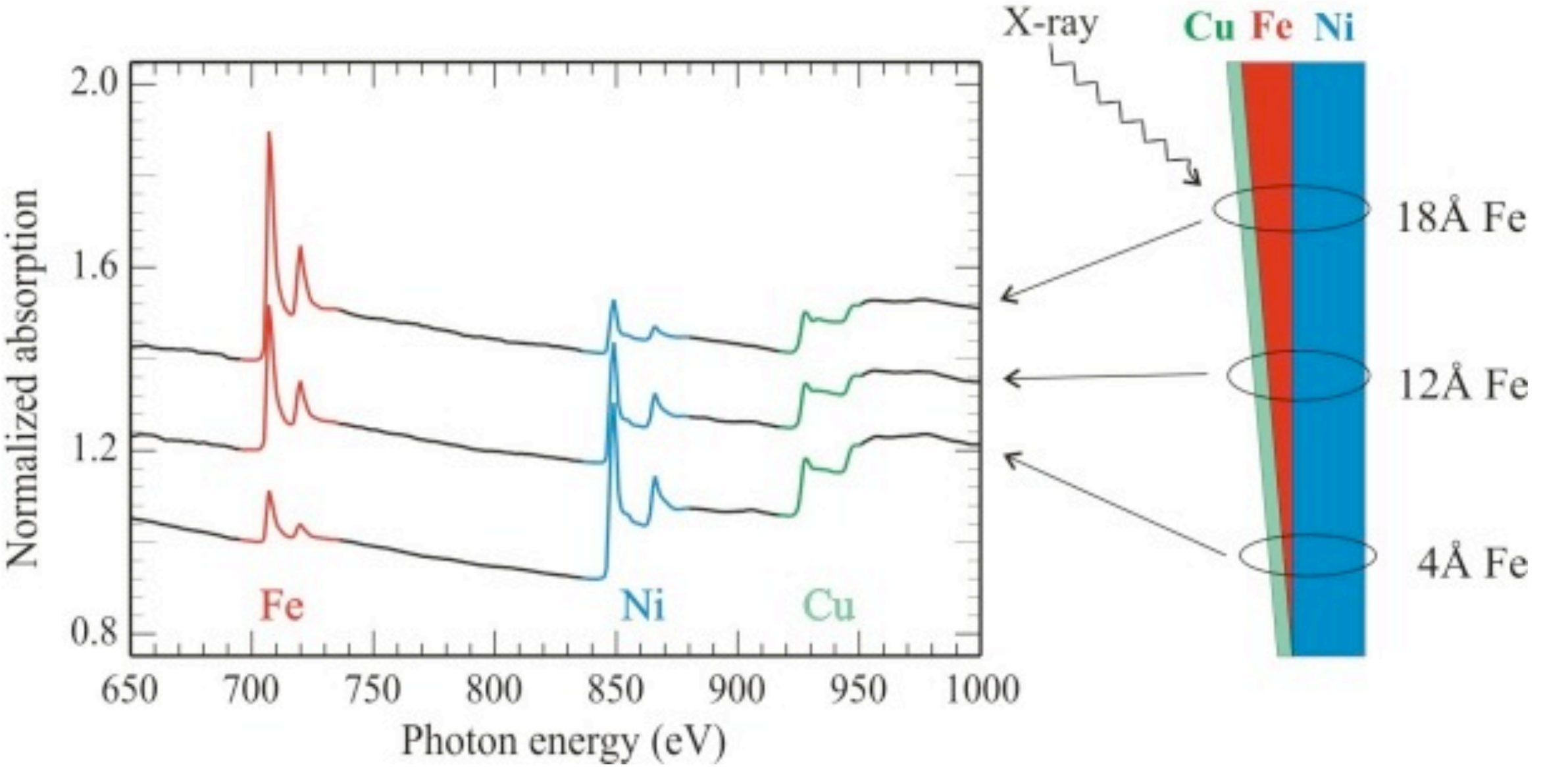

L-edge x-ray absorption spectra of Fe, Co and Ni in the form of the elemental metals and as oxides.

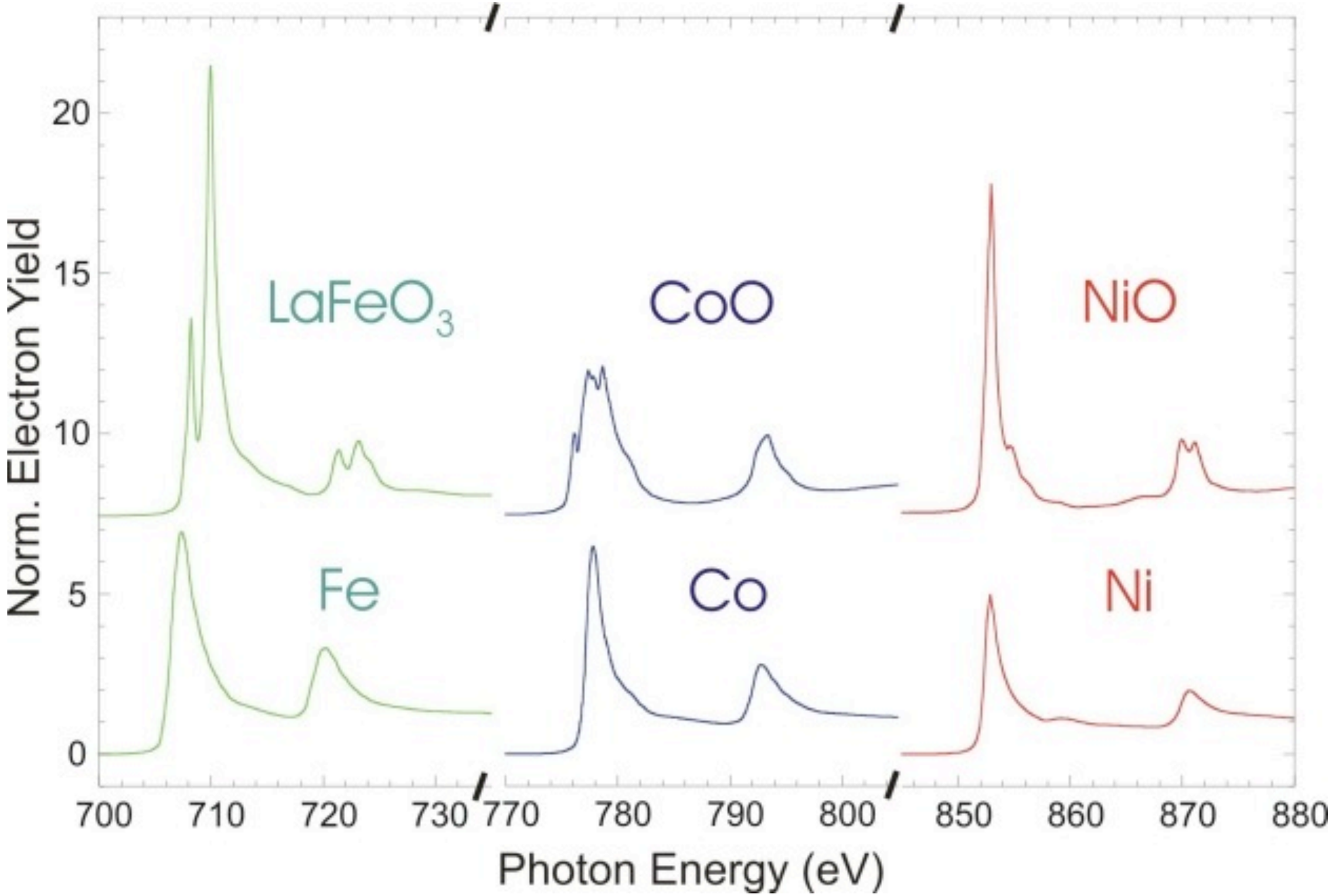

L-edge x-ray absorption spectra of Fe, Co and Ni in the form of the elemental metals and as oxides.

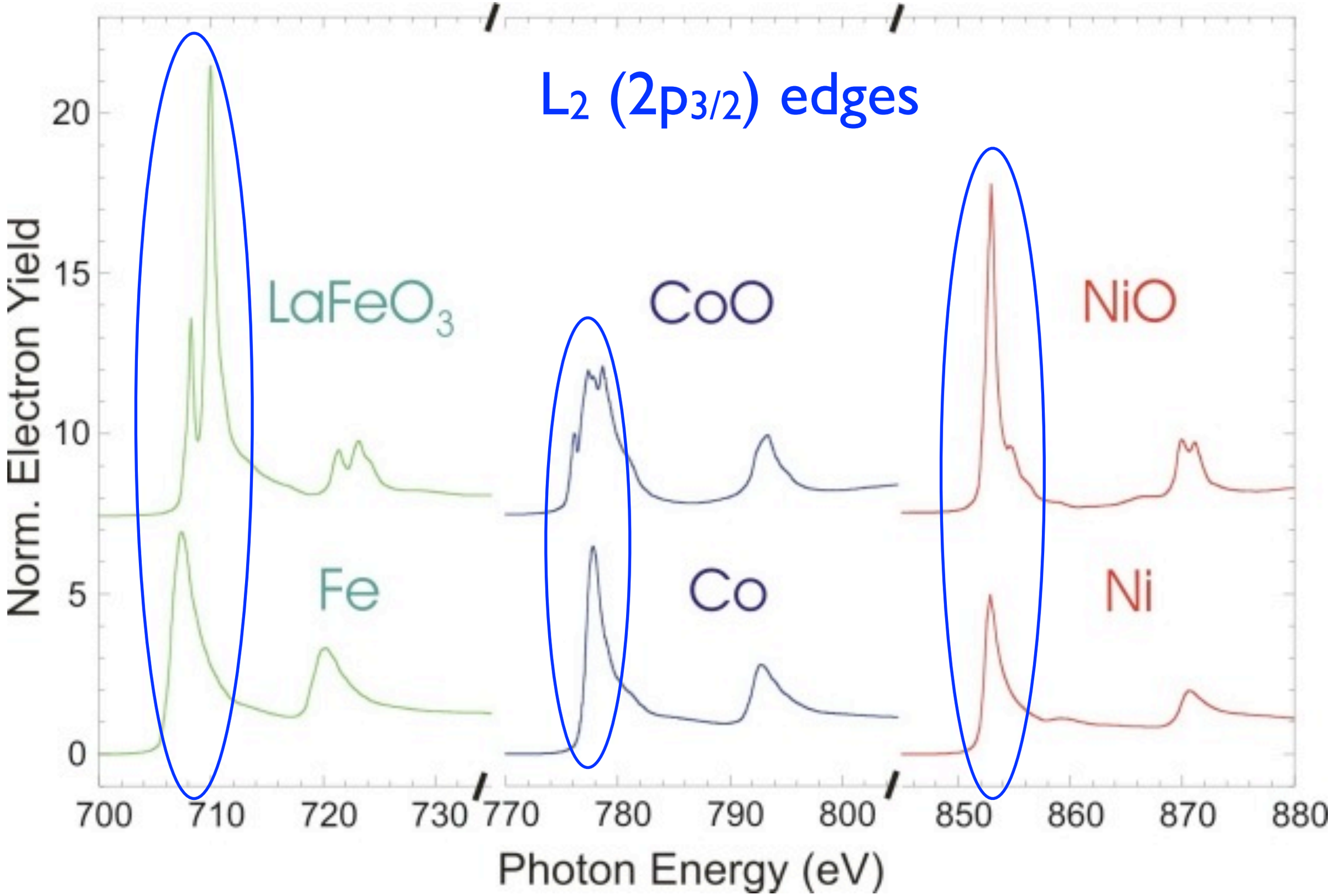

L-edge x-ray absorption spectra of Fe, Co and Ni in the form of the elemental metals and as oxides.

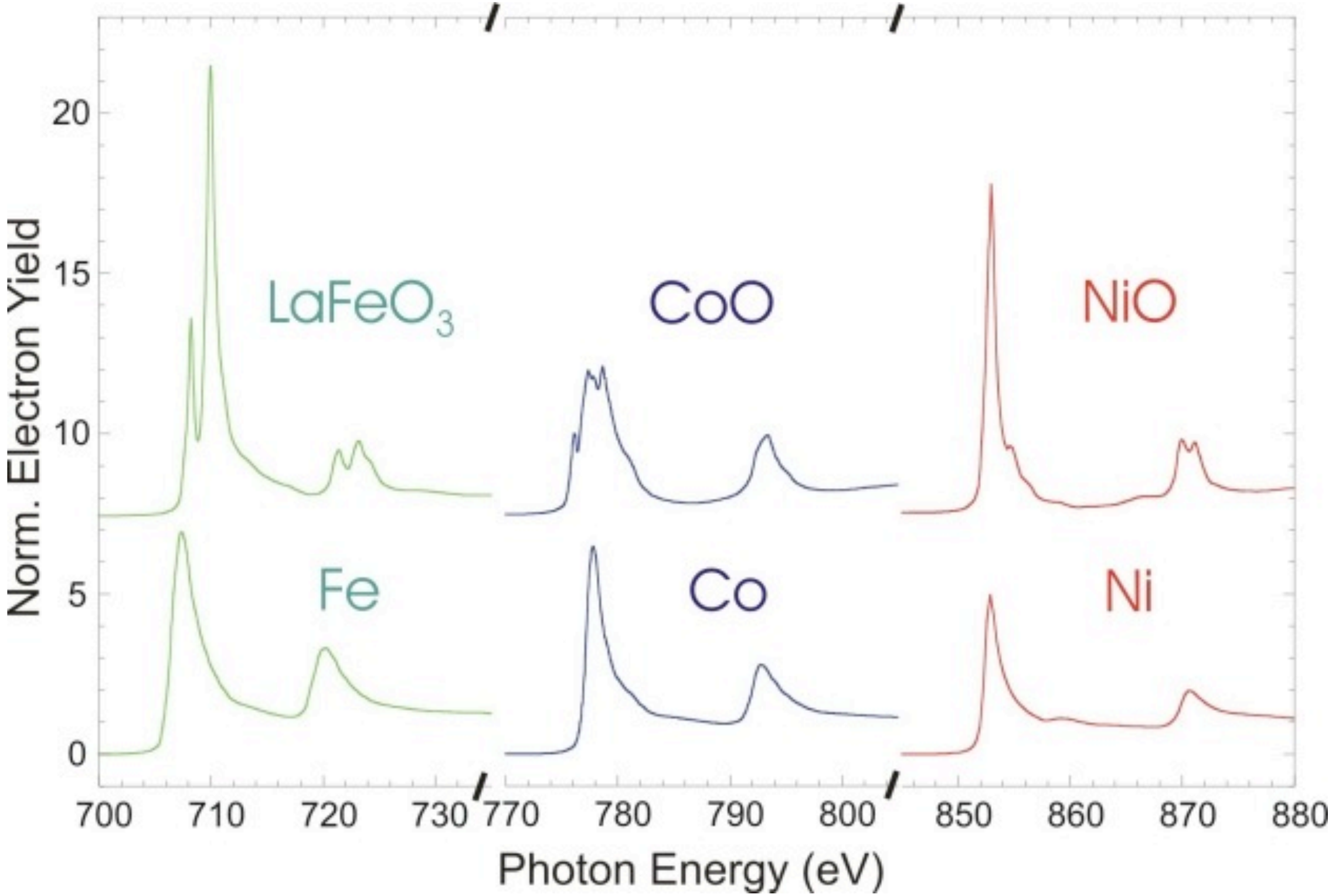

L-edge x-ray absorption spectra of Fe, Co and Ni in the form of the elemental metals and as oxides.

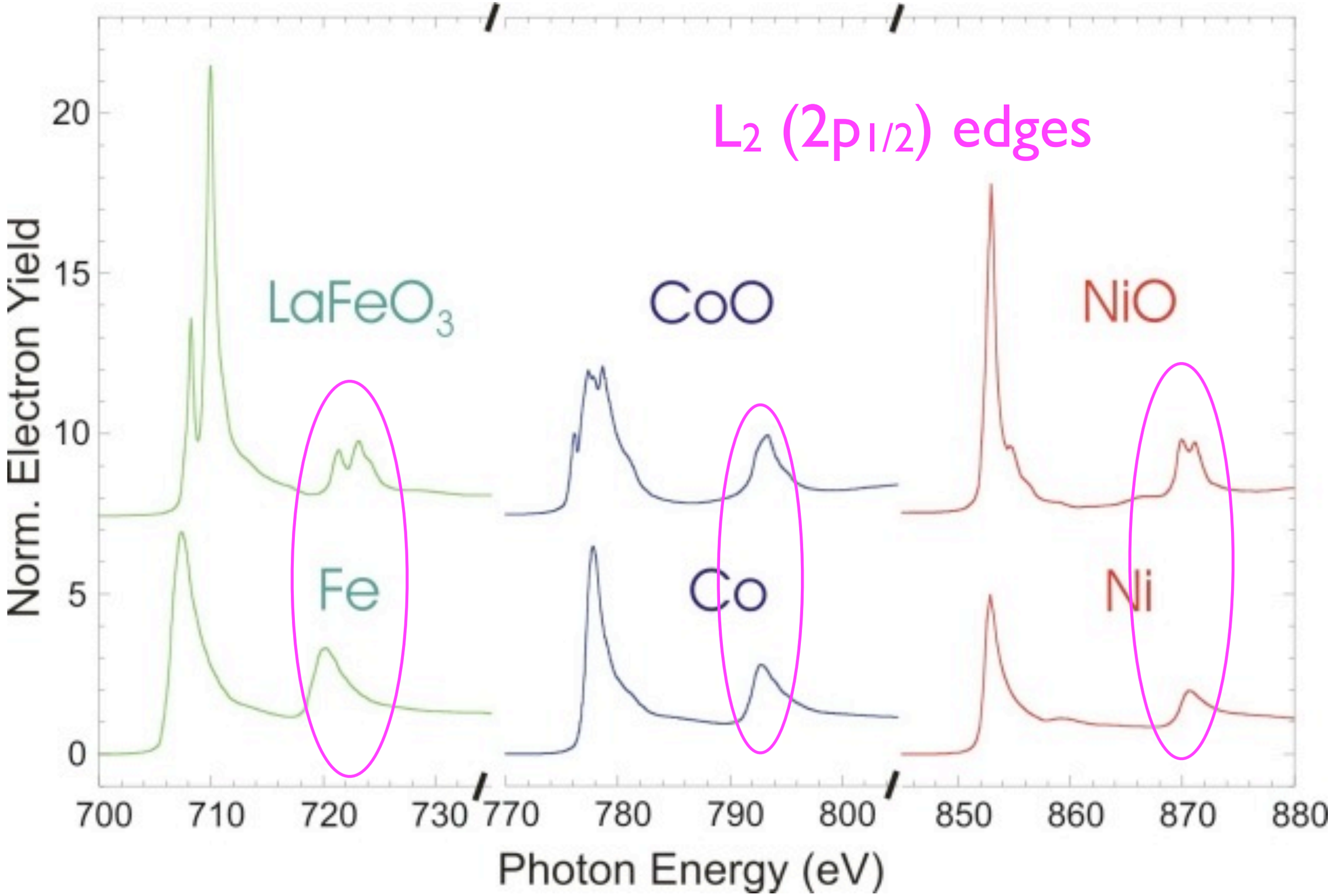

L-edge x-ray absorption spectra of Fe, Co and Ni in the form of the elemental metals and as oxides.

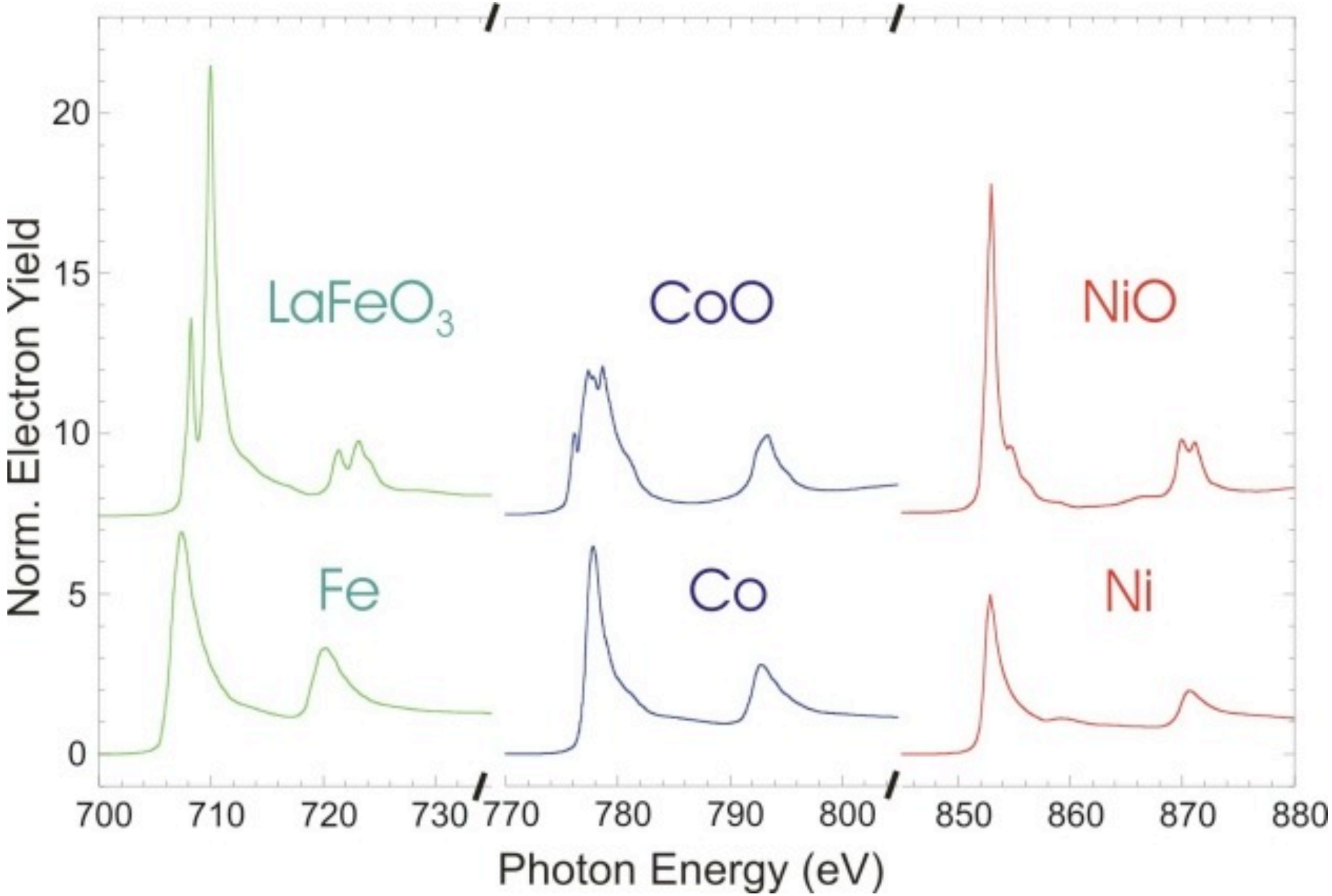

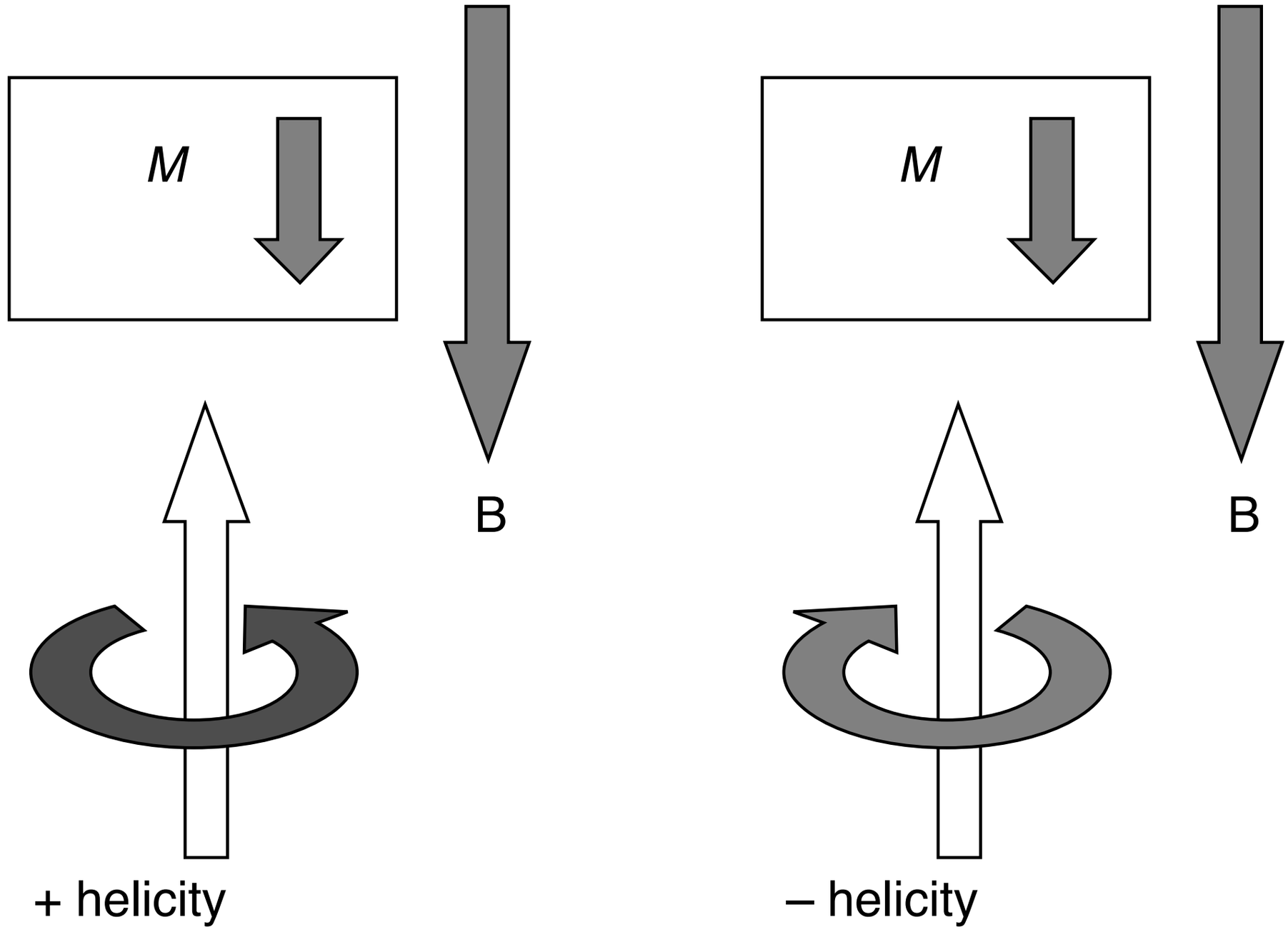

Definition of the intensities $\mu_{\pm}$.

Size of magnetic dichroism effects
The XMLD effect is large only in cases where the absorption edge exhibits multiplet structure.

Circular Dichroism - Ferromagnets

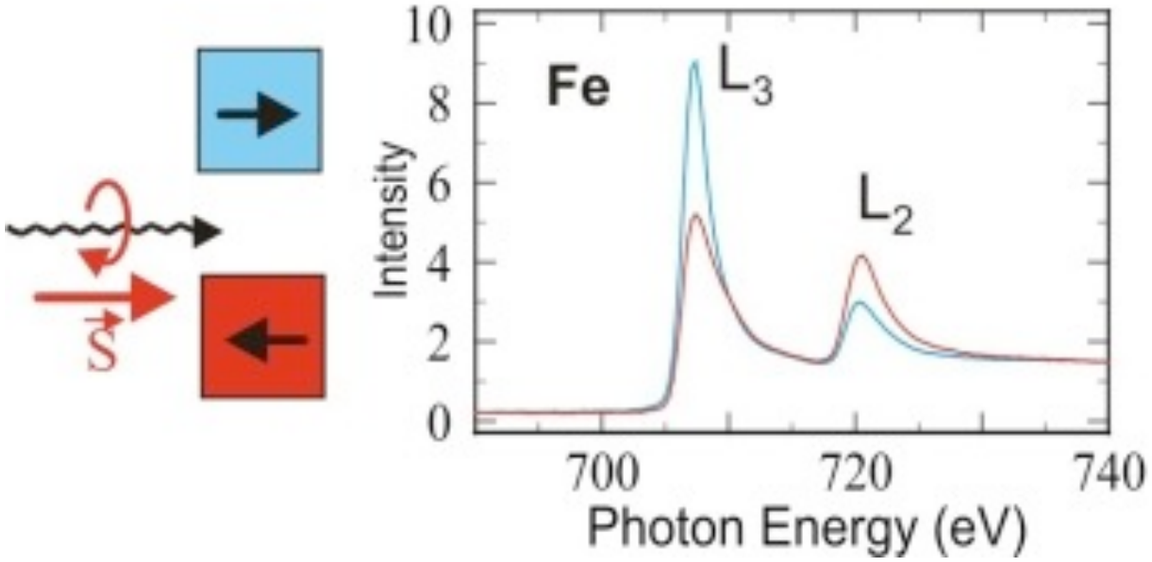

Linear Dichroism - Antiferromagnets

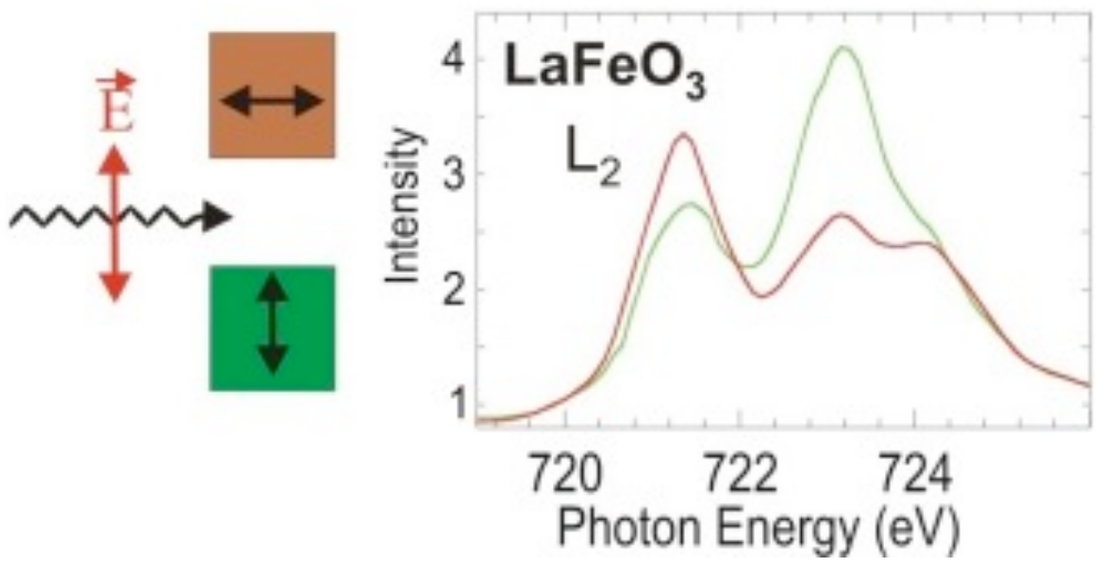

Electronic transitions in conventional L-edge x-ray absorption (a), and x-ray magnetic circular x-ray dichroism (b,c), illustrated in a one-electron model. The transitions occur from the spin-orbit split 2p core shell to empty conduction band states. In conventional x-ray absorption the total transition intensity of the two peaks is proportional to the number of d holes (first sum rule). By use of circularly polarized x-rays the spin moment (b) and orbital moment (c) can be determined from linear combinations of the dichroic difference intensities A and B, according to other sum rules.

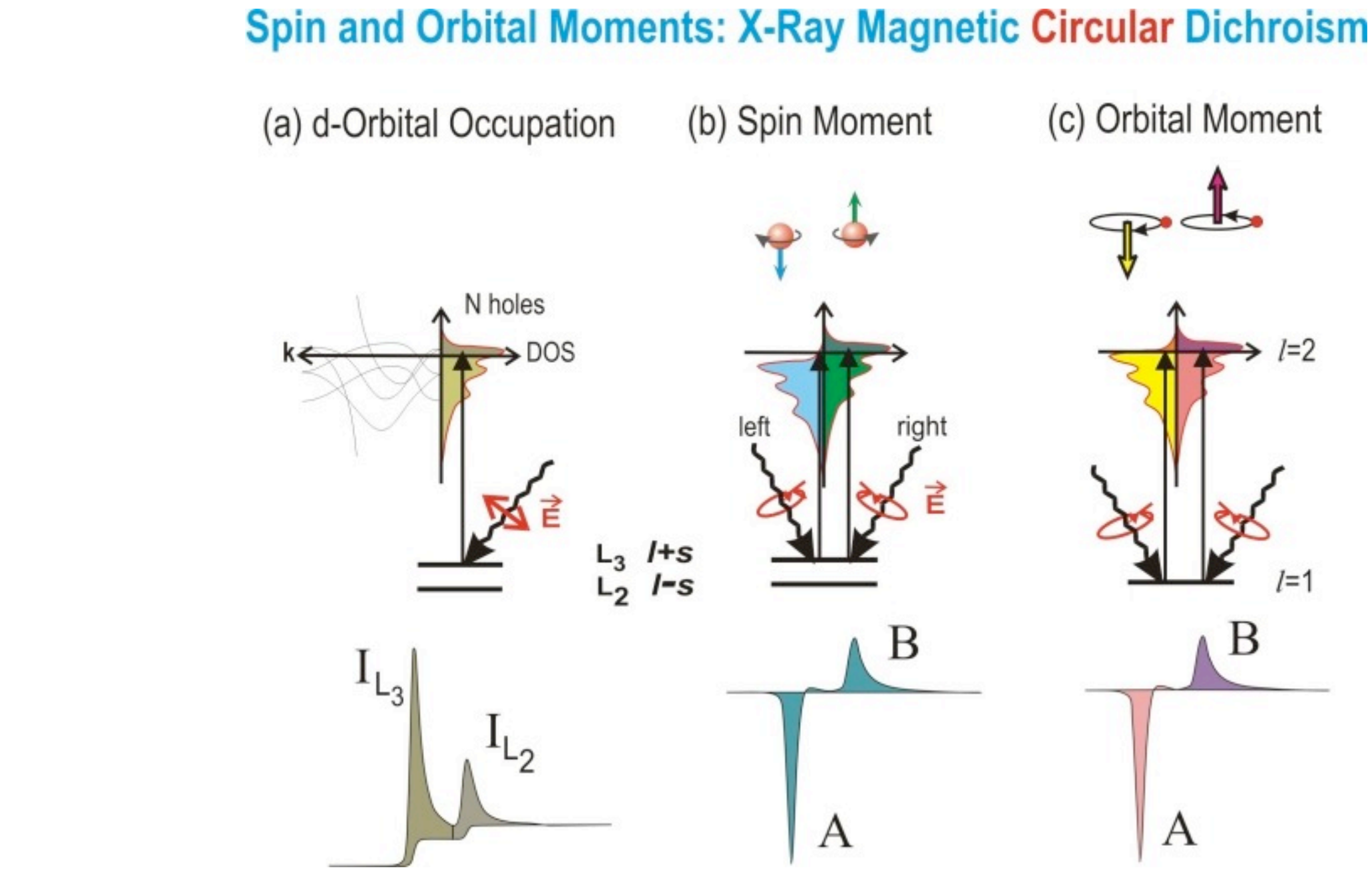

Origin of XMLD for NiO. On the left we show the electronic configurations involved in the x-ray absorption process. In the ground state there are two d holes (d^2 hole configuration) and their energy levels are determined by multiplet and crystal field effects. In the final state, a 2p hole is created by x-ray absorption and one d hole is filled by the excited electron. The resulting pd hole configuration again gives rise to multiplet splitting and the XAS spectrum reflects the multiplet structure. In the paramagnetic state the absorption spectrum of NiO does not exhibit a polarization dependence because of cubic symmetry. In the antiferromagnetic state the spin-orbit coupling leads to a distortion of the charge density and an XMLD effect is observed.

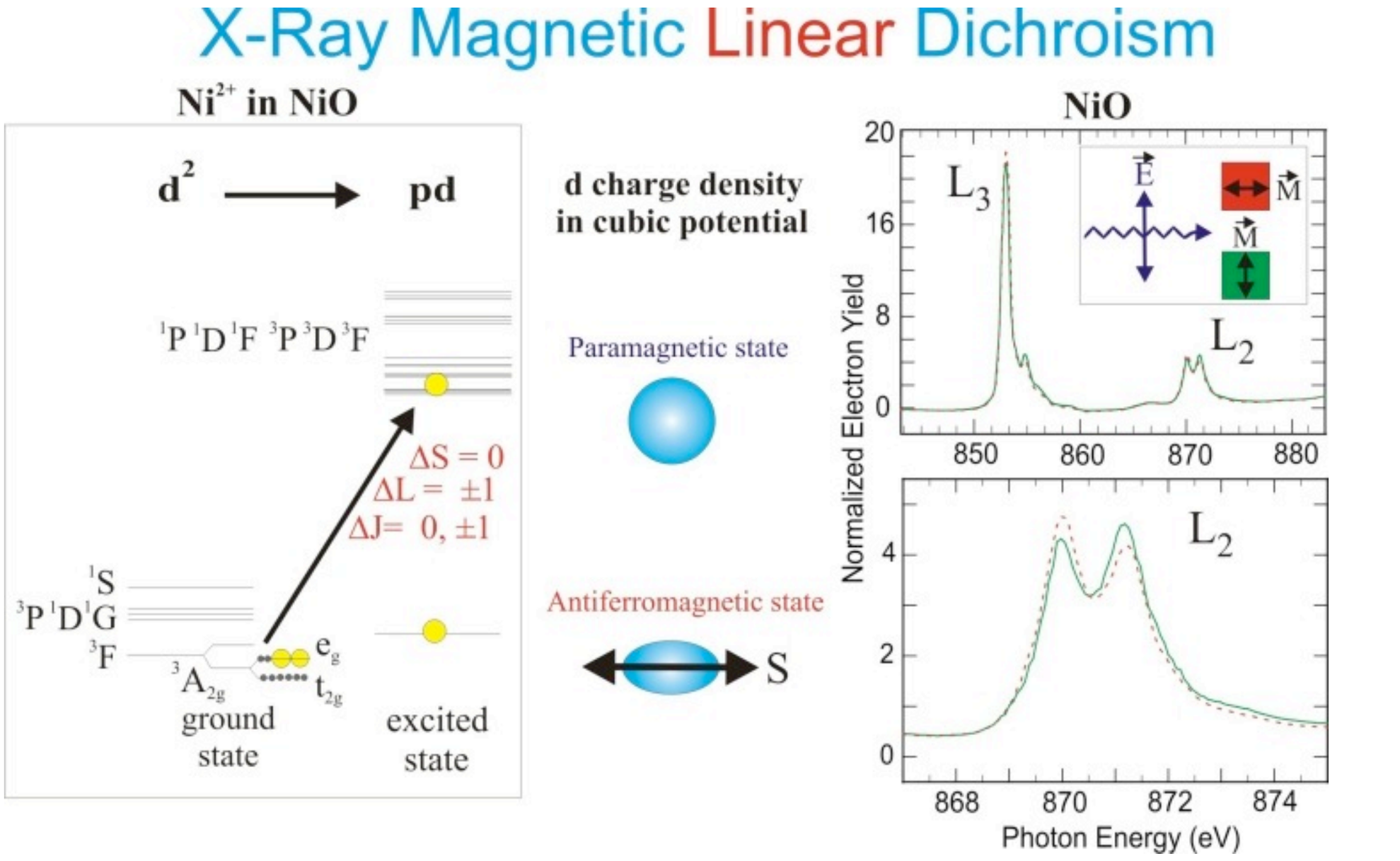

Example: a magnetic alloy

PHYSICAL REVIEW B **73**, 224416 (2006)

Observation of x-ray magnetic circular dichroism at the Ru *K* edge in Co-Ru alloys

H. Hashizume* and K. Ishiji
Photon Factory, KEK, Tsukuba 305-0801, Japan

J. C. Lang, D. Haskel, and G. Srajer
Advanced Photon Source, Argonne National Laboratory, Argonne, Illinois 60439, USA

J. Minár and H. Ebert
Department Chemie und Biochemie, Physikalische Chemie, Universität München, München D-81377, Germany

(Received 16 January 2006; revised manuscript received 19 April 2006; published 13 June 2006)

X-ray magnetic circular dichroism spectra have been measured from dilute Ru alloys of Co at the Ru *K* edge, evidencing the induced magnetization on Ru in contact with ferromagnetic Co. This was made possible using circularly polarized probing beams of approximately 22 keV in energy obtained from a germanium Laue-reflection phase retarder at a synchrotron source. The Ru dichroism is quite small with a main peak of -3×10^{-4} in flipping ratio at about 6 eV above the *K* absorption edge. The spectrum has a very similar profile to the one of the Co *K*-edge dichroism. *Ab initio* calculations indicate that the Ru dichroism is generated by the *p*-orbital magnetic moment on the core-hole site, which is induced through the *p*-*d* hybridization between Co and Ru.

DOI: 10.1103/PhysRevB.73.224416 PACS number(s): 75.30.Et, 07.85.Qe, 75.47.Np, 75.70.−i

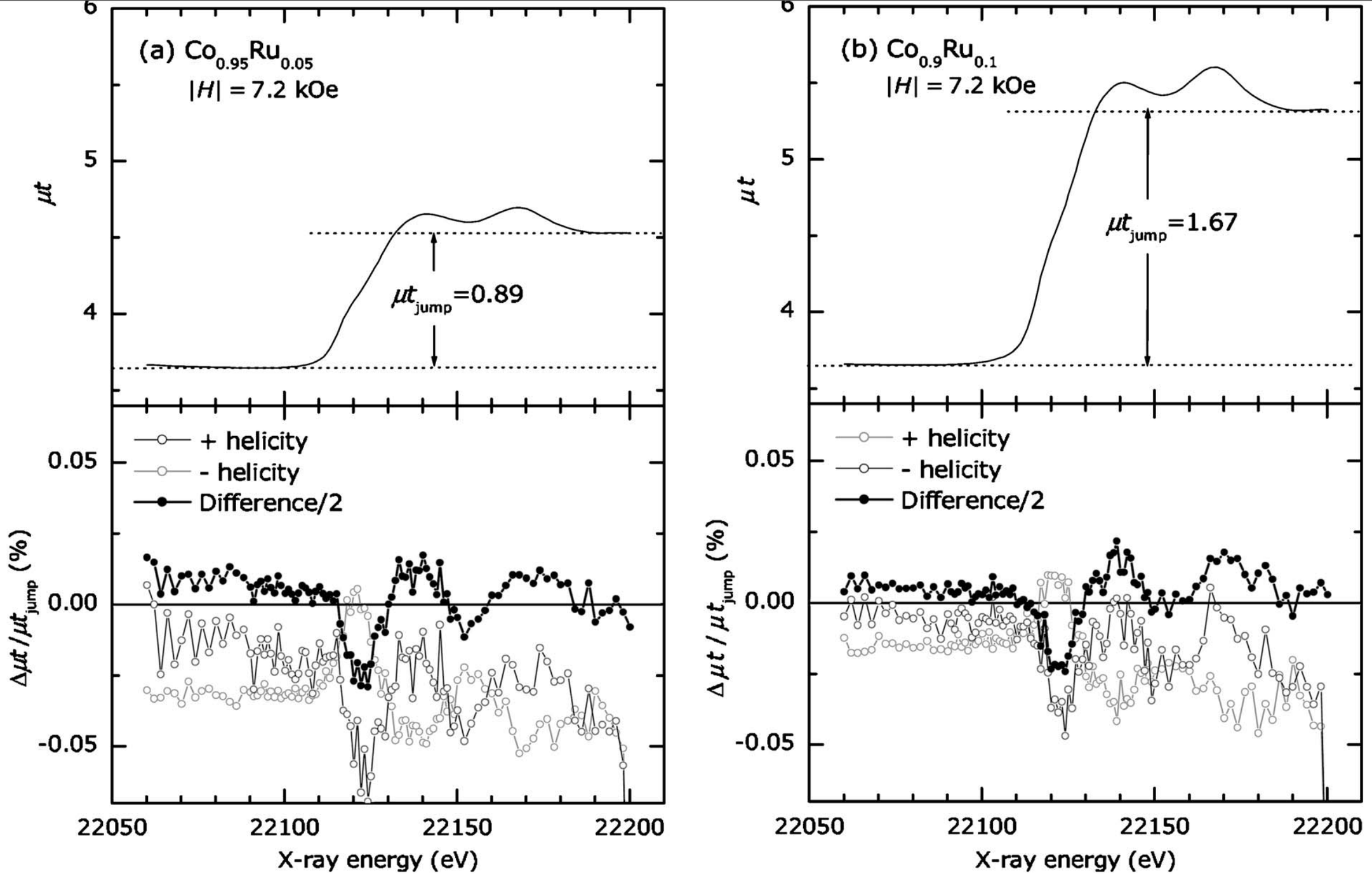

Nonmagnetic (top panel) and magnetic (bottom panel) x-ray absorption spectra measured from the $Co_{0.95}Ru_{0.05}$ (a) and $Co_{0.9}Ru_{0.1}$ (b) samples near the Ru K edge. In the bottom panel, open circles show raw data obtained using the circularly polarized beams of + and − helicities, whereas filled circles show the differences divided by 2, giving the background-free dichroic spectra. X-ray count time per energy point is 320 s (a) and 128 s (b). Data collection time: 20 h (a) and 12 h (b).

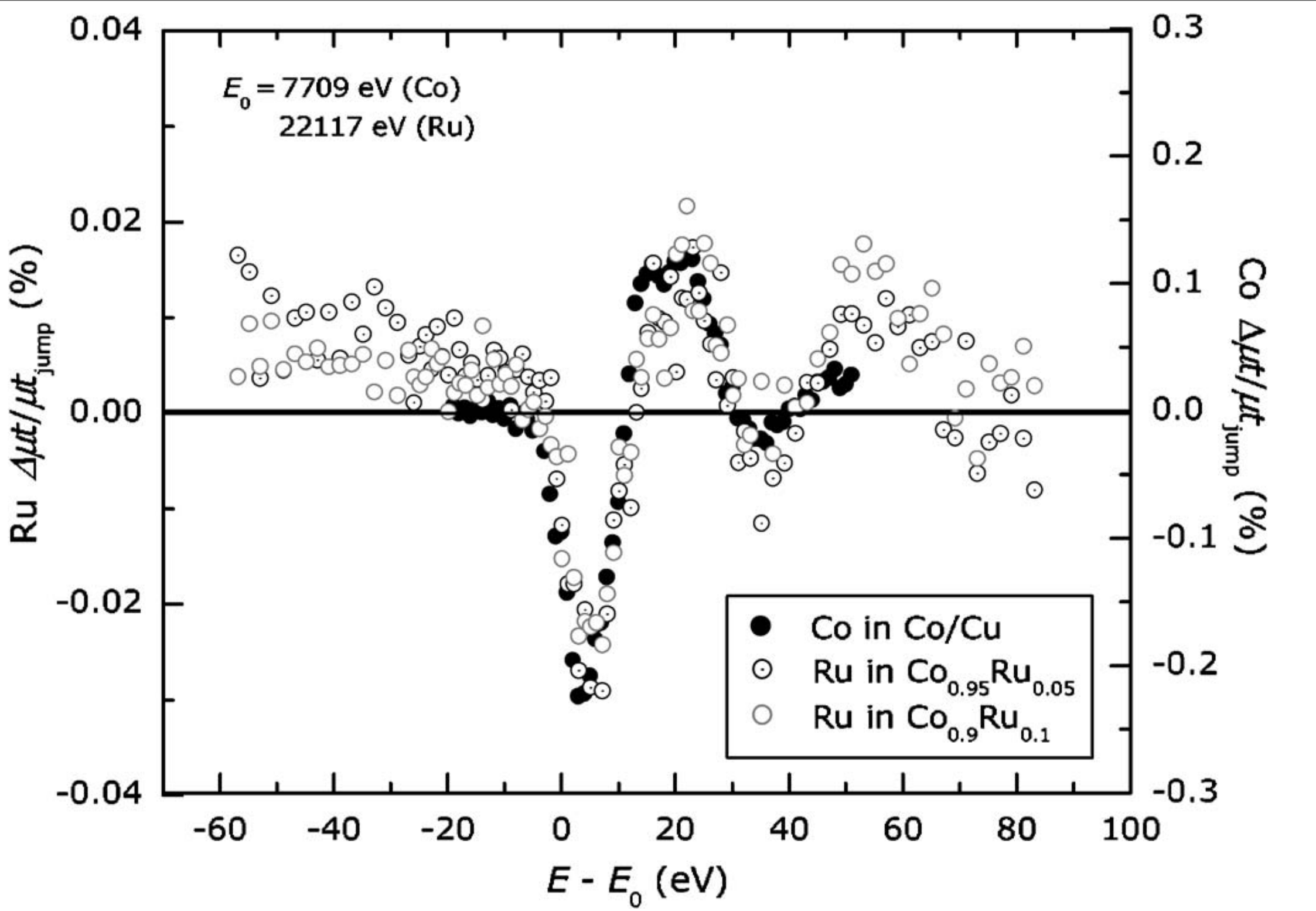

Comparing the dichroic spectra from the $Co_{0.95}Ru_{0.05}$ and $Co_{0.9}Ru_{0.1}$ samples at the Ru K edge with the one from a Co/Cu multilayers at the Co K edge. E_0: absorption-edge energy. Note that the dichroism from induced magnetizations on Ru is one order of magnitude smaller than the one from ferromagnetic Co.

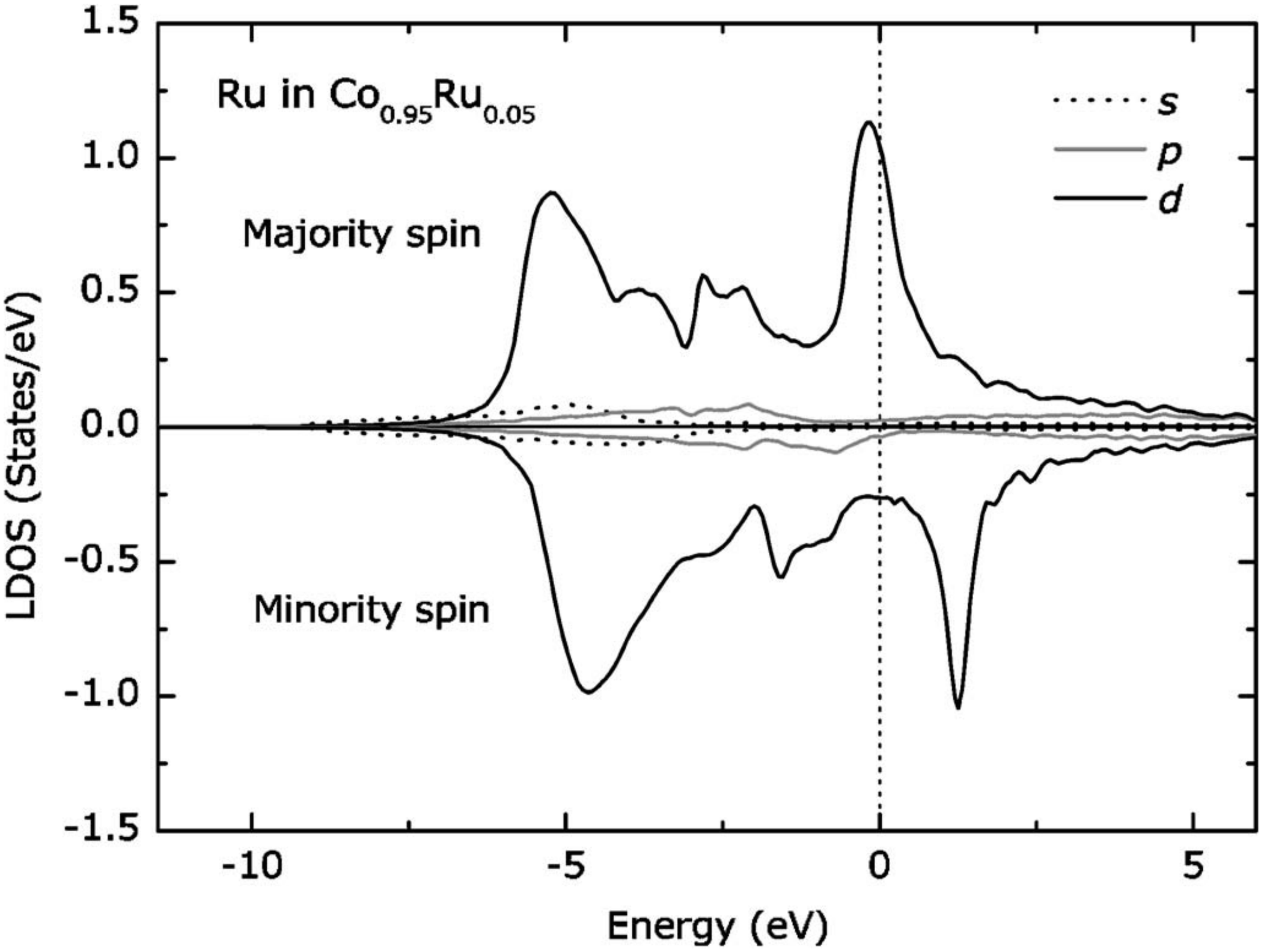

Local density of states (LDOS) including small s and p contributions for $Co_{0.95}Ru_{0.05}$ alloy